ACTIVITY 2

Enhance coherence in eutrophication assessments based on chlorophyll, using satellite data

Part of the EU project JMP EUNOSAT

May 2019

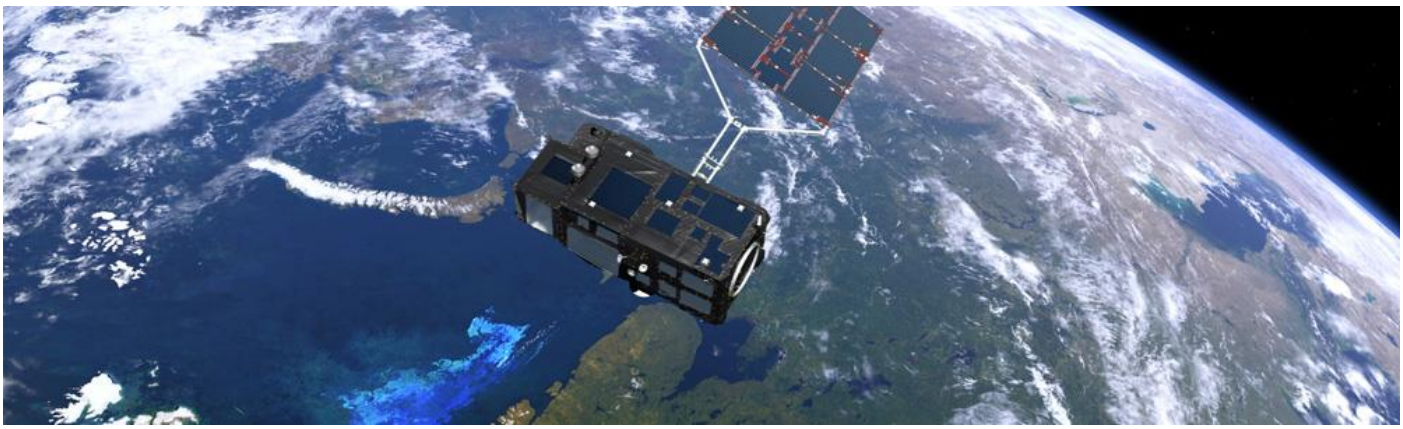

EUROPEAN COMMISSION
DIRECTORATE-GENERAL
ENVIRONMENT
Directorate D - Water, Marine Environment & Chemicals

Co-funded by the European Commission - DG Environment

This report can be cited as:

Van der Zande, D., Lavigne, H., Blauw, A., Prins, T., Desmit, X., Eleveld, M., Gohin, F., Pardo, S, Tilstone, G., Cardoso Dos Santos, J. (2019). **Coherence in assessment framework of chlorophyll a and nutrients as part of the EU project 'Joint monitoring programme of the eutrophication of the North Sea with satellite data' (Ref: DG ENV/MSFD Second Cycle/2016).** Activity 2 Report. 106 pp.

Authors & contributors:

Dimitry Van der Zande[1*], Heloise Lavigne[1], Anouk Blauw[2], Theo Prins[2], Xavier Desmit[1], Marieke Eleveld[2], Francis Gohin[3], Silvia Pardo[4], Gavin Tilstone[4], Joao Cardoso Dos Santos [1]

[1]Royal Belgian Institute of Natural Sciences, Rue Vautier 29, 1000 Brussels, Belgium.

*Corresponding author. Tel.: +3226274130

E-mail address: dvanderzande@naturalsciences.be

[2] Deltares, Boussinesqweg 1, 2629 Delft, The Netherlands

[3] IFREMER, Laboratoire d'écologie pélagique, DYNECO PELAGOS, CS 10070 - 29280 Plouzané, France

[4] PML, Plymouth Marine Laboratory, Prospect Place, The Hoe, Plymouth PL1 3DH, UK

Financial support: EU EMFF Programme Implementation of the second cycle of the MSFD – Achieving coherent, coordinated and consistent updates of the determinations of good environment status, initial assessments and environmental targets (DG ENV/MSFD Second Cycle/2016). Grant Agreement No. 11.0661/2017/750678/SUB/ENV.C2

Acknowledgements: This report is a detailed summary of performed work under Activity 2. The work is co-funded under the Belgian Science Policy (BELSPO) shared cost programme. We thank the project partners for providing access to their national in-situ data bases and technical support. ESA, NASA, ODESA and CMEMS are acknowledged for the provision of satellite products.

Key words: Ocean colour, satellite observations, multi-algorithm chlorophyll-a retrieval, eutrophication assessment

The JMP EUNOSAT project partners are: RWS (NL), RBINS (BE), Deltares (NL), AU (DK), Ifremer (FR), PML (UK), MSS (UK), CEFAS (UK), SMHI (SE), IMR (NO), NIVA (NO), UBA (DE), BSH (DE), NLWKN (DE)

Summary

The European Marine Strategy Framework Directive (MSFD) requires Member States (MS) to achieve Good Environmental Status (GES) of their seas by 2020. Monitoring and assessment should be performed in a coherent, coordinated and consistent manner. The North East Atlantic MSFD Region is divided into four sub-regions: the Wider Atlantic, the Bay of Biscay and Iberian Coast, the Celtic Seas and the Greater North Sea. Each MS is required to develop a marine strategy for their Exclusive Economic Zone (EEZ). Therefore, it is important that MS work together to implement each stage of the Directive in a coherent and coordinated way, ensuring comparability across Europe. The OSPAR Convention is a key forum to facilitate many aspects of the coordination process.

The present report is a deliverable of the EU funded project "Joint monitoring programme of the eutrophication of the North Sea with satellite data' (JMP EUNOSAT). This project aims to develop a coherent monitoring and assessment framework for *chlorophyll a (CHL)*, an indicator relevant for eutrophication (D5) and foodwebs (D4), for the North Sea. The project is organised in 3 activities with the following aims:

a) Derivation of threshold values for Good Environmental Status (GES) for nutrients and algae concentrations with a common a common method for all North Sea countries (activity 1);
b) Generation and validation of a coherent multi-algorithm satellite-based chlorophyll-a product for the North Sea and the suitability of these products for eutrophication assessments (activity 2)
c) Definition of coherent assessment areas with similar ecological and physical functioning (activities 1 and 2 together)
d) Development of a potential design of a future monitoring and assessment programme (activity 3)

The present report describes the results of Activity 2 of the project comprising generation of a coherent satellite-based chlorophyll-a product, examples of eutrophication assessments using the satellite products and an evaluation of the suitability of satellite observations for this purpose.

First, we evaluate publicly accessible satellite-based *chlorophyll a* products available from Copernicus Marine Environment Monitoring Services (CMEMS), European Space Agency (i.e. ODESA) and other data providers (i.e. IFREMER) generated using 1) blue/green-ratio algorithms, 2) red-edge algorithms and 3) artificial network approaches and determine their validity for different water types, giving special attention to optically complex coastal waters. From these products we choose the most suitable products and provide information on the steps needed to upgrade these core ocean color satellite products to operational and coherent monitoring products usable for eutrophication assessment in the Greater North Sea.

We present a quality control procedure for four complementary chlorophyll-a algorithms: the classic empirical blue-green bands ratio algorithm (OC4) and the adapted OC4 for Baltic waters, the OC5 algorithm and finally the Gons (1999) semi-analytic algorithm. Results that do not pass this test are removed (flagged). This quality flagging approach is calibrated and validated using well known ocean color match-up data bases (i.e. CCRR, MERMAID). Subsequently, the best combination of *chlorophyll a* algorithms is

discussed to produce a quality controlled multi-algorithm satellite *chlorophyll a* product based on the best suited algorithm/water type combination.

This step enabled the progression from point-by-point and country-by-country analyses, to basin-wide analysis with data that cover gradients in the ecosystem system. This approach is applied to available satellite data for the period 1998-2017 and the suitability of the blended CHL product for eutrophication assessment is evaluated by a comparison analysis with in-situ datasets for all assessment areas in the Greater North Sea. A validation of the yearly mean and P90 *chlorophyll a* products using the national monitoring *chlorophyll a* data obtained using different analytical techniques (i.e. HPLC, spectrophotometry, fluorometry) yielded a median error of 35.19% and 39.05% respectively. This shows a good general agreement between in-situ and satellite observations.

Considering the spatial and temporal availability of the quality-controlled multi-algorithm *chlorophyll a* products for the period 1998-2017 we can conclude that remote sensing provides opportunities for a synoptic overview of the *chlorophyll a* concentrations of most part of the North Sea. Gathering similar synoptic observations with in-situ observations is difficult or even impossible, especially in off-shore areas. However, there are circumstances where the multi-algorithm remote sensing observations are unsuitable for CHL assessments and where in-situ observations are required to obtain relevant information. There is a significant advantage with the availability of the MERIS sensor (2003-2011) in terms of providing specialized products for optically complex waters which is continued with the Sentinel-3 satellite program. Outside of the MERIS period (1998-2002 and 2012-2016) we observed critically low valid CHL observations in estuaries, the East Anglia Plume, the Wadden Sea, near-shore coastal zones (e.g. UK, BE, NL, GE, DK) and fjords.

With the Copernicus program guaranteeing a reliable source of data to at least 2036, special efforts were made to ensure future integration of Sentinel-3/OLCI data into the processing chain. Sentinel-3/OLCI has a similar spectral band set as MERIS enabling more reliable products for optically complex waters. The full resolution data (300m spatial resolution) are expected to provide more robust CHL estimates in the problematic regions discussed above. Additionally, the Sentinel-2/MSI satellite which is originally designed for land applications can provide *chlorophyll a* products with a spatial resolution of 10m—20m. While these applications are not directly investigated in this study, this option provides useful perspectives for eutrophication monitoring of the near shore coastal waters.

To take the next step towards integration of satellite observations into eutrophication assessments for the North Sea, we investigated: 1) different approaches of aggregating the satellite *chlorophyll a* products, 2) use of different assessment levels and 3) use of new assessment areas.

In a case study focussing on the Dutch part of the North Sea we tested the impact of the different approaches on eutrophication assessment to improve/fine-tune all components before actual implementation. When considering all satellite CHL observations at full resolution, the estimated area *chlorophyll a* mean is for most areas reasonably close to the mean based on in-situ data only when the areas are relatively homogeneous with respect to water quality characteristics. However, in areas with

strong spatial gradients, the assessment results are very sensitive to the area boundaries and the choice of in-situ monitoring locations. A solution was proposed by spatially variable *chlorophyll a* assessment levels with a spatial resolution of 1x1km corresponding to the grid used for the satellite data. This enables a pixel by pixel eutrophication assessment by directly comparing the satellite data with the assessment levels resulting in a more consistent relative exceedance of the assessment levels throughout the assessment area. Consequently, the result is less dependent on the definition of assessment areas. Another possibility is to re-organize the assessment areas into zones that share similar environmental conditions (Final report Activity 1 section 9) which is presented in a case study (section 3).

During the study it was also found that the MSFD system using only two classes (good and bad) is quite limiting in terms of assessing gradual improvement of the status of an assessment area relative to the threshold indicating good environmental status. Using more classes, such as in the WFD, would give more information on changes. Regarding the extent to which good environmental status has been achieved in an assessment area, the satellite-based eutrophication product can easily determine the extent of the area that is not subject to eutrophication, using fixed or variable thresholds, and determine its evolution in time as an objective measure of changes in eutrophication status.

Table of contents

1. Introduction

The Marine Strategy Framework Directive (MSFD) is currently one of the most important drivers for monitoring the coastal and offshore waters in Europe with the objective of reaching a 'good environmental status' (GES) by 2020 (Gohin et al. 2008). It is a crucial legal instrument of the European Commission to protect the marine environment including its ecosystems and biodiversity. Human-induced eutrophication is one of the criteria for assessing the extent to which GES is being achieved. Eutrophication can be defined as the enrichment of water by nutrients causing an accelerated growth of algae and higher forms of plant life to produce an undesirable disturbance to the balance of organisms present in the water and to the quality of the water concerned, and therefore refers to the undesirable effects resulting from anthropogenic enrichment by nutrients (OSPAR, 2017).

The eutrophication status is established by monitoring of nutrients, and chlorophyll-a (CHL)concentration as a proxy of phytoplankton biomass. More specifically, the indicator of choice is the mean or 90-percentile of the CHL concentrations (avg, CHL-P90) over the phytoplankton growing season (e.g. March – September incl.) for a period of six years expressed in µg/l or mg/m³. CHL-P90 represents the CHL level such that 90% of the observations are equal to or less than this value. While in-situ data acquisition is still considered as the main monitoring tool, the European Commission highlighted the need for greater coherence with related EU legislations (Water Framework Directive and Habitats and Birds Directive) and for more coherent and coordinated approaches within and between marine regions and sub-regions (European Commission, 2014).While preparing for the second cycle of MSFD assessment, various OSPAR groups (Intersessional Correspondence Group on Eutrophication (ICG-EUT) and the Hazardous Substances and Eutrophication Committee (HASEC) have identified incomparability of monitoring methods for CHL as a main issue hampering a coherent assessment of the common indicator CHL in the Greater North Sea. Moreover, the assessment levels for CHL, based on background concentrations, have been determined with different methods between member states. This results in different GES determinations across national borders that cannot be explained by differences in water quality (Figure 1.1). Additionally, the budgets for marine monitoring are decreasing in many European countries and MSFD requires countries to measure more variables forcing them to efficiently use monitoring resources.

During recent years there has been a growing tendency to use optical remote sensing as a supporting tool to achieve the monitoring requirements because of severe resource constraints of available ship time and personnel and the need for a coherent assessment of CHL between all OSPAR member statescountries bordering the North Sea. Incoherence in assessment outcomes is most prominent in the North Sea, since the area is divided in national territories of eight countries. Satellite data of CHL combine cheaper data collection with a much improved geographical and temporal coverage compared to traditional in-situ data

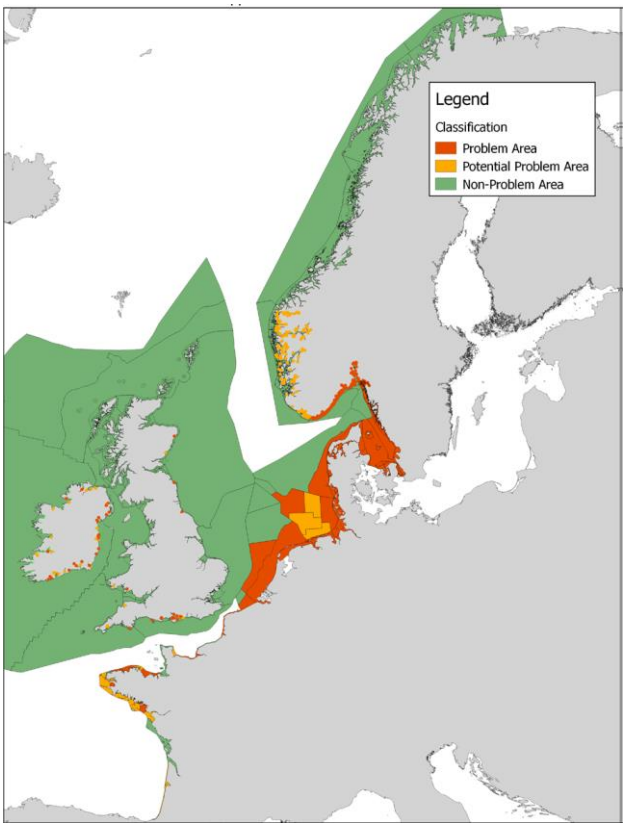

Figure 1.1: Map of problem areas for eutrophication in the OSPAR region (OSPAR, 2017)

Satellite data from ocean color sensors (i.e. SeaWiFS, MODIS, MERIS, VIIRS, Sentinel-3) can provide spatially coherent data on CHL concentrations using CHL retrieval algorithms. There has been considerable success with blue/green-ratio algorithms such as OC4 (O'Reilly et al., 1998) and OC5 (Gohin et al. 2002) in case 1 waters where the variation of optical properties (absorption and scattering) is dominated by phytoplankton and associated material. In contrast, the optical complexity in coastal waters often poses many challenges to the accurate retrieval of biogeochemical parameters using satellite remote sensing (Sathyendranath, 2000; Lee, 2006). CHL retrieval by blue/green-ratio algorithms tend to fail when applied to coastal waters whose optical properties are strongly influenced by non-covarying concentrations of suspended particulate matter (SPM) and coloured dissolved organic matter (CDOM). Such waters are defined as case 2 waters. Several constituent retrieval algorithms for use in case 2 waters have been developed: 1) red-edge algorithms (Gons et al., 2002) taking advantage of the CHL absorption peak near 670 nm and 2) artificial network approaches trained to varying parameter concentrations and optical property ranges specifically developed for use with MERIS data, such as the MERIS Ground Segment Processor -MEGS- (Doerffer and Schiller, 2007) and the FUB/WeW (Schroeder et al., 2007).

The technical objective of the Activity 2 of the JMP EUNOSAT project is to generate a coherent multi-algorithm satellite-based CHL product from publicly accessible satellite-based CHL products available from CMEMS, ODESA and IFREMER. To achieve this, we determine the validity of these core ocean color products for different water types (e.g. clear, turbid or CDOM-rich waters) and upgrade these satellite products to operational and coherent monitoring products usable for eutrophication assessment in the

Greater North Sea through a quality control and merging process. This step enabled the progression from point-by-point and country-by-country analyses, to basin-wide analysis with data that cover gradients in the ecosystem system.

The following sub-activities have been performed:

1) Generation of coherent multi-algorithm satellite-based chlorophyll a products consisting of a quality flagging approach and merging procedure (chapter 2.3) which was applied to a satellite data archive (chapter 2.2) for the period 1998-2017 (chapter 2.4)
2) Validation of coherent satellite-based chlorophyll a product (chapter 2.5)
3) Evaluation of coherent satellite-based chlorophyll a product for eutrophication assessment in a case study for Dutch waters (chapter 3)
4) Evaluation of suitability of satellite data for coherent eutrophication assessment in the North Sea (chapter 4)

2. Generation of coherent satellite-based chlorophyll a product

Part of this section is in preparation for submission to a scientific Journal:

Lavigne, H., Van der Zande, D., Ruddick, K., Cardoso Dos santos, J. Chlorophyll-a algorithm selection in coastal waters. Definition of application flags for OC4, OC5 and Gons algorithms. In prep.

2.1. Introduction

In this section we provide information on the steps needed to upgrade core ocean color satellite products, as delivered by CMEMS, ODESA and IFREMER, to operational and coherent monitoring products usable for eutrophication assessment in the Greater North Sea giving special attention to optically complex coastal waters. Optically complex coastal waters pose many challenges for satellite remote sensing to accurately retrieve biogeochemical parameters such as CHL concentration due to concentrations of suspended particulate matter (SPM) and colored dissolved organic matter (CDOM). Here we evaluate publicly accessible satellite-based CHL products available from Copernicus Marine Environment Monitoring Services (CMEMS), European Space Agency (i.e. ODESA) and other data providers (i.e. IFREMER) generated using 1) blue/green-ratio algorithms, 2) red-edge algorithms and 3) artificial network approaches and determine their validity for different water types, e.g. clear, turbid or CDOM-rich waters. The results of this evaluation are subsequently used to determine the reflectance (i.e. RRS) conditions for which these algorithms can deliver an accurate CHL estimate in complex optical conditions as found in coastal waters. Finally, the best combination of CHL algorithms is discussed to produce a quality controlled multi-algorithm satellite CHL product based on best suited algorithm/water type combination (Figure 2.1). This step enabled the progression from point-by-point and country-by-country analyses, to basin-wide analysis with data that cover gradients in the ecosystem system. The suitability of the blended CHL product for eutrophication assessment is evaluated by a comparison analysis with in-situ datasets for all assessment areas in the Greater North Sea.

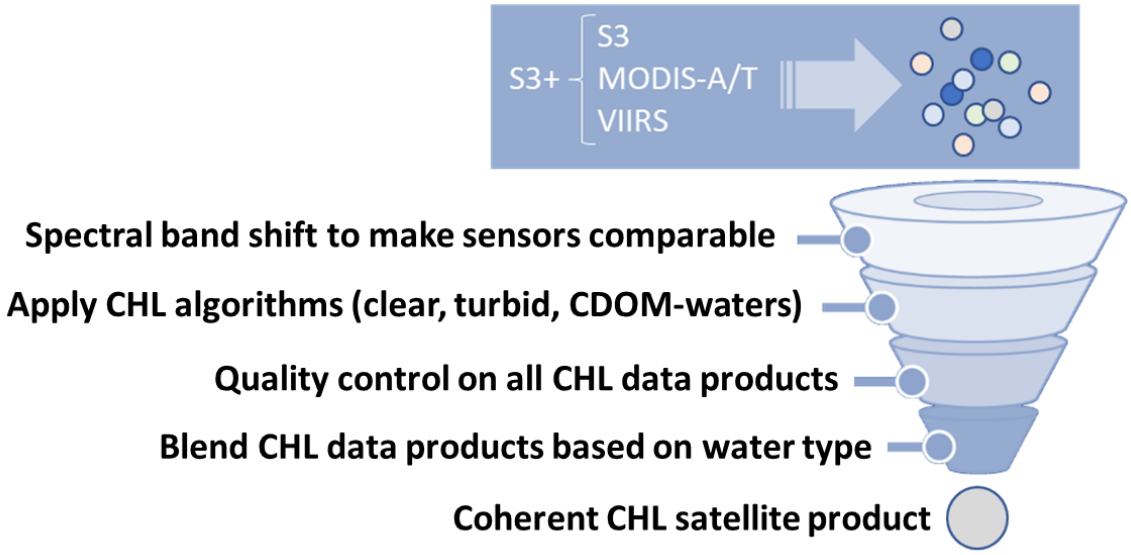

Figure 2.1: Overview of steps needed to generate a quality controlled multi-algorithm coherent satellite CHL product using data from multiple ocean color sensors.

The workflow of this section is:

- Acquisition of core ocean color satellite products from main product services such as CMEMS and ODESA
- Development of quality control protocol for CHL products to generate coherent multi-algorithm satellite CHL product based on best suited algorithm/water type combination
- Validation of coherent multi-algorithm satellite product

2.2. Acquisition of core ocean color satellite products

We started from a collection of operational satellite-based CHL products for the Greater North Sea (Table 2.1) : 1) CMEMS OC5-CI (product 2.1), 2) CMEMS OC4 adapted to Baltic waters (product 2.4 & 2.5), 4) OC4 applied to CMEMS remote sensing reflectance products (product 2.2 & 2.3), 5) MEGS 7.5 applied to the MERIS archive obtained from ODESA online (http://www.odesa-info.eu/, product 2.8), the red-edge algorithm (Gons et al. 2002, product 2.9) applied to remote sensing reflectance spectra (RRS) obtained by applying MEGS 8.1 to the MERIS archive obtained from ODESA online and the FUB-WEW neural network (v4.0.1, product 2.10) applied to MERIS L1b data. An overview of the products and links to their product user manual and quality information document is provided in table 2.1.

Table 2.1: Overview of satellite products and links to their Product User Manual (PUM) and Quality Information Document (QUID).

Ref. No.	Product name & type	Documentation
2.1	OCEANCOLOUR_ATL_CHL_L3_REP_OBSERVATIONS_009_067	PUM: http://marine.copernicus.eu/documents/PUM/CMEMS-OC-PUM-009-ALL.pdf QUID: http://marine.copernicus.eu/documents/QUID/CMEMS-OC-QUID-009-066-067-068-069-088-091.pdf
2.2	OCEANCOLOUR_ATL_OPTICS_L3_REP_OBSERVATIONS_009_066	PUM: http://marine.copernicus.eu/documents/PUM/CMEMS-OC-PUM-009-ALL.pdf QUID: http://marine.copernicus.eu/documents/QUID/CMEMS-OC-QUID-009-066-067-068-069-088-091.pdf
2.3	OCEANCOLOUR_ATL_OPTICS_L3_NRT_OBSERVATIONS_009_034	PUM: http://marine.copernicus.eu/documents/PUM/CMEMS-OC-PUM-009-ALL.pdf QUID: http://marine.copernicus.eu/documents/QUID/CMEMS-OC-QUID-009-034-036-046-047-087-089-090-092.pdf
2.4	OCEANCOLOUR_BAL_CHL_L3_REP_OBSERVATIONS_009_080	PUM: http://marine.copernicus.eu/documents/PUM/CMEMS-OC-PUM-009-ALL.pdf QUID: http://marine.copernicus.eu/documents/QUID/CMEMS-OC-QUID-009-080-097.pdf
2.5	OCEANCOLOUR_BAL_CHL_L3_NRT_OBSERVATIONS_009_049	PUM: http://marine.copernicus.eu/documents/PUM/CMEMS-OC-PUM-009-ALL.pdf QUID: http://marine.copernicus.eu/documents/QUID/CMEMS-OC-QUID-009-048-049.pdf
2.6	OCEANCOLOUR_BAL_OPTICS_L3_NRT_OBSERVATIONS_009_048	PUM: http://marine.copernicus.eu/documents/PUM/CMEMS-OC-PUM-009-ALL.pdf QUID: http://marine.copernicus.eu/documents/QUID/CMEMS-OC-QUID-009-048-049.pdf
2.7	OCEANCOLOUR_BAL_OPTICS_L3_REP_OBSERVATIONS_009_097	PUM: http://marine.copernicus.eu/documents/PUM/CMEMS-OC-PUM-009-ALL.pdf QUID: http://marine.copernicus.eu/documents/QUID/CMEMS-OC-QUID-009-080-097.pdf

2.8	OCEANCOLOUR_MERIS_MEGS75 OCEANCOLOUR_MERIS_MEGS81	PUM: https://earth.esa.int/web/sentinel/user-guides/software-tools/-/article/odesa QUID: http://mermaid.acri.fr/home/home.php
2.9	OCEANCOLOUR_MERIS_GONS	Gons et al. (2002)
2.10	OCEANCOLOUR_MERIS_FUBv4.0.1	Schroeder et al. (2007)

CMEMS products (product 2.1 to 2.7) were directly downloaded from the CMEMS FTP server and are delivered as Analysis Ready Data (ARD) without additional quality flags.

MERIS products (products 2.9) were obtained from the ODESA processor. CHL products were generated using the MEGS7.5 and RRS products using the MEGS8.1 processor. The MEGS7.5 processor produces two CHL products, algal1 and algal2. Algal1 is designed for case 1 waters and is derived using a maximum band-ratio algorithm which uses four wavelengths: 443, 490, 510 and 560 nm (Morel and Antoine, 2007, Morel et al., 2007), while algal2 is computed using a neural-network inversion algorithm designed for case 2 waters (Doerffer and Schiller, 2007), which uses the eight MERIS visible wavelengths: 412–709 nm, except 681 nm to avoid chlorophyll fluorescence effects. It is noted that the MERIS case 2 water (algal2) algorithm is substantially different in design and wavelengths from the MERIS case 1 water (algal1) algorithm. A quality control is performed on RRS, algal1 and algal2 products by removing less reliable data using the standard level 2 flags provided by the MEGS processor (Table 2.2). The choice of which of the two MERIS CHL products to use is made according to the turbid case 2 water flag (case2_s) which produces a single MERIS daily CHL product for further processing. The MEGS7.5 chlorophyll product for turbid waters (algal_2) was updated with the third reprocessing (MEGS8.1) of the MERIS data. Unfortunately, the new version of algal_2 is correlated with the signal from suspended matter resulting in the retrieval of unnatural spatial and temporal patterns of chlorophyll concentration in turbid waters (corresponding to suspended matter variability) making the algal_2 dataset from MEGS 8.1 is not usable in turbid waters (Vanhellemont, 2012**)**

Table 2.2: Overview MERIS quality flags used to remove less reliable data from the RRS and CHL products

Flag Name	Description
land	Pixel classifed as Land in L1B, adjusted radiometrically during L2 pixel classification to allow for geocorrection errors and tidal changes.
cloud	Pixel classified as cloud by the L2 cloud screening algorithm. Sub-pixel, scattered cloud not included.
low_sun	Sun Zenith Angle > 70°
high_glint	Pixel with high sun-glint, which has NOT been corrected. Sunglint reflectance calculated from viewing geometry and wind speed exceeds the medium glint
ice_haze	Pixel with high radiance in the blue, likely to be caused by ice or high aerosol load
case2_anom	Bright water pixel, anomalous scattering water. Flags the presence of Case 2 water
coastline	Coastline flag
pcd_1_13	Confidence flag for MDS 1 to 13 (reflectances). Raised at low sun angles, when atmospheric correction fails or there are difficulties with aerosol correction. Also
pcd_15	Confidence flag for MDS 15 (algal_1). Raised when atmospheric correction fails or there are difficulties with aerosol correction. Also for pixels with
pcd_17	Confidence flag for MDS 17 (algal_2) Raised when PCD_13 is raised, or when the algorithm input or output is outside the expected range.
case2_s	Turbid water, nominally TSM > 0.3gm-3. Indicative of sediment laden coastal water or coccolithophore blooms, sometimes other algal blooms. Raised after
invalid_algal_1	Invalid algal 1 product
invalid_algal2_tsm_ys	Invalid algal 2, TSM and Yellow matter products

The FUB neural network (v4.0.1) was applied to the MERIS Level-1b data archive using the SNAPv6.0 software providing Level-2 CHL products. During the processing the MERIS Level-1b data are masked prior to the retrieval by applying the following combination mask: GLINT_RISK | LAND_OCEAN | BRIGHT | COASTLINE | INVALID. Subsequently, each pixel is checked against the input and output values margin of the trained networks. Additional flags are set in case of a neural network failure for input and output separately. These Level 2 FUB/WeW processor flags of input (in) or output (out) retrieval failure of chlorophyll-a (chl), yellow substance (yel), total suspended matter(tsm) and atmospheric correction (atm) are “chl_in”, “chl_out”, “yel_in”, “yel_out”, “tsm_in”, “tsm_out”, “atm_in” and “atm_out”.

Figure 2.2 shows a CHL product matrix providing an overview of ESA and NASA’s ocean color satellites and the CHL products as described above. Based on literature, an initial selection of the optimal CHL product for a certain appropriate water type (turbid, clear or absorbing waters) is made. There are two considerations to be made here: 1) not all CHL algorithms provide accurate CHL products in all waters (e.g. blue green algorithms fail in turbid waters for lower CHL values as the signal is masked by high scattering effects) and 2) not all algorithms can be applied to all satellites, e.g. the neural networks or red-NIR algorithm cannot be applied to data from NASA’s sensors as those sensors have no 709nm spectral band. This results in a data gap for turbid waters during the periods when no ESA satellites were available. We aim to fill in these data gaps with quality-controlled satellite data using NASA satellites and their algorithms as much as possible. CHL product matrix providing an overview of ESA and NASA’s ocean colour satellites and different CHL products. For turbid coastal waters, there are data gaps for non-MERIS periods as the neural net or GONS CHL products are not available for NASA’s sensors due to the missing of the 709nm band.

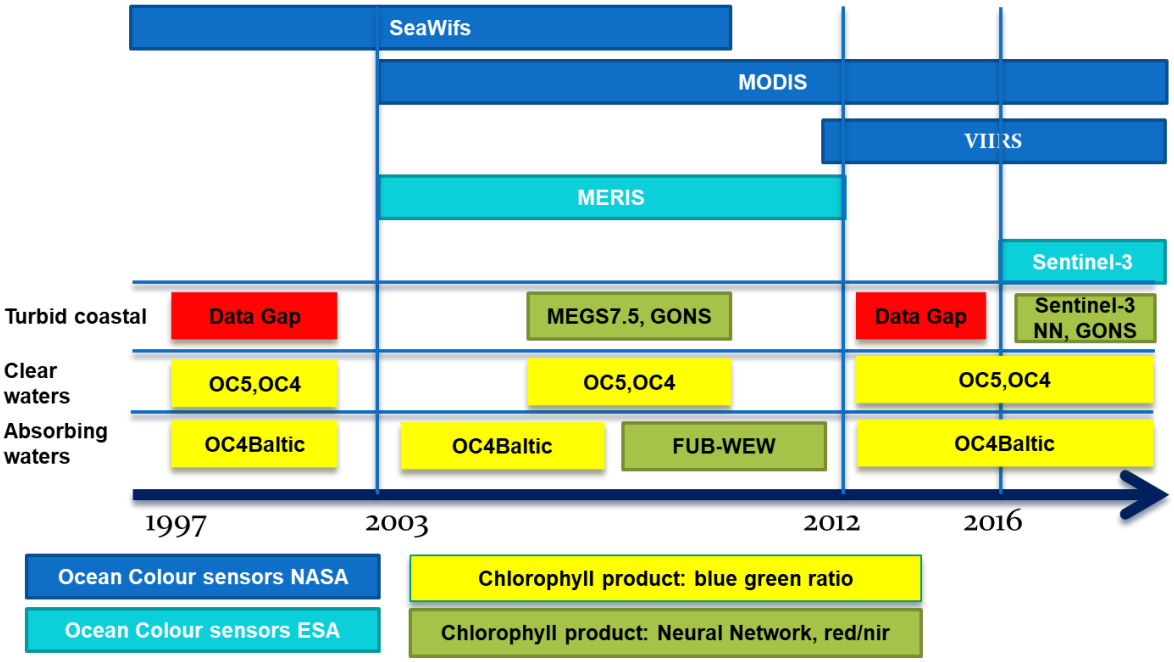

Figure 2.2: CHL product matrix providing an overview of ESA and NASA's ocean colour satellites and different CHL products. Based on literature, the optimal CHL product is linked to its appropriate water type (turbid, clear or absorbing waters). For turbid coastal waters, there are data gaps for non-MERIS periods as the neural net or GONS CHL products are not available for NASA's sensors due to the missing of the 709nm band.

All data where re-gridded to a regular Equirectangular projection in which longitude and latitude steps are constant resulting in a pixel size of 1km. The square region of interest was set to a longitude of 8°W to 13°E and latitude of 48°N to 65°N. The region of interest is shown in figure 2.3 illustrating product 2.1 for April 2010.

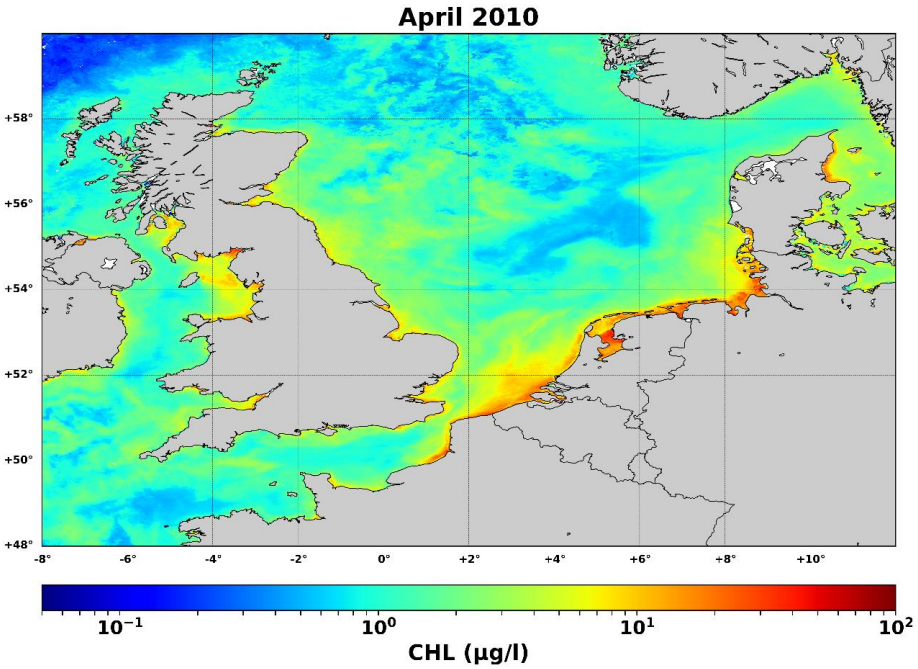

Figure 2.3: CHL (mean) map for April 2010 based on the product 2.1 (table 2.2) demonstrating the JMP-EUNOSAT region of interest.

2.3. Quality control protocol for satellite CHL products

We propose to define simple application rules for four complementary CHL algorithms: the classic empirical blue-green bands ratio algorithm (OC4, O'Reilly et al., 1998) and the adapted OC4 for Baltic waters (Pitarch et al., 2016), the OC5 algorithm (Gohin et al., 2002) and finally the Gons (1999) semi-analytic algorithm. OC4 algorithm is an empirical blue-green band ratio algorithm with a blue band shift from 443 to 510 when CHL concentration increases. This algorithm is adapted to case 1 waters and its median error was estimated to be around 30% for deep waters at global scale (Bailey and Werdell, 2006). Although, OC4 is generally not adapted to coastal waters, it might be suitable for certain coastal zones with optical water properties close the open ocean. The OC5 algorithm is an empirical algorithm based on Look up Tables (LUTs), it has been designed to correct overestimation effects of typical OC4 algorithm in moderately turbid waters or CDOM contaminated waters with a training dataset located in the Bay of Biscay and the English Channel. OC5 LUTs are based on a triplet of entries: CHL estimation with the OC4 algorithm and normalized water leaving radiances at 412 and 560nm. OC5 LUTs have been originally developed for the SeaWiFS sensors (Gohin et al., 2002) but additional LUTs adapted to other ocean colour sensors (MODIS AQUA, MERIS and OLCI) are available (*Francis Gohin pers. com.).* The Gons (1999) algorithm is based on the NIR-red band ratio (i.e. reflectance bands 705nm and 665nm) which is increasing with CHL content. These types of algorithms are only valid in eutrophic waters where the NIR-red signal is significant enough to not being masked by radiometric noise. Among the variety of NIR-red band ratios algorithms (Moses et al., 2009; Dall-Olmo and Gitelson, 2005; Gitelson et al., 2007; Le et al., 2009), we selected the Gons (1999) version because it is semi-analytical which makes it less dependent to validation datasets that the empirical algorithms.

Previously, Lee et al. (2006) and Park and Ruddick (2010) proposed simple calculations based on reflectance to identify case 1 waters where OC4 algorithm is expected to apply. Lee et al, (2006) calculations are based on the average relationship, observed at global scale, between CHL concentration and particulate suspended matter (SPM hereafter) and between CHL and CDOM which allows to distinguish case 1 from case 2 waters. With another approach, Park et al. (2010) provided a quality control flag for the utilization of MODIS CHL estimations derived from the OC4 algorithm, in turbid waters. To process simultaneously oligotrophic and eutrophic waters, switching algorithms using blue-green and NIR-red bands ratio algorithms have also been proposed (Gons et al., 2008; Smith et al., 2018) for specific regions and water type (i.e. case 1 waters in Smith et al., 2018). However, all these approaches are dependent of a specific region or water properties or are not based on the performances of CHL algorithms (Lee et al., 2006). To our knowledge, there do not exist any simple calculations based on water leaving reflectance to limit the application of main CHL algorithms in any complex waters. This section is attempting to fill this gap by providing conditions of application for OC4, OC4BAL, OC5 and Gons (1999) algorithms based on water leaving reflectance.

An in situ/satellite matchups dataset was produced using MEdium Resolution Imaging Spectrometer (MERIS; Rast et al., 1999) reflectances. MERIS was operational from March 2002 to May 2012 which allows the production of a consequent matchups dataset. In addition, its spectral characteristics are very close to the Ocean and Land Colour Instrument (OLCI, Nieke et al., 2012) onboard Sentinel 3 A and B launched in February 2016 and in April 2018 respectively. Then, results presented here aim to be applied on OLCI data.

After the presentation of the data used, the methodology to determinate reflectance conditions for which OC4, OC4Bal, OC5 and GONS algorithms should be applied is presented. Results present the performances of the algorithms before and after quality control as well as the conditions of application themselves. Finally, the best combination of OC4, OC5 and Gons (1999) algorithms is discussed to produce multi-algorithms satellite CHL products and examples of applications on MERIS and OLCI are presented.

No additional quality controls were performed on the MEGS7.5 and FUB CHL products as these neural networks already provide quality flags which were applied.

2.3.1. *In situ data for algorithm investigation (Match-up data)*

A total of 235 situ CHL and MERIS matchups were extracted from the MERMAID database (http://mermaid.acri.fr/home/home.php) from the MEGS 8.1 processing at reduced resolution (RR). In situ CHL was mostly determined with HPLC technique (95%) otherwise with spectrophotometry (5%). The CHL in situ database was completed with measurements published in the Coast Colour Round Robin (CCRR) dataset (Nechad et al., 2015). CCRR database gather in situ optical and biogeochemical data from different coastal regions over the world. All in situ CHL data were extracted and MERIS matchups were extracted from Reduced resolution MEGS8.0 level 2 products downloaded on ODESA platform (http://www.odesa-info.eu/info/). In the CCRR dataset, CHL estimations were derived from fluorometry technique (57%) and HPLC (43%). For the MERMAID and CCRR datasets, MERIS matchups were acquired within a time window of +/- 2.5 hours and resulting values were computed as the median of 9 pixels around the location of the in-situ measurements. Data was accepted if at least 3 valid pixels were available. Then, a final quality control was applied on data to remove data points with negative reflectance values at 443nm. The final dataset included 348 CHL/MERIS matchups from July 2002 to July 2011 with a global spatial distribution with a higher density in the North Sea (Figure 2.4). 235 points came from the MERMAID dataset and 113 points from the CCRR dataset. In the whole dataset, in situ CHL measurements range from 0.05 mg m^{-3} to 31 mg m^{-3}.

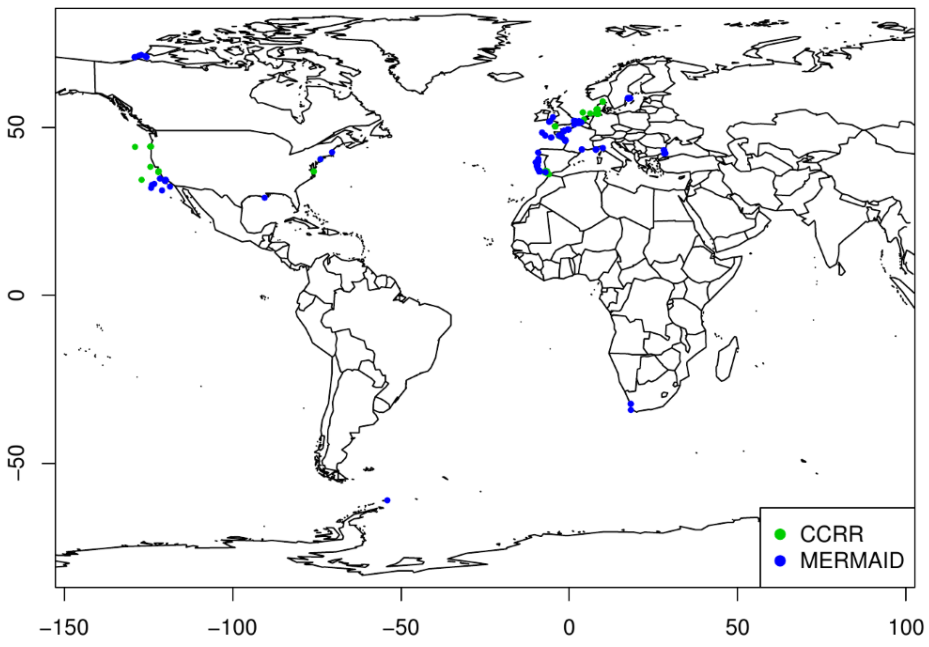

Figure 2.4: Spatial distribution of the in situ CHL observations with a MERIS matchup in the CCRR-MERMAID dataset

From MERIS reflectances, CHL estimations were computed from MERIS dedicated algorithms. The OC4 blue green band ratio algorithm was computed with factors given by Morel and Antoine (2011). The MERIS adaptation proposed by Gons et al. (2002) was used for the NIR-red band ratio algorithm from Gons (1999) and specific MERIS LUTs were used to compute OC5 CHL (Gohin et al., 2002; Gohin and Stanev, 2011). Algorithms are described in the Table 2.3. In the following, CHL estimations from the previous algorithms will be referred as CHL_OC4, CHL_NIR-red and CHL_OC5 respectively.

Table 2.3: Description of the three CHL algorithms considered in this study.

algorithm	reference	description
OC4	Morel and Antoine (2011)	$Chla = 10^{(a+bR+cR^2+dR^3+eR^4)}$ where $R = log_{10}\left(max\left(\frac{\rho_w 443}{\rho_w 560}, \frac{\rho_w 490}{\rho_w 560}, \frac{\rho_w 510}{\rho_w 560}\right)\right)$ $a = 0.4502748, b = -3.259491, c = 3.52271,$ $d = -3.359422, e = 0.949586$
OC5	Gohin et al., (2002)	CHL is a function of CHL_OC4, ρ_w412 and ρ_w560. Specific OC5 LUTS for MERIS where provided by F. Gohin.
NIR-red band ratio	Gons et al., (2002)	$Chla = \frac{1}{0.0146} \cdot \frac{\rho_w 665}{\rho_w 709} \cdot (0.827 + b_b) - 0.429 - {b_b}^{1.06}$ $b_b = \frac{1.61 \cdot \rho_w 779}{(0.082 - 0.6 \cdot \rho_w 779)}$

2.3.2. *Assessment of satellite CHL estimations*

Following recommendations of Baileys and Werdell (2006) satellite CHL estimations was assessed against in situ data with the metrics listed below:

- The median ratio (MR hereafter) is defined as

$$MR = median\left(\frac{Chl\text{-}a_{sat}}{Chl\text{-}a_{situ}}\right) \qquad \text{Equation (2.1)}$$

This metrics allow to measure a potential bias in the CHL estimation. If satellite estimations overestimate CHL concentration MR will be significantly higher than 1, if CHL concentrations are underestimated MR will be significantly lower than 1.

- The semi-interquartile range (SIQR) of the satellite to in situ ratio measures the uncertainty of the data. It is calculated via:

$$SIQR = \frac{Q_3 - Q_1}{2} \qquad \text{Equation (2.2)}$$

Where Q_3 and Q_1 are the third and first quartile of the satellite to in situ CHL ratios.

- The median absolute percent difference (MAPD) indicates the median relative error in percentage. It is computed via

$$MAPD = median\left(100 \times \frac{|Chl\text{-}a_{sat} - Chl\text{-}a_{situ}|}{Chl\text{-}a_{situ}}\right) \qquad \text{Equation (2.3)}$$

2.3.3. Conditions of applicability for OC4 and OC5

ee et al., (2006) have shown that pixels from ocean colour images can be identified as case 1 waters where CDOM and SPM concentrations are functions of CHL concentration. Indeed, CHL can be approximated with the green – blue band ratio (ρ_w560/ρ_w490, named R53 hereafter) and SPM by the reflectance at 560nm (ρ_w560, named R5 hereafter). CDOM is inversely related to the band ratio ρ_w412/ρ_w443 (named R12 hereafter). Hence, in case 1 waters, R12 and R5 are functions of R53 which is the proxy for CHL. To define the average case 1 water relationship between R12 and R53 and between R5 and R53, Lee et al., (2006) considered all pixels of the global ocean and computed a 3-degree polynomial linear regression. All pixels deviating by more than 10% from the average model were considered as case 2 waters. In practice most of the case 2 pixels could be explained by a high CDOM content compared to CHL with points below the minus 10% limit of the R12 and R53 model and/or by high SPM content compared to CHL concentration with points above the plus 10% limit of the R5 and R53 model.

Here we present an approach to determine the applicability of blue-green ratio algorithms (i.e. OC4 and OC5) in case 2 waters by detecting their limits in delivering accurate CHL estimates (APD ≤ 50%) in high SPM and CDOM conditions. The method used is similar to the one proposed by Lee et al. (2006). First, the average model between R12 and R53 (i.e. CDOM limit) and between $\log_{10}$(R5) and R53 (i.e. SPM limit) is computed from data points having a low error (APD ≤ 50%) using a 2-degree polynomial linear regression. The logarithm transformation has been used on reflectance data, but not on reflectance ratios, to better fit with the normal distribution requirements of the linear regression. Two average models for each of the OC4 and OC5 algorithms are then obtained. They have the following form:

$$(R12)_{OC4_{model}} = a + b(R53) + c(R53)^2 = M_{R12_{OC4}}(R53) \qquad \text{Equation (2.4)}$$

$$log_{10}(R5)_{OC4_{model}} = a + b(R53) + c(R53)^2 = M_{logR5_{OC4}}(R53) \qquad \text{Equation (2.5)}$$

$$(R12)_{OC5_{model}} = a + b(R53) + c(R53)^2 = M_{R12_{OC4}}(R53) \qquad \text{Equation (2.6)}$$

$$log_{10}(R5)_{OC5_{model}} = a + b(R53) + c(R53)^2 = M_{logR5_{OC5}}(R53) \qquad \text{Equation (2.7)}$$

Next, the model limits for R12 were determined where high CDOM concentrations are suspected which are expected to result in CHL estimates using OC4 and OC5 with APD > 50%. Similarly, the model limits for $\log_{10}$(R5) are determined where high SPM concentrations are suspected and OC4 or OC5 are not able to provide accurate CHL estimates. These limits are defined as a function of root mean square error (RMSE) such as

$$l_{R12_{OC4}} = M_{R12_{OC4}}(R53) - x_1.RMSE_{R12_{OC4}} \qquad \text{Equation (2.8)}$$

$$l_{logR5_{OC4}} = M_{logR5_{OC4}}(R53) + x_2.RMSE_{logR5_{OC4}} \qquad \text{Equation (2.9)}$$

$$l_{R12_{OC5}} = M_{R12_{OC5}}(R53) - x_3.RMSE_{R12_{OC5}} \qquad \text{Equation (2.10)}$$

$$l_{logR5_{OC5}} = M_{logR5_{OC5}}(R53) + x_4.RMSE_{logR5_{OC5}} \qquad \text{Equation (2.11)}$$

The values of x_1, x_2, x_3 and x_4 were determined by maximizing a cost function which attributes positive points to "good" data points (i.e. low error) and negative points to "bad" data points (i.e. high error) (see Section 2.3.5 for details).

These limit functions allow to constrain the utilization of the OC4 and OC5 algorithms to avoid CHL underestimation in case of high SPM or CDOM content. However, these tests only apply to a certain range of CHL values (Lee et al., 2006) and under certain SPM and CDOM conditions. OC4 and OC5 algorithms applies only on oligotrophic waters (Odermatt et al., 2012; Matsusha et al., 2015; Smith et al., 2018). Based on these studies a first test on CHL_OC4 and CHL_OC5 is applied to verify that CHL_OC4 or CHL_OC5 is lower than 10 $g.m^{-3}$. Looking at the scatter plot of R12 as a function of R53 (Figures 2.12 and 2.14), it appears that some CHL estimates characterized by a high R12 band ratio (R12 > 1.25) are underestimated by OC4 and OC5 algorithms. We suspect for these points a failure of the atmospheric correction algorithms as it is expected that the minimum CDOM concentration is observed in case 1 waters. Data points with a R12 band ratio higher than 1.25 are flagged as "possible atmospheric correction error".

Finally, flowchart on figure 2.5 shows the successive tests applied to each data point to decide if OC4 or OC5 algorithm should be applied on each pixel.

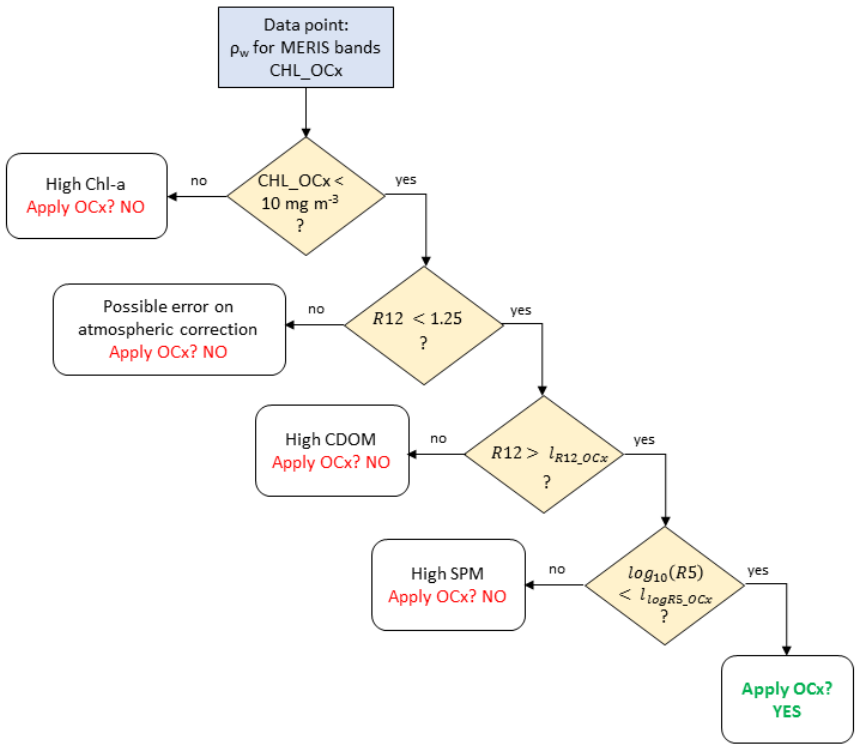

Figure 2.5: Flow chart showing the different steps driving to a decision of application of the OC4 or OC5 algorithms. The expression "OCx" in the chart should be replaced by "OC4" or "OC5".

2.3.4. Conditions of applicability for red-NIR algorithm (Gons)

NIR-red band ratio algorithm is based on the CHL signal in the red-NIR region of the reflectance spectra. This signal is marked by a reflectance minimum at 662 nm followed by a reflectance maximum around 700 nm (Ruddick et al., 2001). This pattern is due to the combined effect of CHL absorption at 662 nm and scattering in the red-NIR region of the spectrum. It is clearly observed in eutrophic and turbid waters but in oligotrophic waters, water leavings reflectances are generally very low and the NIR-red band ratio is strongly affected by radiometric noise driving to very scattered and erroneous CHL estimates (see Figure 2.7, panel C). Hence, decision of application of the Gons et al., 2002 algorithm was based on the CHL and turbidity levels. As for low to mid CHL concentrations, OC4 algorithm is more reliable than NIR-red band ratio algorithm (compare Figure 2.7 panels A and C), CHL_OC4 was used as a proxy of CHL concentration and water leaving reflectance at 620nm (ρ_w620, R6 hereafter) was used as a proxy of turbidity. Then, optimal CHL_OC4 and R6 thresholds were determined by maximizing the same cost function as for OC4 and OC5 algorithms (see Section 2.3.5 for details). These thresholds are named $l_{CHL/red\text{-}NIR}$ and $l_{R6/red\text{-}NIR}$. When CHL_OC4 is higher than $l_{CHL/red\text{-}NIR}$ and when R6 is higher than $l_{R6/red\text{-}NIR}$, red-NIR algorithm can be applied. Finally, an additional check is done to verify that the CHL_red-NIR estimate is at least higher than 2 mg m^{-3}. Figure 2.6 represents the different steps which drive to the application of the NIR-red band ratio algorithm.

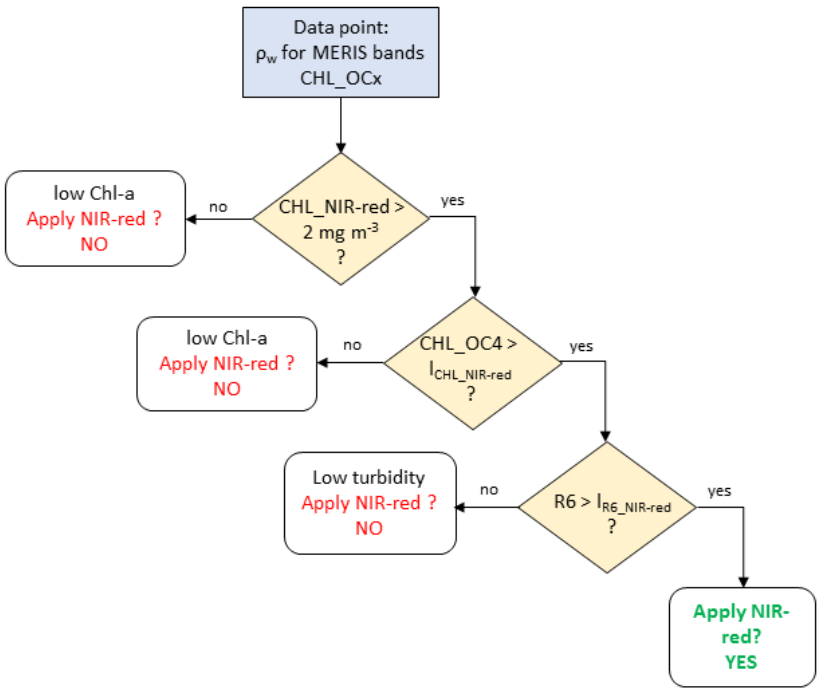

Figure 2.6: Flow chart showing the different steps driving to a decision of application of the NIR-red Gons et al., (2002) algorithm.

2.3.5. Successive sampling

The initial dataset of 348 data points has been randomly divided into two datasets of 174 data points. The first dataset is used to compute the limits of application of the OC4, OC5 and NIR-red band ratio algorithms and the second dataset was used to validate the performances of the selection algorithm developed.

Performances are assessed by comparing the performance of the OC4, OC5 and NIR-red band ratio algorithms when all the points of the validation dataset are considered and the performances of the same CHL algorithms when only points corresponding to the newly developed criteria of selection are considered.

This step of dataset division, training and validation was repeated 100 times resulting in different training and validation datasets. Finally, the median results of the 100 repetitions were used as to define the final selection criteria as reported in Table 2.4.

Table 2.4: List of coefficients necessary to compute l_{R12_OC4}, l_{R12_OC5}, l_{logR5_OC4} and l_{logR5_OC5} and apply algorithm selection methodology presented on Figure 2.7. Note that for the NIR-red_Gons algorithm (Figure 2.7c) $l_{CHL\_NIR\text{-}red}$ = 8.5 mg m^{-3} and $l_{R6\_NIR\text{-}red}$=0.0081.

Model	a	b	c	x	RMSE
M_{R12_OC4}	1.043	-0.226	0.056	0.3	0.212
M_{logR5_OC4}	-2.588	0.676	-0.117	0.4	0.205
M_{R12_OC5}	1.014	-0.079	-0.123	2.1	0.247
M_{logR5_OC5}	-2.624	0.787	-0.125	1.3	0.239

2.3.6. Determination of limit values

To determine the best position of the different limits (l_{R12_OC4}, l_{logR5_OC4}, l_{R12_OC5}, l_{LOGR5_OC5}, $l_{CHL/red\text{-}NIR}$ and $l_{R6/red\text{-}NIR}$), a cost function is defined. This function is defined as

$$CF = \sum_i y_i \text{ with } \begin{cases} y_i = +5 if\, APD_i \leq 30 \\ y_i = +2 if 30 < APD_i \leq 50 \\ y_i = -2 if 50 < APD_i \leq 100 \\ y_i = -5 if\, APD_i > 100 \end{cases}$$ Equation 2.12

i stands for any point in the selection data set. Criteria of selection changes for each algorithm. For the OC4 and OC5 algorithms, the point *i* is in the selection if $R12_i > l_{R12\_OCx}$ and $log10(R5_i) < l_{logR5\_OCx}$. For the NIR-red band ratio algorithm, the point i is in the selection if $CHL\_OC4_i > l_{CHL\_NIR\text{-}red}$ and $R6_i > l_{R6\_NIR\text{-}red}$. APD is the absolute percent difference and is defined as

$$APD = 100 \left| \frac{Chla_{sat} - Chla_{situ}}{Chla_{situ}} \right|$$ Equation 2.13

CF is then defined to increase with the number of "good points" (APD < 50%) in the selection but to decrease with the number of "bad points" in the selection (APD > 50%). By attempting to maximize CF, we look for the best compromise between including the largest number of "good points" in the selection while avoiding "bad points". CF is then computed for a large range of values for each limit. In case of OC4 and

OC5 algorithms, limits value depends of variables x_1, x_2, x_3 and x_4 (see Equations 2.8 to 2.11) and CF is computed for x_1, x_2, x_3 and x_4 ranging between 0 and 5 by step of 0.1. In case of the NIR-red band ratio algorithm, CF is computed for $I_{CHL\_NIR\text{-}red}$ ranging between 0.5 and 50 by step of 0.1 and for $I_{R6\_NIR\text{-}red}$ ranging between 10^{-4} and 10^{-2} by step of 10^{-1}. Then, final limits are defined with the x_1, x_2, x_3, x_4, $I_{CHL\_NIR\text{-}red}$ and $I_{R6\_NIR\text{-}red}$ values which maximize CF.

2.3.7. Performance of CHL algorithms on the CCRR-MERMAID dataset

OC4, OC5 and NIR-red band ratio algorithms have been tested against the whole CCRR/MERMAID dataset (Figure 2.7, Table 2.3). Results show the OC5 algorithm performs the best with a median error of 39% and a slight overestimation (median ratio = 1.17). Most of the points are close to the 1:1 line and uncertainty is estimated with RMSE to be 2.36 mg m^{-3}. OC4 algorithm clearly tends to overestimate CHL concentration as most of the points are above the 1:1 line and the median ratio is 1.92. MAPD is 92.0% far from its performances in case 1 waters (i.e. 30%, Baileys and Werdell, 2006) and the distribution is rather scattered (RMSE = 9.33 mg m^{-3}). These results confirmed the previously observed tendency of the OC4 algorithm to overestimate CHL concentration in coastal waters (Tilstone et al, 2017) and as expected, OC5 algorithm tends to correct this overestimation. A saturation effect for high CHL values was expected by OC4 and OC5 algorithms (Matsushita et al., 2015) but not observed. This might be due to the weak representation of eutrophic waters in our dataset (in the dataset CHL ranges from 0.05 mg m^{-3} to 31 mg m^{-3} only).

The NIR-red algorithm (Gons et al., 2002) performances confirm expected patterns with highly scattered and erroneous CHL estimates for low to moderate CHL values (CHL < 10 mg m^{-3}). In fact, only high in situ CHL values have satellite estimates along the 1:1 line.

The moderate to bad performances of the OC5, OC4 and NIR-red band ratio algorithms on the whole coastal dataset stressed the necessity to define a quality control for each of these algorithms and to avoid their utilization when it is not appropriate.

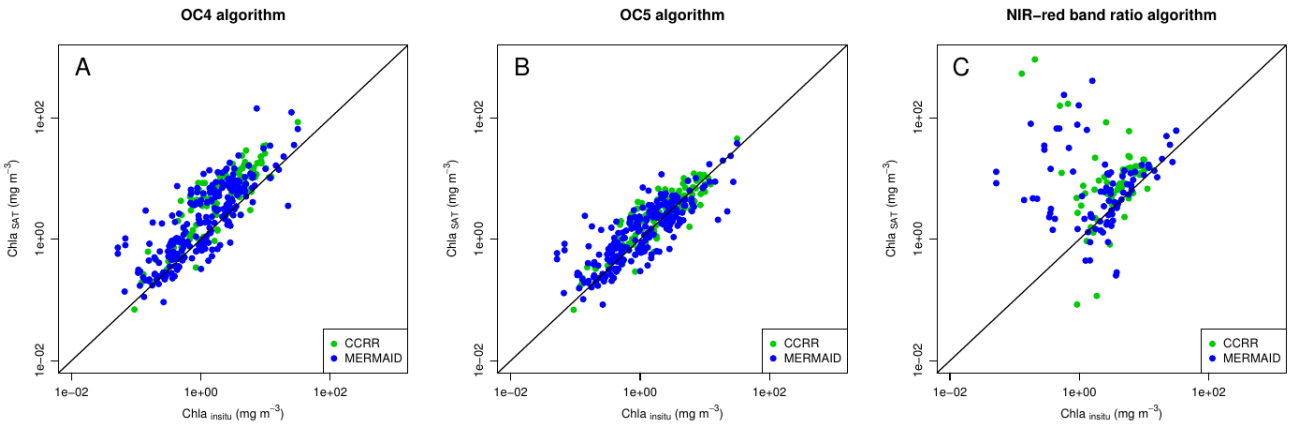

Figure 2.7: in situ CHL as a function of CHL computed from MERIS reflectance with OC4 (panel A), OC5 (panel B) and NIR-red band ratio algorithm (panel C).

2.3.8. Quality control for OC4 algorithm

Figure 2.8 shows the distribution of R53, a proxy of CHL, as a function of R12, inversely related to CDOM (panel A) and of R53 as a function of ρ_w560, a proxy of SPM (panel B). For each point, the relative error

which is measured with the percent difference between the OC4 estimation and the in-situ measurement is indicated with a colour code. Results show that low R12 and high ρ_w560 values at constant R53 value tend to drive to an overestimation of CHL by the OC4 algorithm (red and orange points). This result is consistent with previous findings which pointed out the CHL overestimation by OC4 algorithm in case of high CDOM or SPM.

The different versions of the M_{R12_OC4} and $M_{logR5OC4}$ models computed on the basis of a half dataset (see Section 2.3.5 and Equations 2.8 and 2.9, solid grey lines on Figure 2.8) are quite close to each other and are well represented with the median model (thick solid black lines figure 2.8). The limits l_{R12_OC4} and l_{logR5_OC4} under which and above which, respectively, a data point is not selected to be processed with OC4 (dotted lines on Figure 2.8) are quite close to the model lines suggesting that OC4 is only adapted to a narrow range of SPM and CDOM conditions. This drives to the selection of a small percentage (about 25%) of coastal data points to be retained but the performances of the algorithm are significantly improved when applied to the subset (see Figure 2.9, Table 2.2). Figure 2.9 show the distribution of each performance metrics when applied to the whole validation dataset (blue boxplots) and when applied to selected subsamples after application of the OC4 quality control (yellow boxplots). For the OC4 algorithm (top panels on Figure 2.8), the boxplot comparison shows a clear improvement of all metrics when the quality control is applied to OC4. When the quality control (coefficients are given in Table 2.4) is applied to the whole CCRR-MERMAID dataset, only 92 data points (26%) are selected but the OC4 performance are much higher and comparable to the one observed in the training-validation phase and displayed on Figure 2.8. These performances reach also the levels expected of a remote sensing CHL algorithm.

Table 2.6: Performances of the OC4, OC5 and NIR-red band ratio algorithm when they are tested against the whole dataset and when they are tested only against the selected data points (referred with the "QC" mention).

	N	MR	SIQR	MAPD	slope	intercept	RMSE	r^2
OC4	348	1.92	1.12	92.0%	2.15	0.73	9.33	0.47
OC5	346	1.17	0.50	39.1%	0.85	0.59	2.36	0.69
NIR-red	348	-0.90	17.1	420%	4.92	-37.80	156.2	0.02
OC4 QC	92	1.25	0.42	37.3%	1.23	0.11	1.00	0.73
OC5 QC	231	1.09	0.44	31.9%	0.63	0.86	1.44	0.62
NIR-red QC	44	1.17	0.34	39.5%	0.92	1.34	5.22	0.65
Merged	259	1.25	0.46	34.9%	1.34	-0.15	3.02	0.79

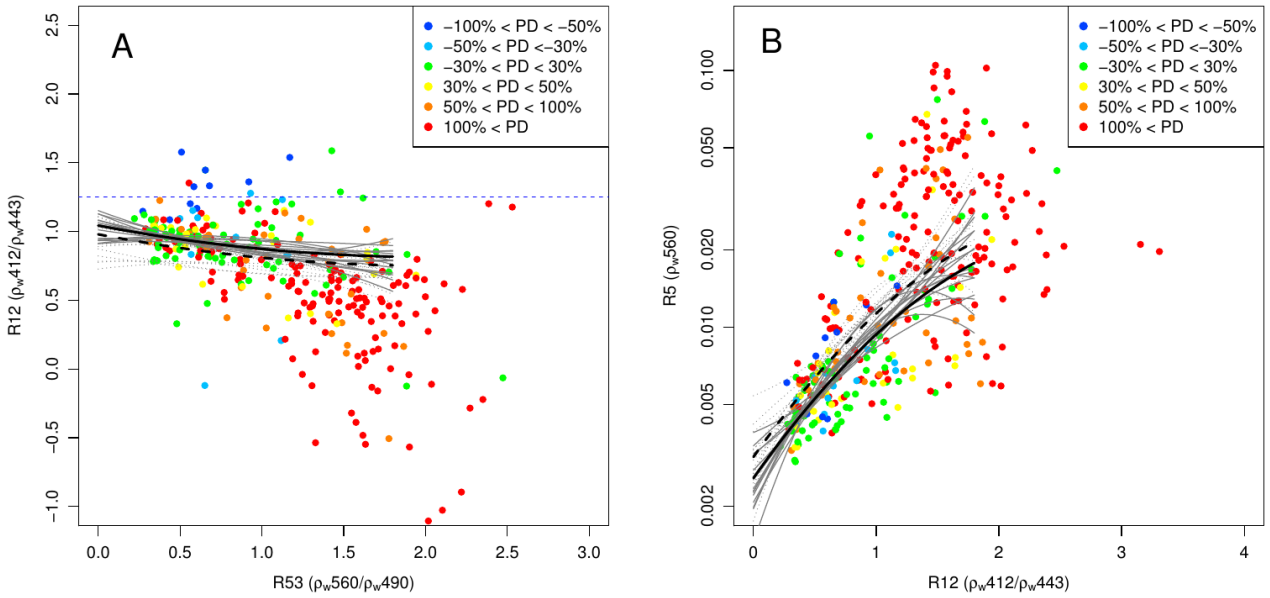

Figure 2.8: R12 as a function of R53 (panel A) and R5 as a function of R12 (panel B). Color of dots refers to the error (percent difference, PD) of the OC4 algorithm compared to in situ measurements. Grey lines show 20 examples of models (solid lines, M_{R12_OC4}, panel A and $M_{logR5OC4}$ panel B) and limits (dotted lines, l_{R12_OC4} panel A and l_{logR5_OC4} panel B) computed from a random training dataset (50% of the whole dataset, see Section 2.3.5 for details). Thick black solid and dotted lines show the final model and limits. In panel A, dotted blue line show the upper limit (R12=1.25) of the R12 variable. Coefficients are given in Table 2.3.

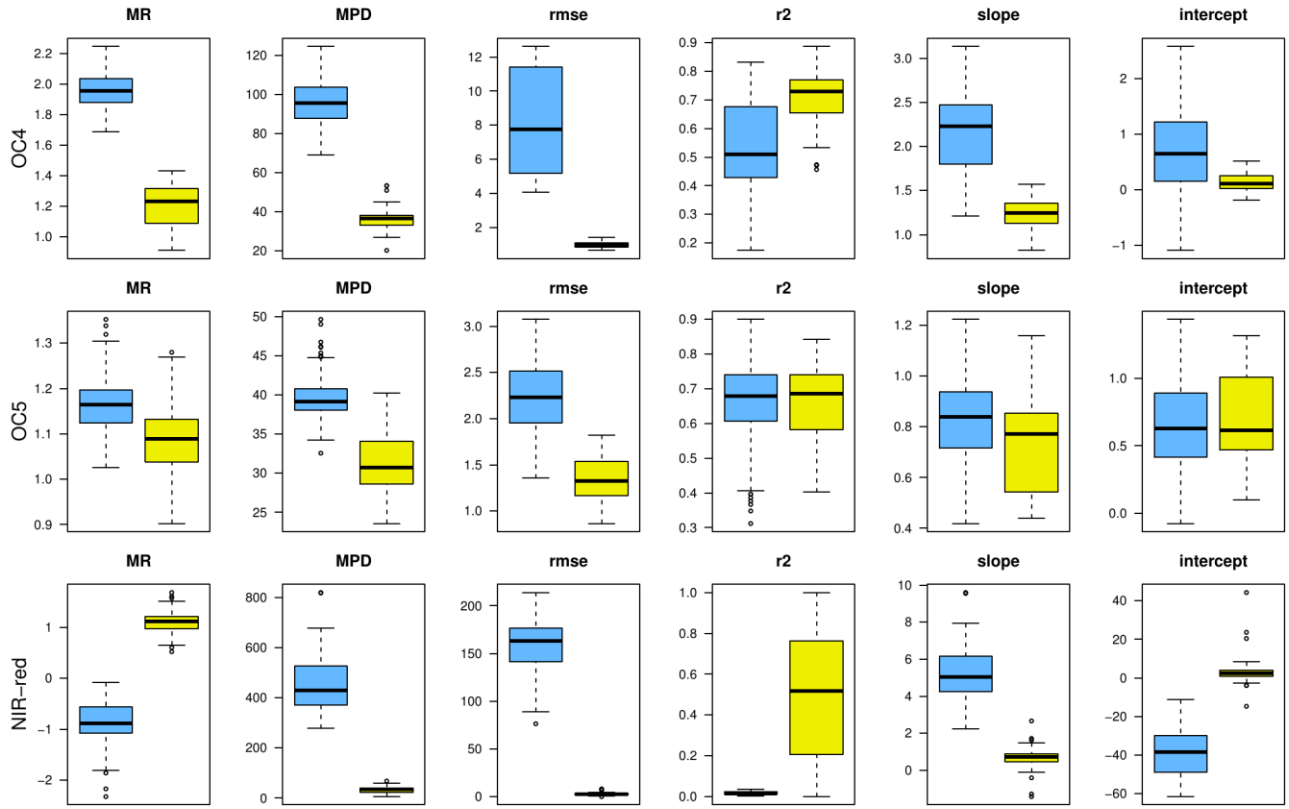

Figure 2.9: Box-plots comparing the performances of the OC4 (top panels), OC5 (middle panels) and NIR-red band ratio (bottom panels) algorithms on the full validation dataset (blue-boxplots, 50% of the whole CCRR-MERMAID dataset randomly selected) to the subset of points selected to application of the algorithm (yellow box-plots).

2.3.9. Quality control for OC5 algorithm

Figure 2.10 shows that the OC5 algorithm performs for a wider range of R12 and ρ_w560 at constant R53 than OC4. Green points are sparser on Figure 2.10 than on Figure 2.8 and the limit curves: lR12_OC5 and llogR_OC5 are further from MR12_OC5 and Mlog5_OC5 than it is the case with the OC4 algorithm on Figure 2.8, confirming that OC5 performs well for a larger range of CDOM and SPM values than OC4. Nevertheless, it appears that for very low R12 and high ρ_w560 values, OC5 tends to overestimate CHL which shows the necessity to also constrain OC5 algorithm.

Regarding performances with and without quality control, Figure 2.9 shows that the quality control allows to reduce the OC5 positive bias (MR is reduced), as well as the uncertainty (RMSE reduced) and the relative error. In fact, for most of the simulations MDP ranges between 28% and 35% against 38% to 41% when OC5 is applied to the whole validation dataset. Only r^2, the coefficient of determination of the linear regression between in situ and satellite estimates, as well as the slope and the intercept of the linear model doesn't really improve after applying the quality control. This effect can be explained by the fact that the CHL range is slightly reduced (all points with CHL_OC5 > 10 mg m^{-3} are eliminated). Overall, the performances of the 100 repetitions in the training-validation phase are in agreement with the performance of the OC5 algorithm with quality control (coefficients given in Table 2.3) tested over the whole CCRR-MERMAID dataset (Table 2).

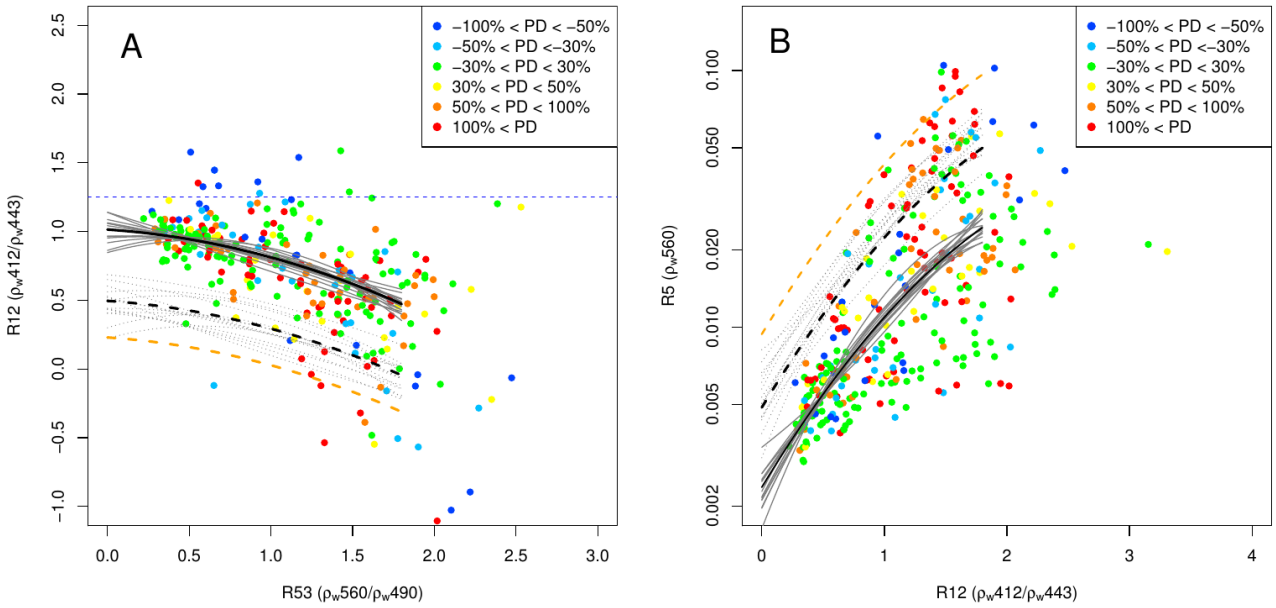

Figure 2.14: R12 as a function of R53 (panel A) and R5 as a function of R12 (panel B). Color of dots refers to the error (percent difference, PD) of the OC5 algorithm compared to in situ measurements. Grey lines show 20 examples of models (solid lines, M_{R12_OC4}, panel A and $M_{logR5OC4}$ panel B) and limits (dotted lines, l_{R12_OC4} panel A and l_{logR5_OC4} panel B) computed from a random training dataset (50% of the whole dataset, see Section 2.3.5 for details). Thick black solid and dotted lines show the final model and limits. In panel A, dotted blue line show the upper limit (R12=1.25) of the R12 variable. Coefficients are given in Table 2.4. Orange dotted lines represent the limits of application of the OC5 algorithm in case of extended utilisation of the algorithm (see Section 2.3.12)

2.3.10. Quality control for red-NIR ratio algorithm

Figure 2.11 shows the distribution of CHL_OC4 as a function ρ_w620 with a colour code indicating the performance of the NIR-red band ratio algorithm for each point. For low CHL_OC4 values (CHL_OC4 < 5 mg m^{-3}) and low ρ_w620 values ($\rho_w620 < 0.002$), NIR-red algorithm is failing for almost all points with generally a strong underestimation (dark blue points) or a strong overestimation (red points). It clearly appears that a certain threshold for CHL_OC4 and ρ_w620 is necessary to obtain accurate estimates of CHL by this algorithm. In most of the 100 simulations performed, these thresholds calculated on a randomly defined training dataset (50% of the CCRR-MERMAID dataset) ranges between 7.5 mg m^{-3} and 12 mg m^{-3} for CHL and between 0.007 and 0.0085 for ρ_w620. The final threshold defined as the median of the 100 simulations are 8.5 mg m^{-3} for CHL_OC4 and 0.0081 for ρ_w620. Given the very poor performances of the NIR-red band ratio algorithm when applied to the whole CCRR-MERMAID dataset the selection algorithm clearly improves the NIR-red band ratio algorithm performance. With data selection, algorithm is almost unbiased (MR ranges between 0.97 and 1.2) and the median error reaches acceptable values (MPD ranges between 23% and 40%). The linear regression model between in situ and satellite values is also close to 1:1 line with a coefficient of determination mostly ranging between 0.20 and 0.76 for the different simulations. In comparison to OC4 and OC5, the algorithm's uncertainty measured with RMSE is higher with most of the RMSE values ranging between 2.3 and 3.4 mg m^{-3}. This specificity can be explained by the fact that NIR-red band ratio algorithm applies for high ranges of CHL concentrations driving to a higher uncertainty in absolute values. Finally, the performance of the red-NIR algorithm with the quality control is in agreement with the performances of the red-NIR algorithm performances of the 100 repetitions in the training-validation phase and shown on Figure 2.9 (bottom panels).

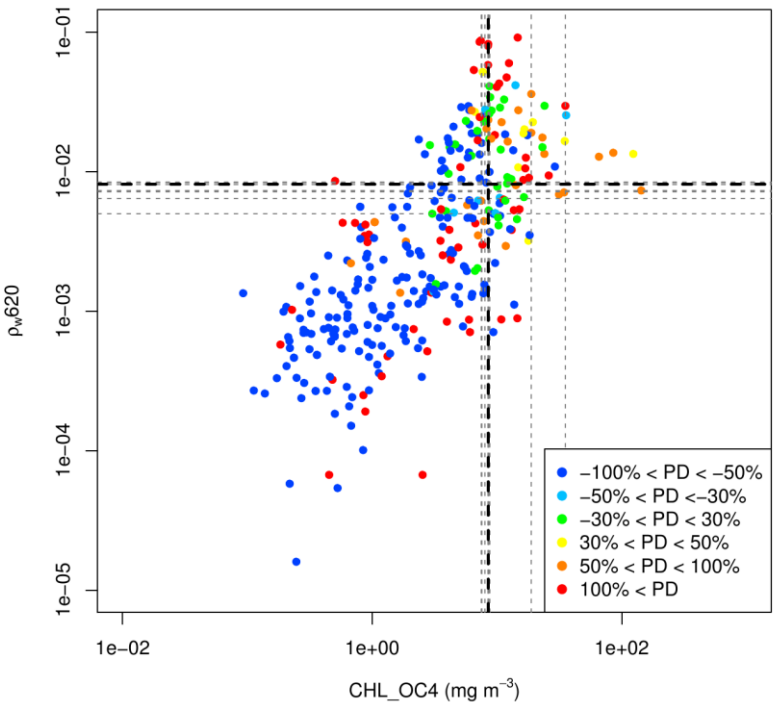

Figure 2.11: ρ_w620 as a function of CHL_OC4. Color of dots refers to the error (percent difference, PD) of the NIR-red Gons et al. (2002) algorithm compared to in situ measurements. Grey lines show 20 examples of limits for CHL_OC4 (vertical lines) and ρ_w620 (horizontal lines) computed from a random training dataset (50% of the CCRR-MERMAID dataset). Thick black dotted lines show the final limits lines.

2.3.11. Quality control for OC4_Bal algorithm

The algorithm developed by Pitarch et al. (2016) for Baltic Sea (named OC4_BAL hereafter) was also tested with CCRR-MERMAID database. Although this algorithm was developed for SeaWiFS sensor, it was tested against the MERIS MEGS8.1 database. As, there is only a 1% difference between reflectance at 555 nm (SeaWiFS band) and at 560 nm (MERIS bands ,Melin and Sclep, 2015) results were not significantly impacted by band shifting. Results on Figure 2.12 show that OC4_BAL underestimates CHL concentration when CHL is lower than 1 mg m-3. The same methodology as the one applied to OC4 and OC5 algorithms was applied to OC4_BAL results (Figure 2.13) show that there is no clear impact of reflectance at 560nm and only a limit based on R12 (proxy of CDOM) could be developed. Finally, we decided to apply this algorithm only when CHL_OC4_BAL was between 1 and 10 mg m-3 and when R12 was upper the limit (dotted line on Figure 2.13).

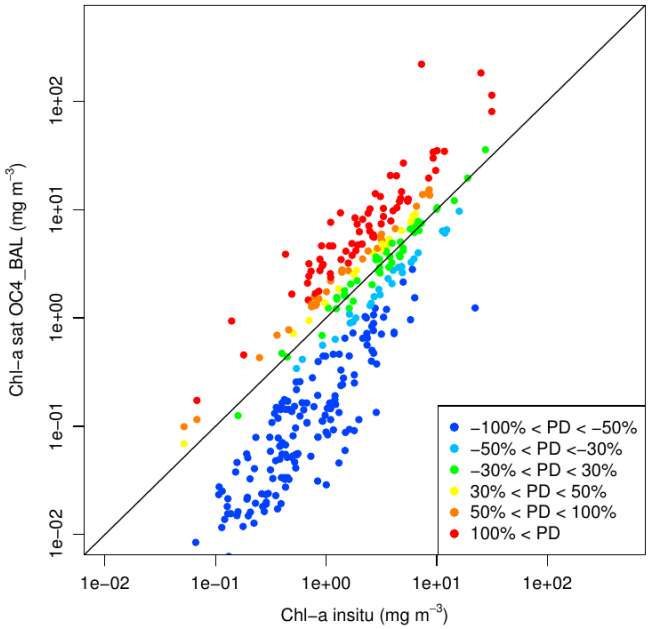

Figure 2.12: CHL in situ as a function of satellite CHL estimation with OC4_BAL algorithm. Color code is for error measured with the percent difference between in situ observation and satellite estimation.

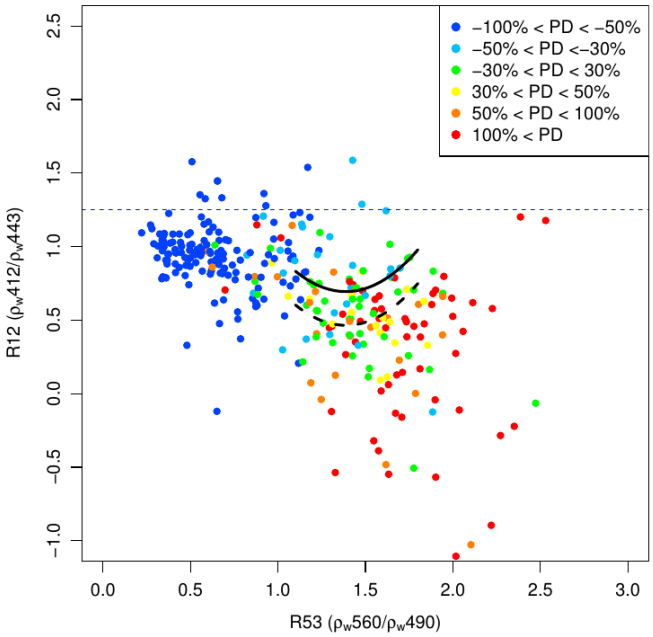

Figure 2.13: R12 as a function of R53. Color code indicates the percentage error of the OC_BAL algorithm in estimation CHL. Solid line is the average model when only low error points are considered (APD < 50%) and the dotted line is lower limit of application of the OC4_BAL algorithm.

2.3.12. *Best algorithm combination and limits of used dataset*

This section presents conditions of application to determine if OC4, OC4_Bal, OC5 and NIR-red_Gons algorithms should be applied on a pixel basis. Each algorithm has its own rules which are independent of the other algorithm performances. So, it happens that a certain pixel can be processed by two algorithms or by none algorithm. In fact, all points which validate conditions of application of the OC4 algorithm also validate the OC5 algorithm and in the CCRR-MERMAID dataset 19 points verified the conditions of application of OC5 and NIR-red_Gons algorithms. To determine how to handle these particular cases we tested on the intersection subsets the performances of each algorithm which applies as well as their average. Results are presented in table 2.7 (OC4/OC5) and table 2.8 (OC5/NIR-red_Gons). For the OC4/OC5 intersection, results show that OC4 still tends to overestimate CHL (MR=1.25) whereas OC5 slightly underestimate CHL (MR=0.92). OC5 presents the best MAPD but it seems that the linear model is slightly better with OC4. Finally, the point by point average of OC4 and OC5 CHL estimations presents interesting results with almost no bias (MR=1.05), a MAPD less than 30% and a linear model very close to the 1:1 line. Regarding the OC5 and NIR-red band ratio algorithms, OC5 presents better results regarding the accuracy of the CHL estimation (see MR and MAPD on Table 2.8) but the linear regression model is pretty poor with a slope of 0.17 and a r^2 of 0.19 suggesting that OC5 CHL estimations for this subset of points are rather constant. The average model seems then to be a good option to improve this aspect while keeping acceptable accuracy and uncertainty (MR=1.41 and RMSE=2.67). Hence, we would recommend to apply a point by point average if OC4 and OC5 or OC5 and NIR-red_Gons algorithms are valid for a same in pixel. In addition, this methodology allows to smooth discontinuities that might be produced by an algorithm shift when processing satellite images. Performances of the final algorithm selection and combinations are presented on table 2.6 (line named “merged algorithm”) and figure 2.14.

The process allowed to estimate CHL for 74.4% of the data point. The average error is of 35% and the points are well aligned along the 1:1 line (see Figure 2.14, r^2 of the linear regression = 79%). Most of points (64%) are within the plus or minus 50% error range which can be consider as an acceptable error on CHL estimation in coastal water. The majority of points out of this range present an overestimation of the in situ CHL measurements.

One of the weakness of this methodology for CHL estimation is its ability to estimate CHL in only 74.4% percent of the cases. By applying it on a set of MERIS images we observed that during winter season most of the North Sea could be labelled as "not processed" because of too high SPM levels. To help fixing this point we proposed to extend the conditions of utilization of the OC5 algorithm as this algorithm present the best results on the whole CCRR-MERMAID dataset. Hence, we propose extra extended values for x_3 (extended x_3=3.2) and x_4 (extended x_4=2.5) to define extended limits l_{R12_OC5} and l_{logR5_OC5} respectively (see also the orange dotted lines on Figure 2.10). These values have been chosen on the basis of tests performed on MERIS images and on the properties of the CCRR-MERMAID dataset. On one hand they have to allow to perform most of the images but on the other hand new R12 and ρ_w620 limits has to be in the CCRR-MERMAID dataset range for these variables. These extended OC5 conditions allowed to process 42 additional data points (in grey on the Figure 2.14). These data points present a MAPD of 70% and a significant overestimation. However, it might be interesting in some applications to process the most of the satellite image keeping in mind that for some part of the CHL image, accuracy in lower with possibly an overestimation. Overall, when added to the whole dataset, these additional data points only slightly decrease the performance metrics (compare on Table 2.6, lines named "merged" and "merged / OC5 extended").

Finally, one might wonder on the global benefit of this "complex" algorithm selection method compared to the only utilization of the OC5 algorithm as it shows the best performances compared to OC4 and NIR-red_Gons algorithms. The CCRR-MERMAID dataset represents mostly average coastal water properties and extreme water properties in terms of turbidity, CDOM and CHL are certainly lower-represented in this dataset. As it has been proved that OC5 tends to fail in case of high CDOM or SPM concentrations (see Figure 2.10) or in case of eutrophic waters (Tilstone et al., 2017), it is then important to determine limits of application of this algorithm and to propose alternative algorithms when possible. Whatever the limits: "optimized" or "extended", the future user will be certain to use OC5 within its conditions of application and will be aware of the associate uncertainty. In case of ultra-oligotrophic case 1 waters (CHL < 0.15 mg m^{-3}) which is out of the scope of the paper, we would recommend to future user to switch to the OC4 only algorithm or to the CI approach (Hu, 2012) as it is already performed in several satellite CHL products (i.e. CMEMS product 2.1 in table 2.1)

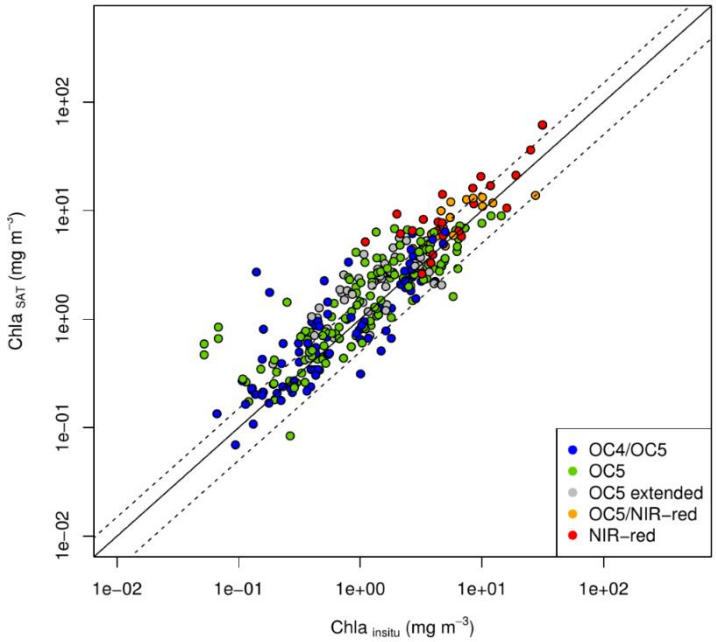

Figure 2.14: In situ CHL observations as a function of satellite CHL estimations after having applied algorithm selections and multi-algorithms merging methodologies presented in this paper. Color code indicates for each point which CHL algorithms has been selected. Dotted lines represent the ±50% error interval.

Table 2.7: Comparison of the performances of the OC4, OC5 and point by point average OC4-OC5 algorithms on the subset of points where OC4 and OC5 apply.

	N	MR	MAPD	slope	intercept	RMSE	r^2
OC4	92	1.25	37.3%	1.23	0.11	1.00	0.73
OC5	92	0.92	27.0%	0.76	0.26	0.66	0.70
average: OC4-OC5	92	1.05	29.4%	1.00	0.185	0.82	0.72

Table 2.8: Comparison of the performances of the OC5, NIR-red band ratio and point by point average OC5 – NIR-red algorithms on the subset of points where OC5 and NIR-red apply.

	N	MR	MAPD	slope	intercept	RMSE	r^2
OC5	19	1.18	34.3%	0.17	5.65	2.07	0.19
NIR-red	19	1.67	66.7%	0.66	5.54	4.12	0.46
average: OC5-NIR-red	19	1.41	44.0%	0.41	5.60	2.67	0.45

2.3.13. Application to MERIS data

Four, clouds free, images of the Atlantic French coast and North Sea have been selected from the MERIS archive to represent different seasons. The developed methodology for CHL algorithm selection has been applied to each image (Figure 2.15) and final CHL maps have been produced (Figure 2.16). Results show that OC5 algorithm is dominant most of the year in this region except for certain locations and periods. Because of high turbidity, the winter image (2008/02/11) shows that CHL concentration can be processed only if extended conditions of the OC5 algorithm are accepted. In addition, some spots flagged as "high SPM" with the OC5 algorithm cannot be processed by none of the three CHL algorithms presented here.

These spots generally correspond to very turbid zones visible on the RGB true color image. In the image of the 2004/05/24, a large area offshore the French Atlantic coast was also flagged as “No algo” surrounding by “OC5 ext”, this spot which occurs during the spring bloom season was identified as a Coccolithophores bloom from the RGB image. Coccolithophores have a calcite envelope which scatters light, affecting standard CHL algorithms and explaining the flag “high SPM” returned by the OC5 test algorithm. OC4 algorithm was only applied in the image of the 2005/09/19 off shore the French Atlantic coast. At this season, main rivers discharge is low and off shore Atlantic waters are expected to be close to case-1 waters. NIR-red band ratio algorithm is applied in very coastal areas: the South Eastern UK coast with the Tames estuary, the Severn estuary on the South Western UK coast and the Belgium and Netherland coasts during spring and summer. These regions correspond to very turbid and eutrophic regions (Ruddick et al., 2003). Although, a few pixels are concerned by the NIR-red band ratio algorithms, they are very important for coastal environment monitoring and eutrophication reporting such as the MSFD. It is then important to process these pixels with the best care. CHL maps (Figure 2.16) shows that CHL ranges between 0.5 and more than 8 mg m^{-3} with highest values along the UK, Belgium and Netherland coast. In the English Channel and central North Sea, CHL is highest in spring and summer with values reaching 3 mg m^{-3} in the English Channel and more than 7 mg m^{3} in the North Sea.

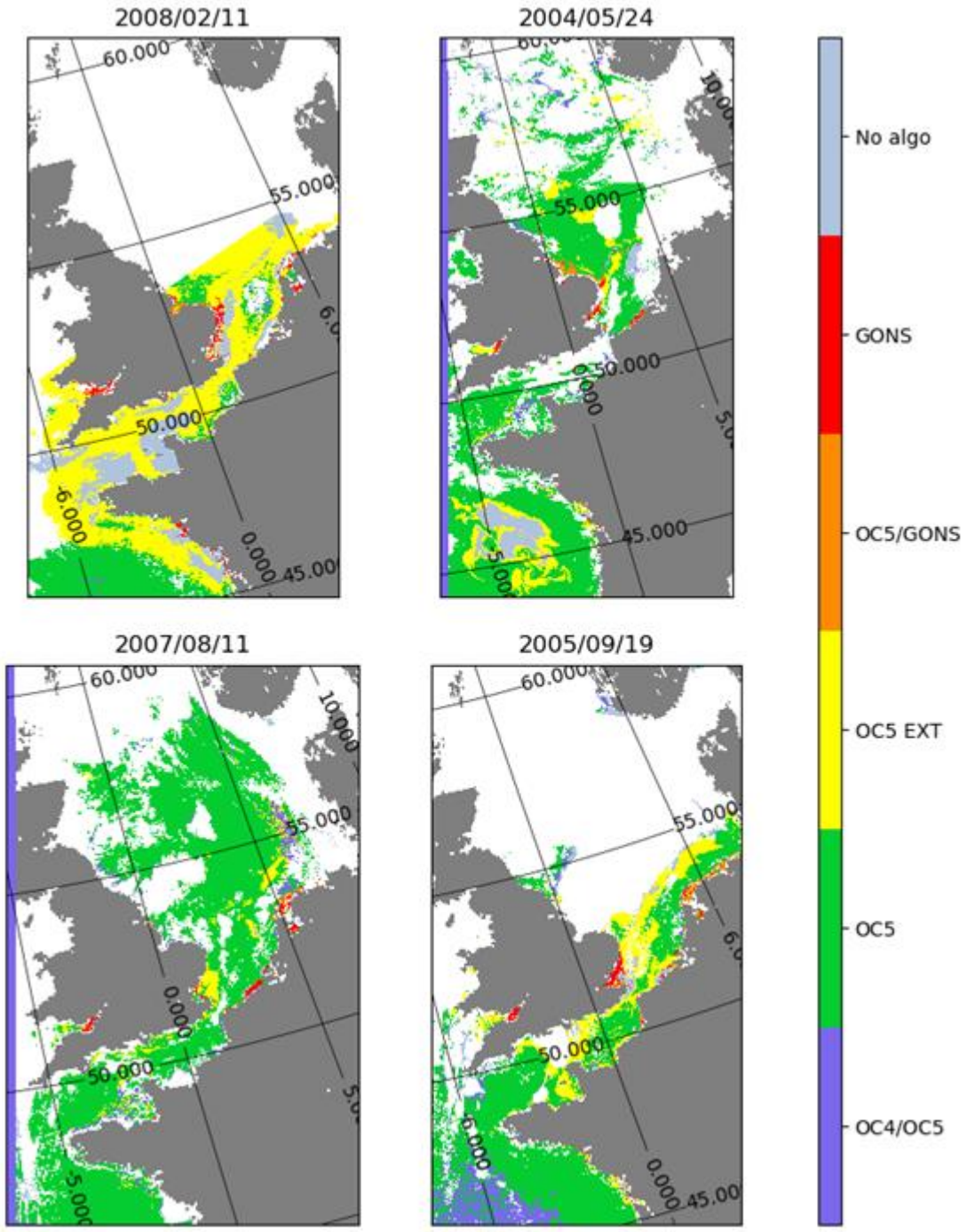

Figure 2.15: Results of application of the CHL algorithm methodology developed in this paper on 4 MERIS images processed from ODESA (http://www.odesa-info.eu/info/) with MEGS8.1 version.

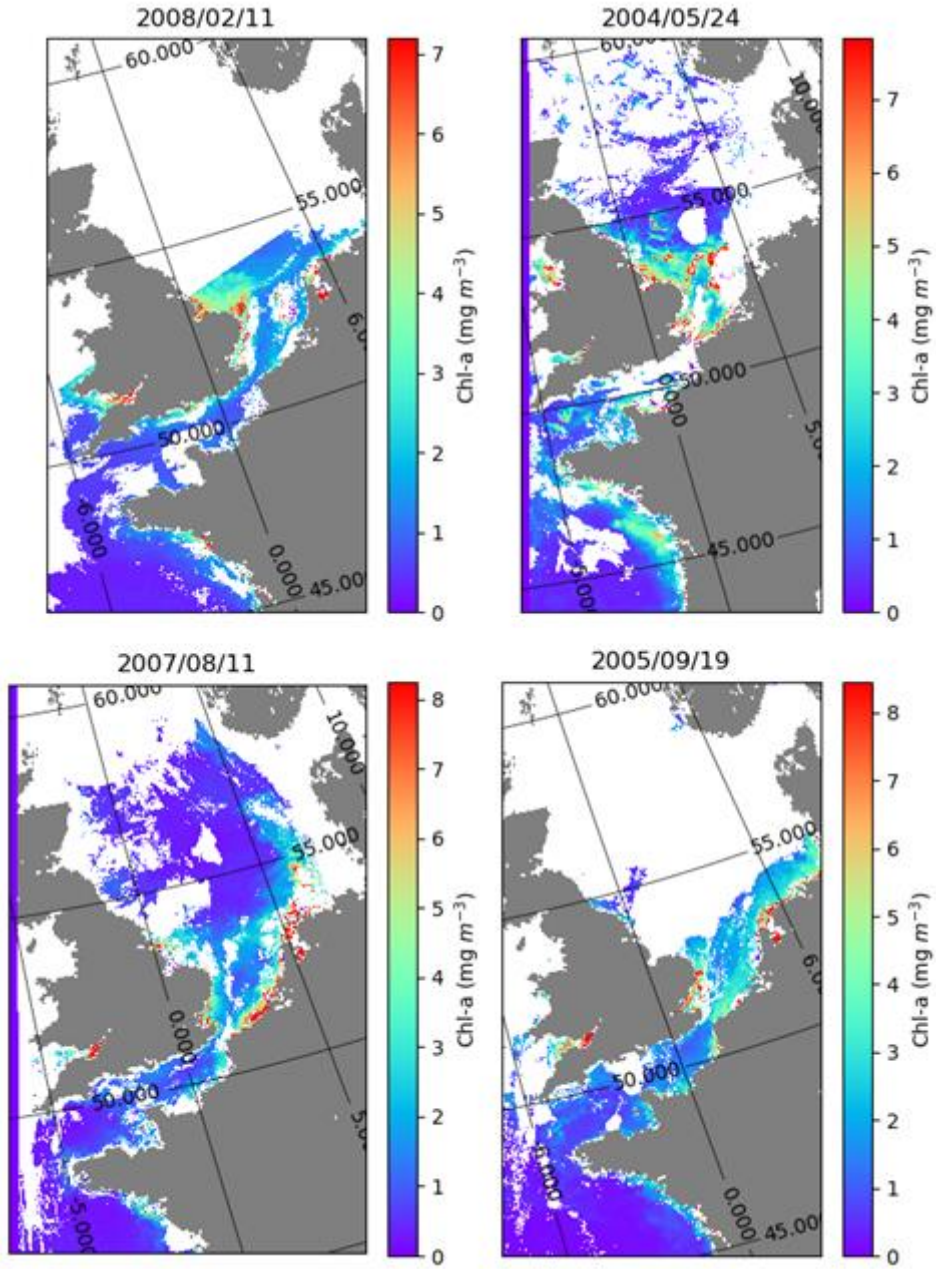

Figure 2.16: For the same images as Figure 2.15, resulting CHL maps.

2.3.14. Application to Sentinel-3 OLCI data

A first tentative to apply the algorithm selection methodology is presented on an image taken on 2017/06/18 from the OLCI instrument onboard the Sentinel 3A satellite. L1 data have been downloaded at the reduced resolution and processed with the POLYMER atmospheric correction processor (Steinmetz et al., 2011). This atmospheric correction algorithm is dedicated to complex waters and show positive results on OLCI when compared with aeronet stations (Zibordi et al., 2009) located in the North Sea (results not shown). Although a future validation of OLCI CHL_OC5 is needed, OC5 LUTs published for MERIS were applied to the OLCI data that have comparable spectral bands. Figure 2.17 shows a large application of the OC5 algorithm with some areas offshore the French and UK coast regions were the OC4 algorithm is also valid. Along the coast, the OC5 algorithm is accepted in its extended conditions due to higher turbidity. Offshore the coast, in the Irish Sea other spots show the "OC5 EXT" flags. These areas correspond to blooms of Coccolithores as also observed on the MERIS image of the 2014/05/24. Finally, the NIR-red_Gons algorithm is selected in the Wadden Sea North of Netherlands. CHL map shows values ranging between 0.15 and 8 mg m^{-3}, similarly to the MERIS images, we observed highest CHL value along the coast close to estuaries and higher CHL values in the North Sea than in the English Chanel. Results presented here need to be validated against in situ measurements, but as a first observation they are consistent with MERIS results which suggests that the present methodology should be easily adaptable to OLCI data. The benefit of the 705 nm band on OLCI instrument combined with the present approach should definitively help to better estimate CHL concentration from space in coastal waters for the next decade.

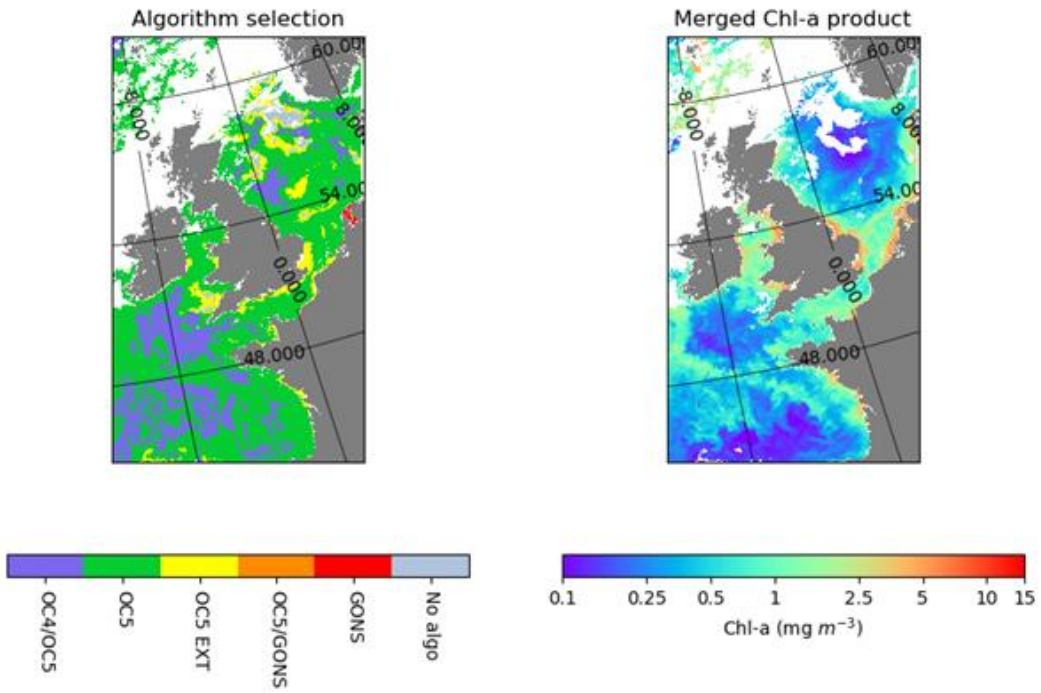

Figure 2.17: results of application of the CHL algorithm methodology developed in this paper on the OLCI reduced resolution image taken on 2017/06/18. Left panel show algorithm selection and right panel resulting CHL map. OLCI image has been processed from level 1 with the POLYMER atmospheric correction (Steinmetz et al., 2011).

2.3.15. *Conclusion Quality control protocol*

From a dataset of 358 in situ CHL / MERIS matchups, conditions of application for the OC4, OC5 and NIR-red_Gons algorithms were determined using water leaving reflectance only. OC4 and OC5 conditions of application are based on ρ_w412/ρ_w443 and ρ_w560, as a function of ρ_w560/ρ_w490 and NIR-red_Gons conditions of application depends of CHL_OC4 and ρ_w620. Results showed that with a pixel selection, performances of the three selected algorithms are improved and almost reach the standards expected in open ocean. After combining these algorithms, 74% of the dataset could be processed with a median error of 34% (Table 2.6). Methodology was then tested on four MERIS images of European waters and show that OC5 algorithm is dominant except in very turbid and eutrophic waters along the coast. In these locations, the NIR-red band ratio algorithm helps filling the gap. Finally, a test was performed on an OLCI-A image. Although some validations are still needed for the OLCI sensors, results show some agreements with MERIS applications which suggest that the present methodology should be easily adaptable to OLCI data. Then we expect that this methodology combined with OLCI data will help to monitor CHL in coastal waters which is essential for certain applications like eutrophication management.

2.4. Merging of QC on JMP-EUNOSAT satellite archive

With the ability to determine the validity of the chlorophyll-a algorithms per water type on a pixel-per-pixel basis we performed the quality control procedure described in section 2.3 to the core satellite products described in section 2.2. An example is provided in Figure 2.18 A&B with the application of this approach on satellite observations for the 8th of April 2010 for the OC4 and OC5 products showing an algal bloom in the Belgian and Dutch coastal waters. Figure 2.18 C&D shows a classification map indicating the water types where the OC4 and OC5 algorithms are applicable indicating that the OC5 algorithm can be applied in more situations compared to the OC4 algorithm. The OC4 algorithm is inaccurate in the English Channel and South-East UK due to high concentrations of suspended matter (SPM).

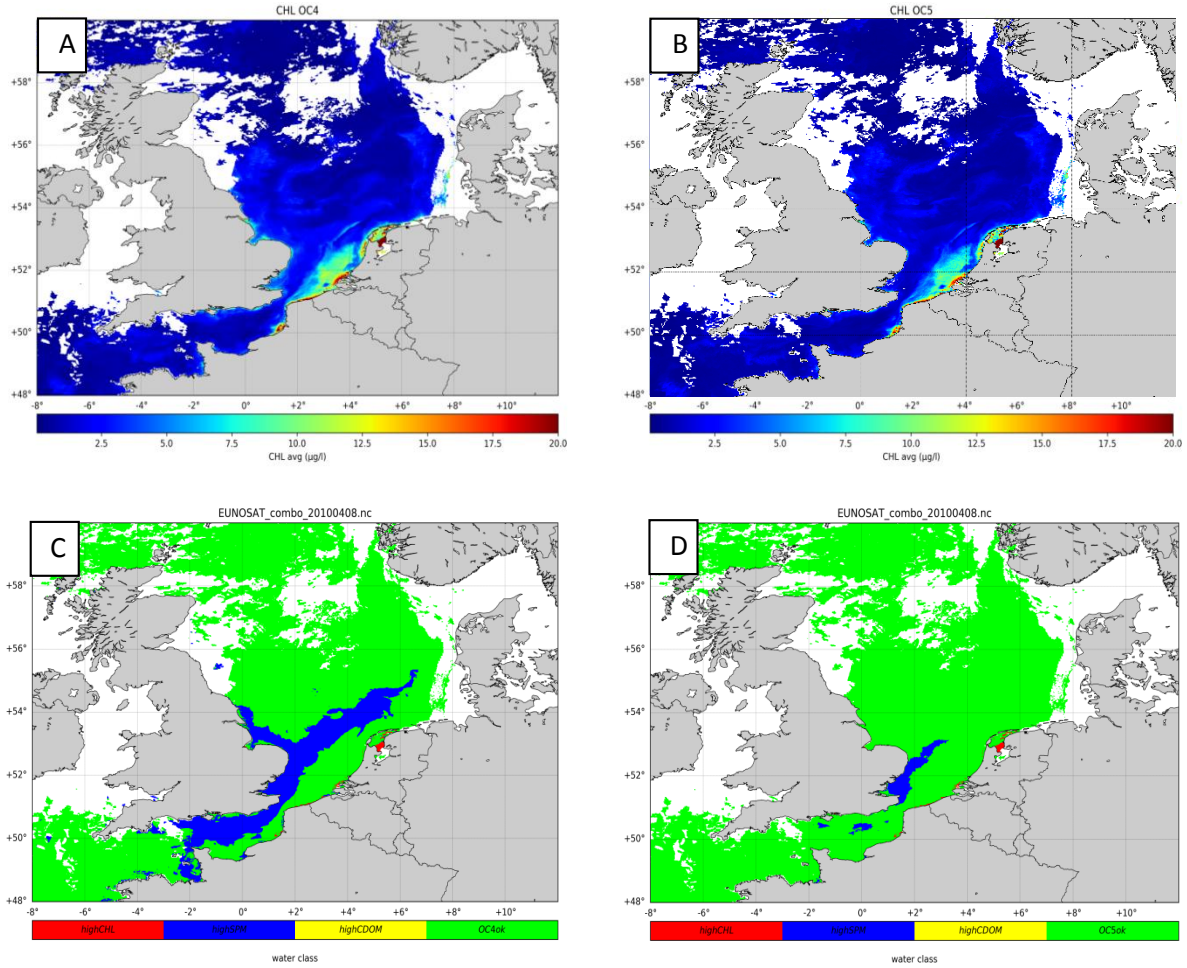

Figure 2.18. (A & B) Chlorophyll-a CHL products generated using the OC4 and OC5 algorithms for the 8th of April 2010 showing an algal bloom in the Belgian and Dutch coastal waters. (C & D) Water type classification map in dicating the water types where the OC4 (C) and OC5 (D) algorithms are applicable indicating that the OC5 algorithm can be applied in more situations compared to the OC4 algorithm. The OC4 algorithm is inaccurate in the English Channel and South-East UK due to high concentrations of suspended matter (SPM). White regions are masked due to cloud cover.

In the next phase a blending process is applied to join the quality-controlled chlorophyll-a datasets based on best suited algorithm/water type combination. A schematic overview of this process is provided in figure 2.19 showing three quality-controlled product lines: OC5 (or OC4) for clear waters, red-NIR ratio

products for turbid waters and FUB-WEW/OC4Bal products for the Skagerrak-Kattegat region. Clear and turbid waters are defined by the quality control procedures of the respective product lines. The three product lines are sequentially merged together with the priority rule of 1) turbid waters, 2) clear waters and finally 3) Skagerrak-Kattegat. This logical rule set is based on validation results presented in section x.

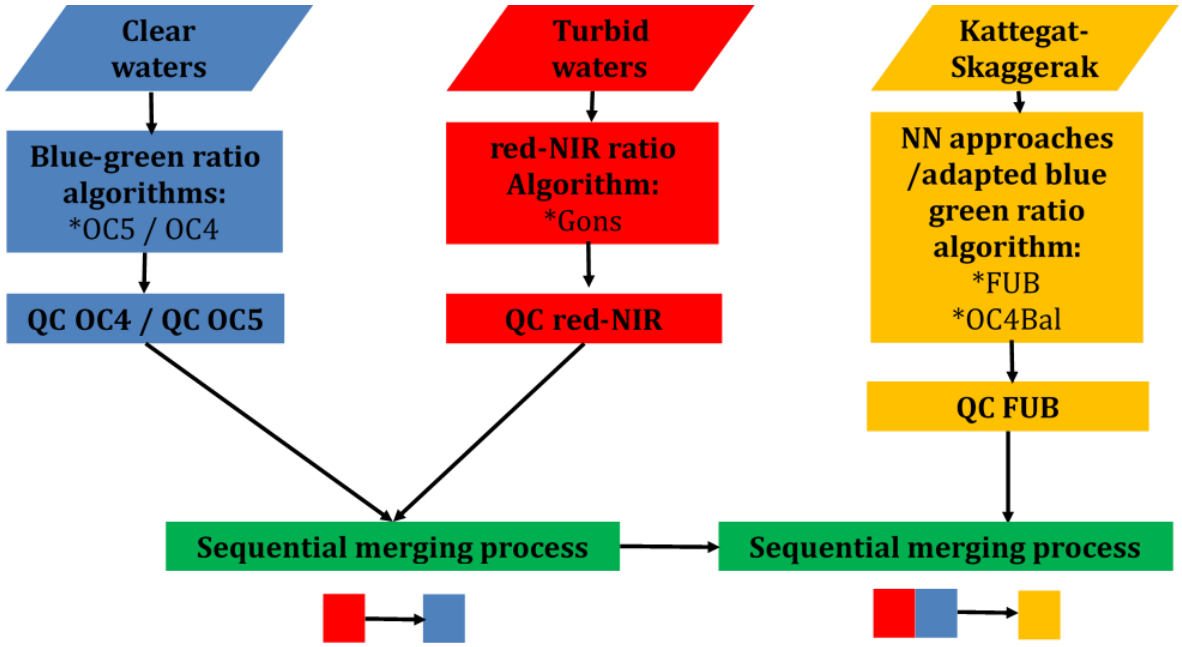

Figure 2.19. Schematic overview of CHL product processor to generate a coherent CHL product based on three quality-controlled product lines: OC5 (or OC4) for clear waters, red-NIR ratio products for turbid waters and Neural Net and the OC4Bal products for Kattegat-Skaggerak region. Clear and turbid waters are defined by the quality control procedures of the respective product lines. The three product lines are sequentially merged together with the priority rule of 1) turbid waters, 2) clear waters and finally 3) Kattegat-Skaggerak.

A demonstration of the blending process is presented if figure 2.20. This shows the different quality controlled CHL products (i.e. OC5QC, GonsQC, FUB/OC4Bal) for the 13th of April 2010. These products were merged on a pixel by pixel basis with a priority rule given to GonsQC (turbid waters) and then OC5QC (clear waters) for the North Sea area. For the Skaggerak-Kattegat area (CDOM rich waters), the pixels were filled with CHL-FUB and OC4Bal CHL products with a priority given to CHL-FUB.

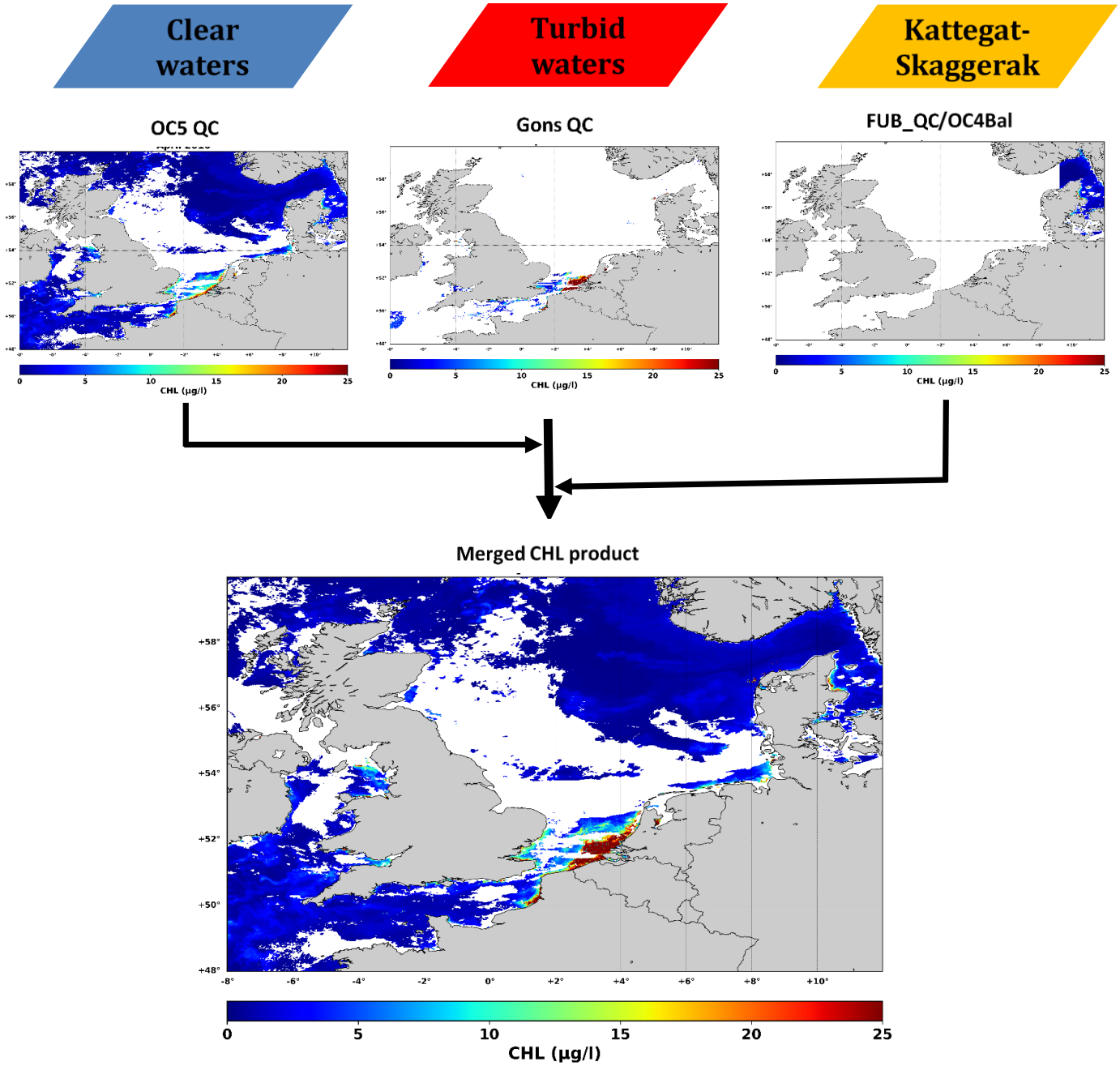

Figure 2.20: Blending process of different quality controlled CHL products on a pixel per pixel basis. The different quality controlled CHL products (i.e. OC5, red-NIR Gons, FUB/OC4Bal) for the 13th of April 2010 are presented in the top row. These CHL products are merged together on a pixel-per-pixel basis with a priority rule given to red-NIR Gons and then OC5 filling up the North Sea with the most appropriate algorithms available. Subsequently, the Skagerrak-Kattegat region are filled with the FUB/OC4Bal product. White regions are masked due to cloud cover.

2.5. Intercomparison of satellite products with ship-based observations

The validation of satellite ocean color data products is a critical component in establishing their measurement uncertainties, assessing their scientific utility, and identifying conditions for which their reliability is suspect. Such efforts require a considerable amount of high quality in situ data, preferably consistently processed. In this project we follow the approach of Bailey and Werdell (2006) for validating satellite data products using in situ measurements as ground truth. In the process of generating a coherent satellite-based CHL product for the greater North Sea it is key to understand the uncertainties of the core ocean color satellite products under a variety of water conditions. In this study, we use the comprehensive JMP-EUNOSAT in situ data base for our initial validation efforts consisting of regional in situ data collected in the national monitoring programs of the North Sea countries as it is a data set of sufficient size, quality, and diversity to support a comprehensive validation. While in situ measurements are some times referred to as 'ground-truth' measurements, they are rarely 'absolute truth'. Full characterization of the inherent error of the field measurement is essential for any validation effort. Unfortunately, such information is seldomly available for in situ observations of CHL. Additionally there is currently no consensus between the North Sea countries on the method used to assess in situ CHL concentrations ranging from HPLC measurements to spectrophotometry and fluorimetry. Still, to enable the acceptance of satellite-based in national monitoring programs it is key to compare the satellite products to the national/regional in situ data which is officially used in MSFD monitoring efforts.

The validation of satellite-products is performed by:

- Match-up analysis between satellite and in situ observations in the greater North Sea
- Match-up analysis between multi-temporal composite CHL satellite and in situ products (yearly)
- Time series intercomparison for key stations to investigate if satellite observations can capture the CHL dynamics

2.5.1. In situ data for CHL product validation

See section report Activity 1 section 3 for more details.

Observed data have been received and processed from all countries around the North Sea. The observed data differed between countries in sampling depth, sampling frequency, the variables that were measured, analysis methods and the units that were used. We pre-processed the data to create a more coherent dataset.

We first:

- converted all data to the same units;
- selected only surface CHL observations allowing measurements up to 3m depth. We neglected data of deeper water layers since our analysis will focus on concentrations in the upper mixed layer that can be observed with satellite;

- We allowed CHL observations obtained using different analytical techniques (i.e. HPLC, spectrophotometry, fluorimetry) to allow direct comparison with methods currently used by different North Sea countries.

A spatial distribution of the stations is presented in fig 3.1 of the final report of Activity 1.

2.5.2. *Match up protocol*

When directly comparing satellite and in-situ observations it is important to consider differences in both spatial and temporal scales of both data sources. The spatial resolution of the core ocean color products is 1km while a traditional in situ observation can be considered a point measurement. Given the different in spatial scales, the ground truth data are ideally collected in regions where the spatial variability of the geophysical parameter under consideration is relatively stable for an area several times the spatial resolution of the satellite-based instrument (Gordon et al., 1983). This accounts for possible navigation errors in the satellite data and minimizes the effect of small-scale spatial variability on the measured in situ data. Subpixel geophysical variability is effectively averaged by spaceborne remote sensors, while in situ instrumentation does not adequately characterize this variability. Satellite navigation may not be accurate to a pixel (Patt, 2002), therefore, a box of some number of pixels (e.g. 3×3) is defined, centered on the location of the in-situ measurement. This box allows for the generation of simple statistics, such as the mean and standard deviation, to assist in the evaluation of spatial stability, or homogeneity, at the validation point. Further, the use of a multi-pixel box increases the possibility of an in-situ measurement being available for validation by increasing the chance that the satellite retrieval will have enough clear pixels to be useful. Following, the closest pixel to the in-situ location need not be clear, so long as the valid pixels in the box meet the homogeneity requirement.

Satellite data are navigated to identify the pixel that corresponds with each in situ location. As the in-situ data are rarely collected exactly when the satellite views their location, we assign a temporal threshold in our definition of coincidence. This time window is defined to be short enough to reduce the effects of temporal variability in the in-situ data, yet sufficiently large to allow for the greatest possibility of a match. For the homogeneous water masses under consideration, we assigned a ±2 h window around the satellite overpass.

The in-situ data base (section 2.5.1) was directly compared to the satellite CHL archive (section 2.2) to extract match-ups fulfilling the above described criteria. For the satellite data it was required that at least 5 of the 9 pixels in the defined box (3x3 pixels centered on the in-situ location) be valid (i.e. unflagged) to ensure statistical confidence in the mean values retrieved. The arithmetic mean and standard deviation of the non-masked pixels is determined. To minimize the effect of outliers on the calculated mean value, especially for the case of coastal locations, a filtered mean value is also calculated:

$$\text{Filtered mean} = \frac{\sum_i (1.5 * \sigma - \bar{X}) < X < (1.5 * \sigma + \bar{X})}{N}$$

With $\bar{X}$ the unfiltered mean value, σ the standard deviation of the unfiltered data and N the number of values within ±1.5*σ. A revised pixel count (total minus masked pixels minus filtered pixels) is computed. A coefficient of variation (filtered standard deviation divided by the filtered mean, CV) is computed. Satellite retrievals with extreme variation between pixels in the defined box (CV > 0.15) are excluded.

Next to the daily match-ups, complete CHL time series were extracted from the satellite products archive following the approach described above resulting in a filtered mean value for each day that data was available. These time series were extracted for each station in the in-situ data base. Next, monthly means were calculated for both the satellite and in situ data to avoid impact from irregular sampling when calculating the average and 90-percentile CHL concentrations for a yearly growing season which was defined as March to October inclusive for this comparison. Time series were considered adequate for validation if both satellite and in-situ data were available for each of the 8 months in the growing season.

A linear regression is computed between log transformed in situ and satellite CHL observations and the following metrics were considered to assess the CHL:

- The slope and the intercept of the regression line allow to see how the model is close to the 1:1 line.
- The coefficient of determination of the model (r^2) measures the part of variability explained by the model. This coefficient is highly dependent of the dataset range.

Additional calculated accuracy descriptors are:

- The median absolute difference → $MAD = median\left(\left|CHL^{sat} - CHL^{in\ situ}\right|\right)$
- The median absolute percent difference (MAPD) indicates the median relative error in percentage. It is computed via
  $MAPD = median\left(100 \times \frac{\left|CHL^{sat} - CHL^{in\ situ}\right|}{CHL^{in\ situ}}\right)$
  Where CHL^{sat} and $CHL^{in\ situ}$ are the satellite and in situ observations respectively.

2.5.3. Match-up analysis: satellite vs in-situ observations

The quality controlled and merged satellite-based chlorophyll-a observations are compared to *in situ* observations collected in national monitoring programs. Differences between in situ and satellite CHL observations are quantified based on the 3762 match ups between the in-situ data archive as described in section 2.5.1 and the satellite archive with the quality controlled and merged CHL products as described in section 2.4. Figure 2.21 shows the scatterplot of in-situ observations versus satellite observations with the data coloured per country. Considering all available data, the uncertainty is estimated with MAD resulting in value is 1.89 µg/l which corresponds to a MAPD of 45.26%. The satellite products tend to overestimate CHL values when CHL is less than 1µg/l resulting in a slope of 0.64 and relative high scatter (r^2 = 0.60) around the 1:1 line for higher CHL values. Detailed validation results per country are provided in table 2.9. MAPD values range from 29.24% (Belgium) to 89.83% (UK CEFAS) showing big differences between

countries which can be explained by differences in water types at the monitoring stations, CHL estimation techniques (i.e. HPLC, spectrophotometry, fluorimetry) and proximity to the coast.

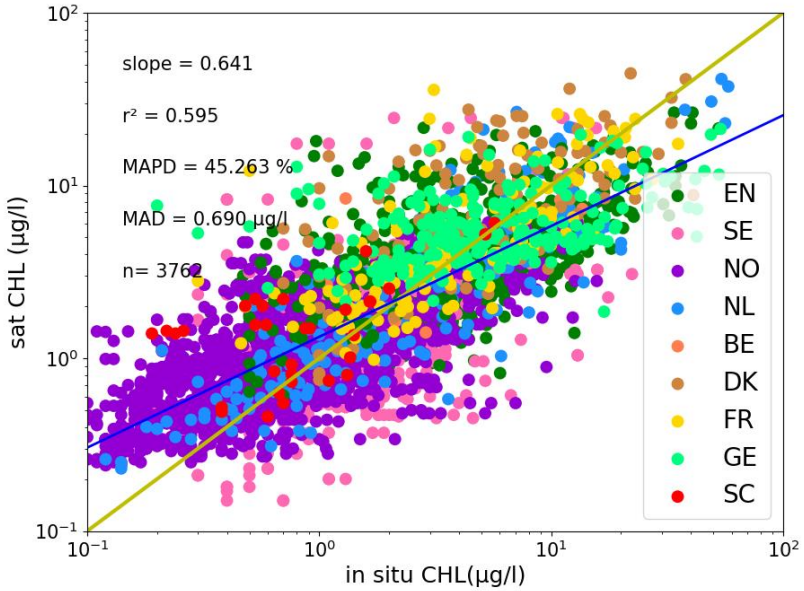

Figure 2.21: Scatterplots of in situ and satellite CHL observations for the North Sea countries. The relationship between both data sets are described by the Median Absolute Difference (MAD), Median Absolute Percentage Error (MAPD). The determination coefficient (r^2) and the slope characterizes the regression.

Table 2.9: Statistical results of the daily match up analysis per country.

Country	MAD (µg/l)	MAPE (%)	R^2	Slope	Intercept	nr	Method
BE	1.85	29.24	0.71	0.79	0.11	14	HPLC
NL	2.47	39.90	0.75	0.78	0.06	216	HPLC
DK	3.49	54.56	0.40	0.57	0.48	129	SPEC
FR	1.45	35.48	0.49	0.60	0.32	148	SPEC
UK CEFAS	2.34	89.83	0.41	0.61	0.41	121	HPLC
UK SB	0.95	34.84	0.51	0.49	0.19	1059	FLUO
SC	0.48	39.39	0.70	0.89	0.69	33	SPEC
GE	2.27	50.78	0.17	0.20	0.60	237	HPLC + SPEC
SE	0.78	58.85	0.16	0.44	0.00	317	FLUO
NO	0.71	66.65	0.42	0.44	0.99	1464	SPEC
Combo	0.69	45.26	0.60	0.64	0.12	3762	all

While the daily match up analysis provides an accuracy assessment for singular CHL observations, eutrophication assessments are performed based on multi-temporal aggregates of CHL observations. In this section the capability of the satellite observations to capture the yearly CHL dynamics is assessed by calculating the mean and 90-percentile values over a CHL growing season defined as March-October incl. Differences between in situ and satellite CHL yearly mean CHL concentrations are quantified based on the 956 match ups. Figure 2.262 shows the scatterplot of yearly averaged in-situ observations versus satellite observations with the data coloured per country. Considering all available data, the uncertainty is estimated with MAD resulting in value is 1.23 µg/l which corresponds to a MAPD of 35.19% which is an

improvement to the daily match up results. The linear regression results in a slope of 0.86 with data close to the 1:1 line (r^2 = 0.59). Detailed validation results per country are provided in table 2.10. MAPD values range from 12.97% (UK smart buoys) to 54.10% (Scotland). For the 90-percentile products the uncertainty is estimated with MAD resulting in value is 2.32 µg/l which corresponds to a MAPD of 39.05 %. The linear regression results in a slope of 0.79 with data close to the 1:1 line (r^2 = 0.53) (Figure 2.23, Table 2.11). We observe an increase in scatter (higher r^2 values) and MAPD values when comparing the CHL-P90 matchups with the mean indicating that the statistical variable 'mean' provides more stable results compared to the CHL-P90 which is more sensitive to sampling frequency (Van der Zande et al., 2011).

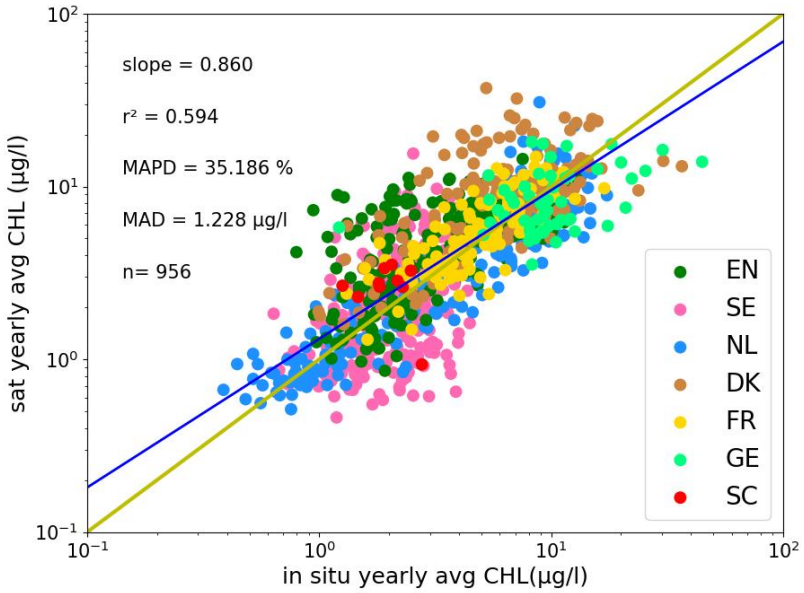

Figure 2.22: Scatterplots of yearly mean CHL concentrations based on in situ and satellite CHL observations for the North Sea countries. The relationship between both data sets are described by the Median Absolute Difference (MAD), Median Absolute Percentage Error (MAPD). The determination coefficient (r^2) and the slope characterizes the regression.

Table 2.10 Statistical results of the match up analysis of yearly mean CHL estimates per country.

Country	MAD (µg/l)	MAPE (%)	R^2	Slope	Intercept	nr	Method
BE	****	***	***	***	***	***	***
NL	1.83	27.98	0.84	0.88	0.01	202	HPLC
DK	3.03	53.78	0.41	0.59	0.59	133	SPEC
FR	1.13	22.98	0.58	0.78	0.20	113	SPEC
UK CEFAS	1.11	36.40	0.34	0.62	0.35	211	HPLC
UK SB	0.53	12.97	0.70	0.61	0.14	17	FLUO
SC	0.83	54.10	0.33	0.63	1.65	10	SPEC
GE	3.23	39.56	0.16	0.30	0.61	55	HPLC + SPEC
SE	0.90	43.05	0.19	0.72	0.04	216	FLUO
NO	****	****	****	***	***	2	SPEC
Combo	1.23	35.19	0.59	0.86	0.12	956	***

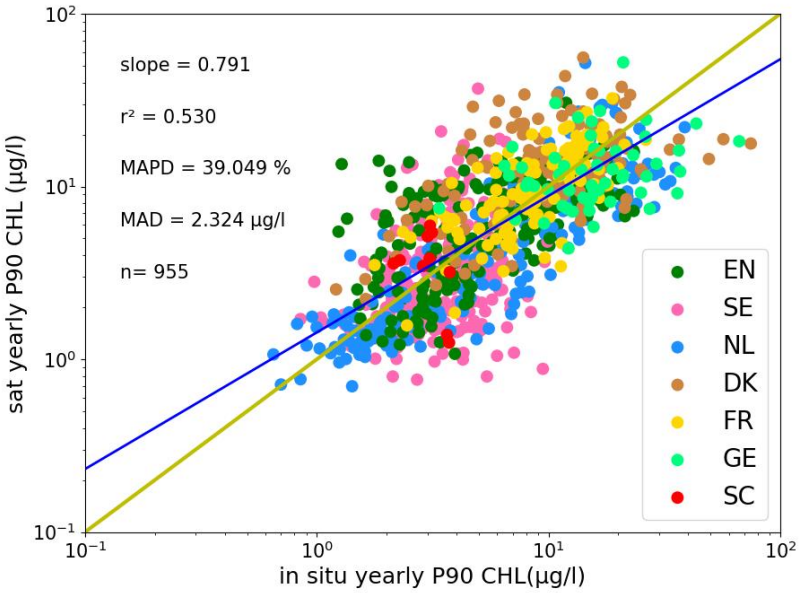

Figure 2.23: Scatterplots of yearly 90-percentile CHL concentrations based on in situ and satellite CHL observations for the North Sea countries. The relationship between both data sets are described by the Mean Absolute Difference (MAD), Mean Absolute Percentage Error (MAPD). The determination coefficient (r^2) and the slope characterizes the regression.

Table 2.11: Statistical results of the match up analysis of yearly 90-percentile (P90) CHL estimates per country.

Country	MAE (µg/l)	MAPE (%)	R^2	Slope	Intercept	nr	Method
BE	****	***	***	***	***	***	***
NL	4.06	34.50	0.77	0.87	-0.01	202	HPLC
DK	4.87	49.74	0.29	0.47	0.65	132	SPEC
FR	2.47	29.45	0.50	0.77	0.26	113	SPEC
UK CEFAS	1.97	36.45	0.30	0.54	0.39	143	HPLC
UK SB	1.28	20.95	0.67	0.53	0.20	17	FLUO
SC	1.11	47.99	0.20	0.63	2.39	10	SPEC
GE	6.28	42.14	0.08	0.22	0.81	55	HPLC + SPEC
SE	1.69	48.30	0.12	0.54	0.20	216	FLUO
NO	****	****	****	***	***	2	SPEC
Combo	2.32	39.05	0.53	0.79	0.16	955	***

Figure 2.24 shows an example of a yearly mean and P90 CHL map for the growing season (March-Oct incl.) for three years (2000, 2007, 2016, other years not shown) with an overlay in situ station markers showing the in situ CHL values with the same color scheme as the satellite data. Each of these markers represents a point in the scatterplots presented in figure 2.22 and 2.23. This representation shows the ability of the satellite observations to capture the spatial CHL patterns which are not captured by the in-situ

observations. The national monitoring zones are overlaid in black providing an opportunity to assess the ability of an in-situ station to capture the CHL variability in a specific zone.

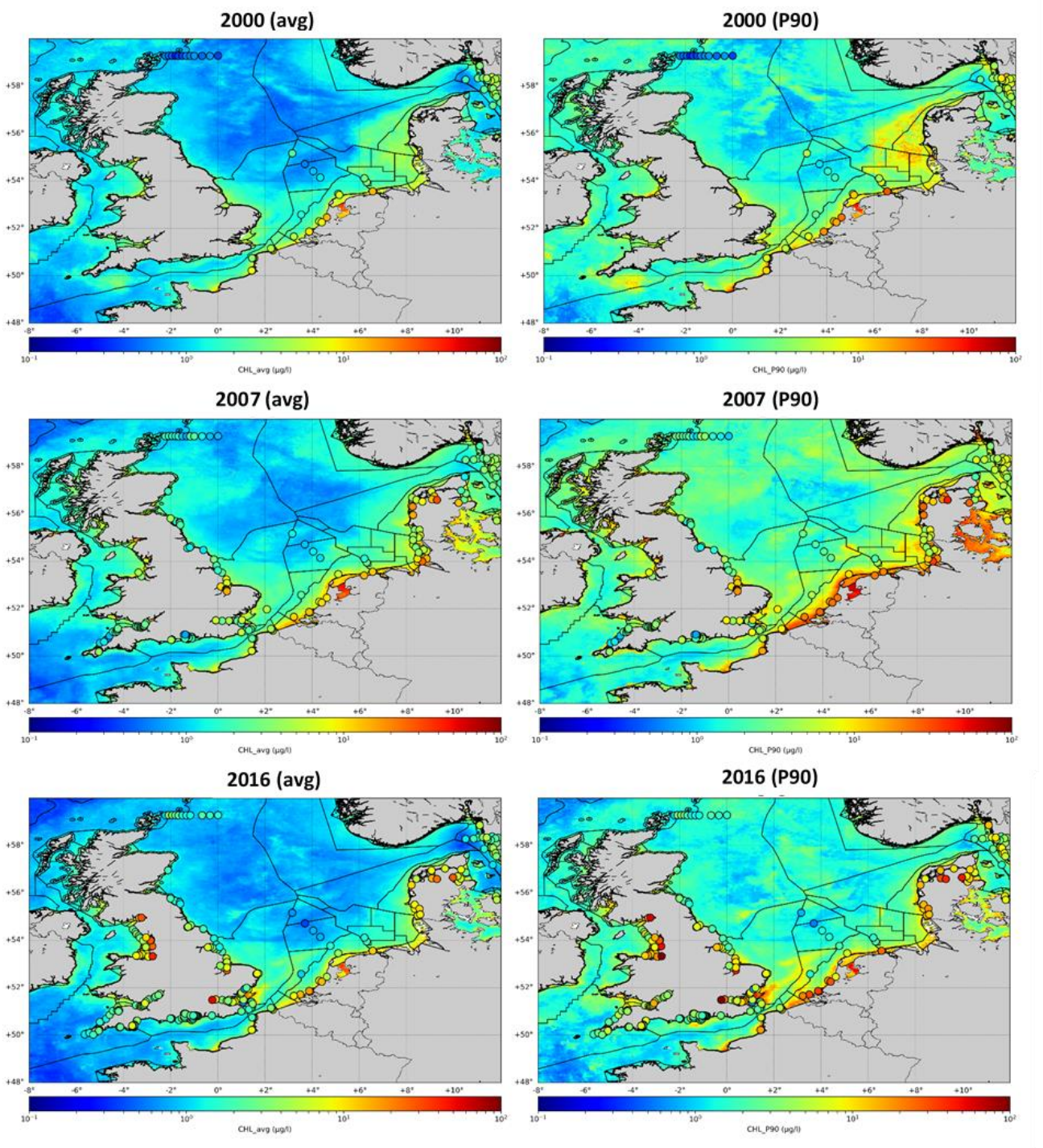

Figure 2.24: Mean and 90-percentile map of the blended and quality controlled CHL product for the growing season (March-Oct incl.) for the years 2000, 2007 and 2016 with an overlay in situ station markers showing the in situ CHL values with the same color scheme as the satellite data providing a spatial interpretation of the intensity of the algal blooms in the North Sea. The national monitoring zones are overlaid in black

CHL time series were extracted for the national monitoring stations for the period 1998-2017 showing the ability of the satellite data to capture the temporal CHL dynamics. These data were provided to all partners to enable a direct assessment of the quality of the satellite observations for their specific stations. Examples of such time series are demonstrated in figure 2.25 showing a 90-percentile map of chlorophyll a for the growing season (March-Oct incl.) of 2003 providing a spatial interpretation of the intensity of the algal blooms in the North Sea. Additionally, a direct comparison of chlorophyll-a time series is provided for the national monitoring stations Stonehaven (Scotland), Rottumerplaat (the Netherlands), 330 (Belgium) and Boulogne (France) for the year 2003 showing the ability of the satellite data to capture the temporal chlorophyll a dynamics. For the time series of satellite data we extracted a 3 x 3 macro-pixel with 1 x 1 km pixels of which the center pixel contains the monitoring station location. The resulting time series are presented in monthly bins as in situ data is mostly collected on a monthly basis in these stations. The satellite data is presented as boxplots to demonstrate the increased availability of satellite data compared to *in situ* sampling, i.e. 20-50 observations per growing season depending on the location, cloud cover and water conditions.

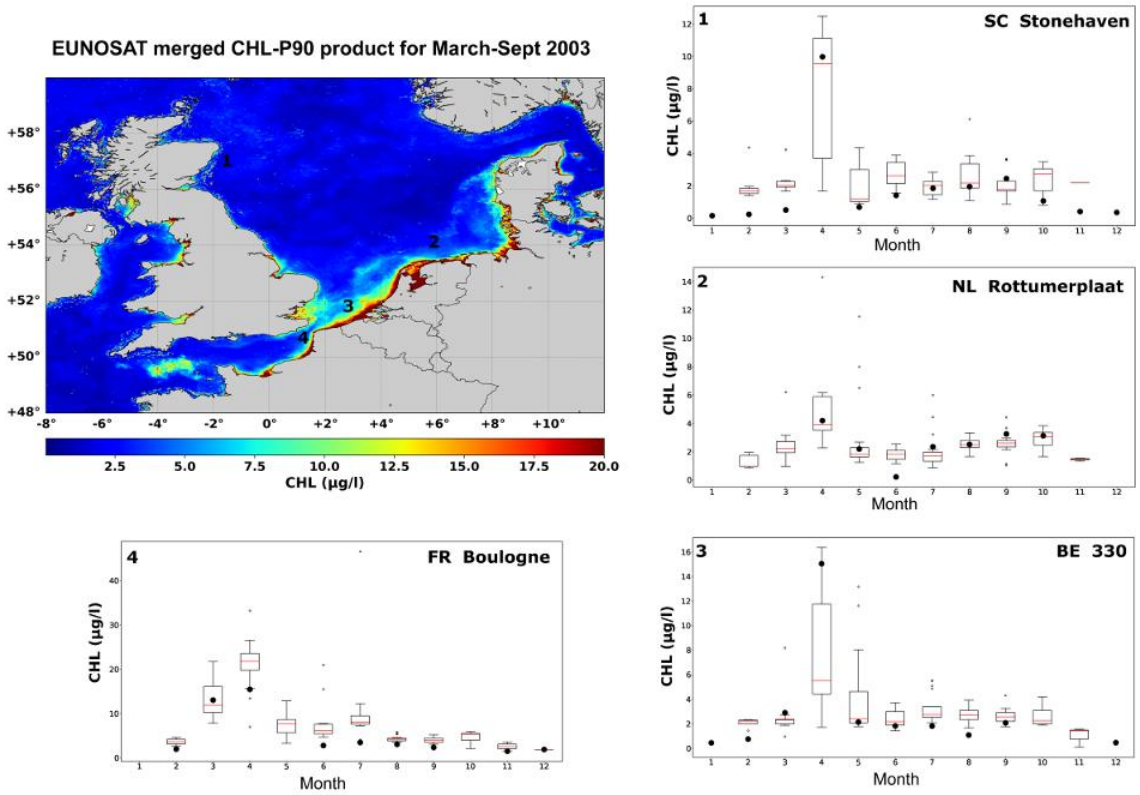

Figure 2.25: Map of the 90th percentile of the blended and quality-controlled CHL product for the growing season (March-Oct incl.) of 2003 providing a spatial interpretation of the intensity of the algal blooms in the North Sea. Additionally, a direct comparison of CHL time series, presented as boxplots, is provided for the national monitoring stations Stonehaven (Scotland), Rottumerplaat (The Netherlands), 330 (Belgium) and Boulogne (France) for the year 2003 showing the ability of the satellite data to capture the temporal CHL dynamics. Black dots represent the mean monthly in-situ CHL concentration, the boxplots show the monthly satellite-based CHL concentration with box extending from the lower to upper quartile values of the data, with a line at the median and the whiskers showing the 10-and 90-percentiles.

2.6. Conclusions

CHL concentration is a critical parameter for the users of ocean color satellite images in the North Sea. Satellite data from ocean color sensors (i.e. SeaWiFS, MODIS, MERIS, VIIRS, Sentinel-3) can provide spatially coherent data on CHL concentrations using CHL retrieval algorithms such as with blue/green-ratio algorithms (e.g. OC4, OC5), red-NIR algorithms (e.g. Gons) or Neural Networks (e.g. MEGS, FUB). However, because of the optical complexity of coastal waters, retrieving accurate CHL estimates is still challenging. The CHL algorithms are often regional or only apply to a certain water type (e.g. clear waters, turbid waters, CDOM rich waters) making it difficult to apply them to a region such as the North Sea as water properties are so variable spatially that only one algorithm is generally not adapted to the whole study area. To fill this gap, we proposed a methodology to determine the reflectance conditions for which these algorithms can deliver an accurate CHL estimate in complex optical conditions as found in coastal waters. Results show that by applying the quality control per algorithm, performances of the selected algorithms are improved and almost reach the standards expected in open ocean (i.e. 30% error).

Next, the best combination of quality controlled CHL algorithms is determined to produce a quality controlled multi-algorithm satellite CHL product based on best suited algorithm/water type combination. The suitability of the blended CHL product for eutrophication assessment was evaluated by a comparison analysis with *in situ* datasets for all assessment areas in the greater North Sea. After combining multiple algorithms, a daily match up analysis with in situ observations resulted in a median error of 45.26%. Eutrophication assessments for the MSFD are performed on multi-temporal composites of these daily CHL products, i.e. mean or P90 over a growing season. A validation of the yearly mean and P90 CHL products yielded a median error of 35.19% and 39.05% respectively showing a good general agreement between in-situ and satellite observations.

A more detailed intercomparison between in-situ and satellite CHL observations per country showed differences which can be explained by:

- **differences in water types at the monitoring stations**. While there is a selection of an optimal CHL algorithm per water type, the complex condition of coastal waters generally results in less accurate CHL estimates compared to clear waters. It is especially difficult to quarantee high quality CHL products in CDOM rich waters (e.g. Kattegat, German Wadden Sea).
- **In-situ CHL estimation techniques**. Ocean colour algorithms are generally calibrated using HPLC in situ measurements. In this study, the in situ data set used for validation consisted of CHL estimates obtained through different techniques, i.e. HPLC, spectrophotometry, fluorimetry. Thus including the inconherency between these methods into the validation results. Additionally, the monitoring frequency of both satellite and in situ observations can play an important role when comparing multi-temporal CHL products (e.g. mean, P90)

- **proximity to the coast.** In coastal waters, CHL concentration might be extremely high (Smith et al., 2018) and water leaving reflectance canaffected by non algal particulates (high turbidity) and/or CDOM by riverine output which varies independently of phytoplankton biomass. This results in very complex optical conditions where spectral ratio algorithms generally fail pushing the need for more complex approaches such as neural networks. Often, satellite product providers apply a buffer flag around land pixels to exclude these difficult conditions.

The quality control and merging procedure was tested on Sentinel-3 OLCI images. Although more validation results are still needed for the OLCI sensors, results show good agreements with the applications on MERIS images which suggest that applied the presented methodology will help to accurately estimate CHL in the North Sea for the Sentinel-3 era which will continue up to 2036.

3. Evaluation of coherent satellite-based chlorophyll a product for eutrophication assessment

3.1. Introduction

The Water Framework Directive (WFD) and the Marine Strategy Framework Directive (MSFD) are currently the most important drivers for monitoring the coastal and offshore waters in Europe with the objective of reaching a 'good environmental status'. Human-induced eutrophication is one of the criteria for assessing the extent to which good environmental status is being achieved. The eutrophication status is established by monitoring the CHL concentration as it is a proxy of phytoplankton biomass. More specifically, the indicator of choice is a multi-temporal statistical descriptor such as the mean or 90 percentile (P90) of CHL over the phytoplankton growing season for a period of 6 years expressed in µg/l. While a growing season may have different definitions depending on the country applying them, in this exercise we use the Dutch definition as March-September incl. With in-situ data acquisition still considered as the main monitoring tool, in this section we investigate the impact of use of satellite data using different approaches on eutrophication assessments:

- satellite data vs in-situ data for coherent CHL assessment
- traditional vs newly proposed (WP1) assessment levels (threshold values in MSFD terminology)
- traditional vs newly proposed (WP1) assessment regions

In this case study we focus on the Dutch part of the North Sea due to the availability of sufficient in-situ and satellite observations. We state that the assessment results presented here are **NOT** proposed as 'the new OSPAR assessment for 2022'. We combined available models and satellite algorithms for the first time to demonstrate a novel approach for coherent assessments to improve/fine-tune all components before actual implementation. The assessment provided here should reflect trends in eutrophication. To minimize random effects of observation timing, location and method of sampling we focus on 6-year means with CHL time series at fixed monitoring sites. To enhance the assessment, we use the full archive of quality controlled and merged satellite-based CHL products taking advantage of their high spatial and temporal resolution.

3.2. Satellite data and in-situ data for coherent CHL assessment

Ecological assessments for the Marine Strategy Framework Directive (MSFD) require monitoring data of chlorophyll-a to assess the eutrophication status of Dutch marine waters. Traditionally, such monitoring data have been acquired by bi-weekly to monthly monitoring cruises by ship (Dutch national monitoring program MWTL). The use of satellite data for monitoring CHL in marine waters for assessments could enable more reliable assessments at lower costs than traditional monitoring by ships. In the section 3.1 we present a quality controlled merged satellite-based CHL product and validation results have shown that this type of observations can provide data on CHL with an appropriate accuracy and precision. While the satellite data could not reproduce individual in-situ observations exactly, because of the higher resolution in space and time, the estimates of growing season means would still be more accurate than estimates based on monthly monitoring data at selected locations.

Including high spatial resolution data into an eutrophication assessment requires different data processing and results may differ from the traditional assessments based on in-situ data. The objective of this case study is to evaluate how different data sources (in-situ vs satellite data) and data processing methods affect the assessment results. In this section we start from the same method that has been used in the most recent OSPAR assessment for Dutch marine waters for 2006 – 2014 (Baretta-Bekker, 2016) but we focus on the period 2006-2011. We have chosen this period because MSFD assessments are carried out at a 6-year frequency, so we evaluate assessment results for a six-year period. Furthermore, this period overlaps with the period used for the 2006-2014 OSPAR assessment and for this period MERIS satellite data are available. Satellite data from MERIS can provide more accurate chlorophyll-a estimates than MODIS data in turbid coastal waters. We perform the assessment at 3 spatial aggregation methods:

- Assessment per individual MWTL location
- Assessment per assessment area, as area means
- Assessment per grid cell of 1 x 1 km in the satellite data, with spatially variable assessment thresholds

OSPAR assessments use 4 indicators: nutrients, chlorophyll, *Phaeocystis* and oxygen. This study focusses on possible changes in assessment results due to a change in assessment method, by including satellite data. Satellite data can only provide information on the chlorophyll-a indicator. Therefore, we focus only on possible changes in assessment results for the chlorophyll indicator. In the latest OSPAR assessment oxygen was not a problem in any of the Dutch assessment areas. *Phaeocystis* is being reconsidered as indicator. It may be excluded from future assessments for the North Sea. We exclude these indicators from the present study, since we don't expect them to affect future eutrophication assessments for the North Sea. The assessment of nutrients is not affected by the use of satellite data, but the overall assessment result is affected by nutrients.

In this study we focus on the marine assessment areas: Coastal waters, Southern Bight offshore, Oyster grounds and Dogger Bank. The estuarine assessment areas: Wadden Sea, Western Scheldt and Ems-Dollard are disregarded in this study. In these shallow turbid waters, with many intertidal areas, satellite data of traditional ocean color satellites are relatively unreliable. The Sentinel-2 satellite for inland waters has a

higher spatial resolution and therefore we expect this satellite to provide more useful data for the deeper parts (gullies). In shallow areas where the sediment reflects sunlight optical satellite data (water colour) cannot be used to retrieve chlorophyll-a concentrations.

3.2.1. Data description

Chlorophyll-a concentrations of 2006 – 2011 from the MWTL monitoring programme by Rijkswaterstaat have been used as in-situ data. Only the locations that are used for the OSPAR assessment have been used, for the marine assessment areas (see Table 3.1 and Figure 3.1). These data have been sampled at 3 m below the surface and samples were analyzed in the laboratory with HPLC to determine chlorophyll-a concentrations.

Table 3.1: Overview of MWTL monitoring locations per assessment area that have been used for the latest OSPAR assessment

Coastal waters	Goeree 2 km
Coastal waters	Goeree 6 km
Coastal waters	Noordwijk 10 km
Coastal waters	Noordwijk 2 km
Coastal waters	Noordwijk 20 km
Coastal waters	Rottumerplaat 3 km
Coastal waters	Rottumerplaat 50 km
Coastal waters	Rottumerplaat 70 km
Coastal waters	Schouwen 10 km*
Coastal waters	Terschelling 10 km
Coastal waters	Terschelling 4 km
Coastal waters	Walcheren 2 km
Coastal waters	Walcheren 20 km
Dogger Bank	Terschelling 235 km
Oystergrounds	Terschelling 100 km
Oystergrounds	Terschelling 135 km
Oystergrounds	Terschelling 175 km
Southern Bight off-shore	Noordwijk 70 km
Southern Bight off-shore	Walcheren 70 km

*Since there are no chlorophyll data available for Schouwen 10 km in the years 2006 – 2011, we have omitted this station from this study

CHL time series were extracted from the quality controlled multi-algorithm products archive (section 2.4) for each of the MWTL stations as described in table 3.1 using the method described in section 2.5.2. to enable a direct comparison. Additionally, CHL time series were created for each of the Dutch marine areas (i.e. Coastal waters, Southern Bight offshore, Oyster grounds and Dogger Bank) by calculating the mean CHL for each region per satellite image.

3.2.2. OSPAR assessment levels and areas

For the OSPAR assessments in Dutch coastal waters 7 assessment areas are distinguished (Figure 3.1). The marine areas: “Coastal waters”, “Southern Bight offshore”, “Oystergrounds” and “Doggerbank” are in scope for this study. Traditionally the area mean chlorophyll concentrations are estimated from the MWTL locations (black dots in Figure 3.1) within these assessment areas. The assessment level for the 90-percentile chlorophyll-a concentrations are twice as high as the assessment levels for growing season means. The 90-percentile of chlorophyll-a concentrations for the assessment is also estimated as twice the

mean of observed chlorophyll-a concentrations. The assessment of 90-percentiles of chlorophyll-a concentrations is actually redundant in the present assessment method. Table 3.2 summarizes the assessment levels for season mean DIN, DIP and chlorophyll concentrations in the 4 marine areas that are in scope for this study. The assessment level for DIN is salinity dependent. The number in table 3.2 is the assessment level at a salinity of 30 psu.

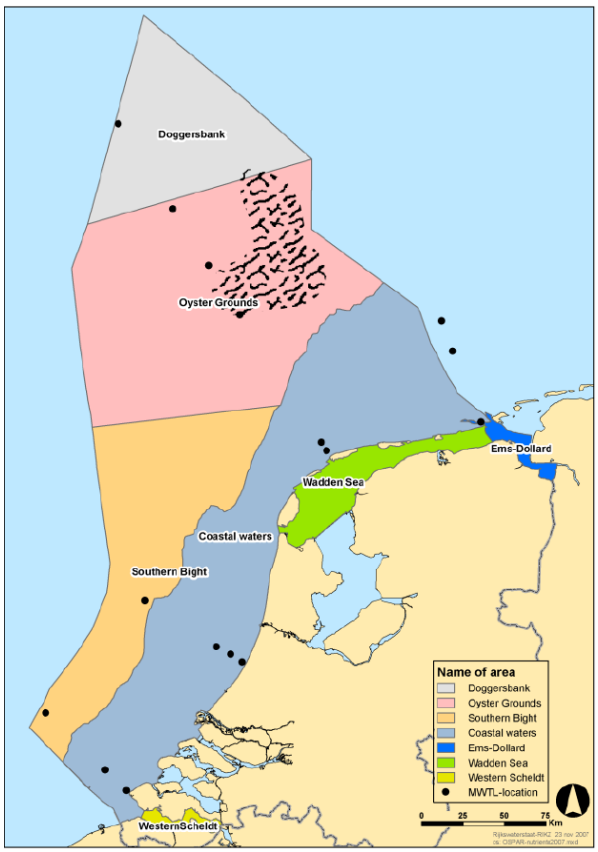

Fig 3.1: Assessment areas in the latest OSPAR assessment. Black closed circles represent MWTL monitoring locations used for the assessment

Table 3.2: Assessment levels for growing season mean CHL concentrations per assessment area.

Indicator	Coastal waters	Southern Bight	Oystergrounds	Doggerbank
Winter DIN	30	15	15	15
Winter DIP	0.8	0.8	0.8	0.8
Growing season chlorophyll-a	7.5	2.25	2.25	2.25

Next, monthly means were calculated for both the satellite and in situ data to avoid impact from irregular sampling when calculating the average and 90-percentile CHL concentrations for a yearly growing season which was defined as March to October inclusive for this comparison. Time series were considered adequate for validation if both satellite and in-situ data were available for each of the 8 months in the growing season.

3.2.3. OSPAR assessment levels and areas

The most recent application of the OSPAR Comprehensive Procedure to Dutch marine waters is from 2016 (Baretta-Bekker, 2016). In this report in-situ data from the years 2006 – 2014 were used for the assessment. Figure 3.2 shows the overall outcome of the assessment. The Oyster Grounds and Dogger Bank were non-problem areas, while all other subareas were classified as problem areas. In Figure 3.2 the assessment results are shown for per indicator: DIN/DIP, CHL, the nuisance phytoplankton indicator species (i.e. *Phaeocystis*) and oxygen. Assessment levels for CHL are only exceeded in the assessment area Wadden Sea. The Southern Bight offshore area is a problem area based on the number of cells/l of *Phaeocystis* only. In the assessment areas: Coastal Waters, Wadden Sea, Western Scheldt, and Ems-Dollard the assessment levels of several indicators (nutrients and Phaeocystis, and in some cases chlorophyll) were exceeded. Oxygen concentrations in are above the minimum assessment levels in all areas. If the indicator *Phaeocystis* will not be used in the future then coastal waters will only be assessed as problem area because of excess nutrient concentrations.

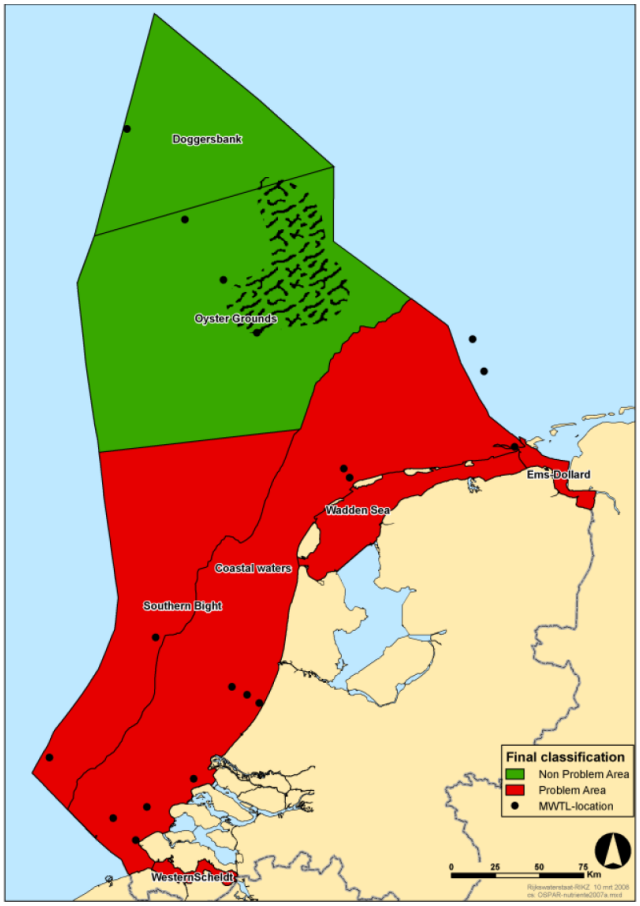

Fig 3.2: Overall OSPAR assessment results for eutrophication for the years 2006-2014

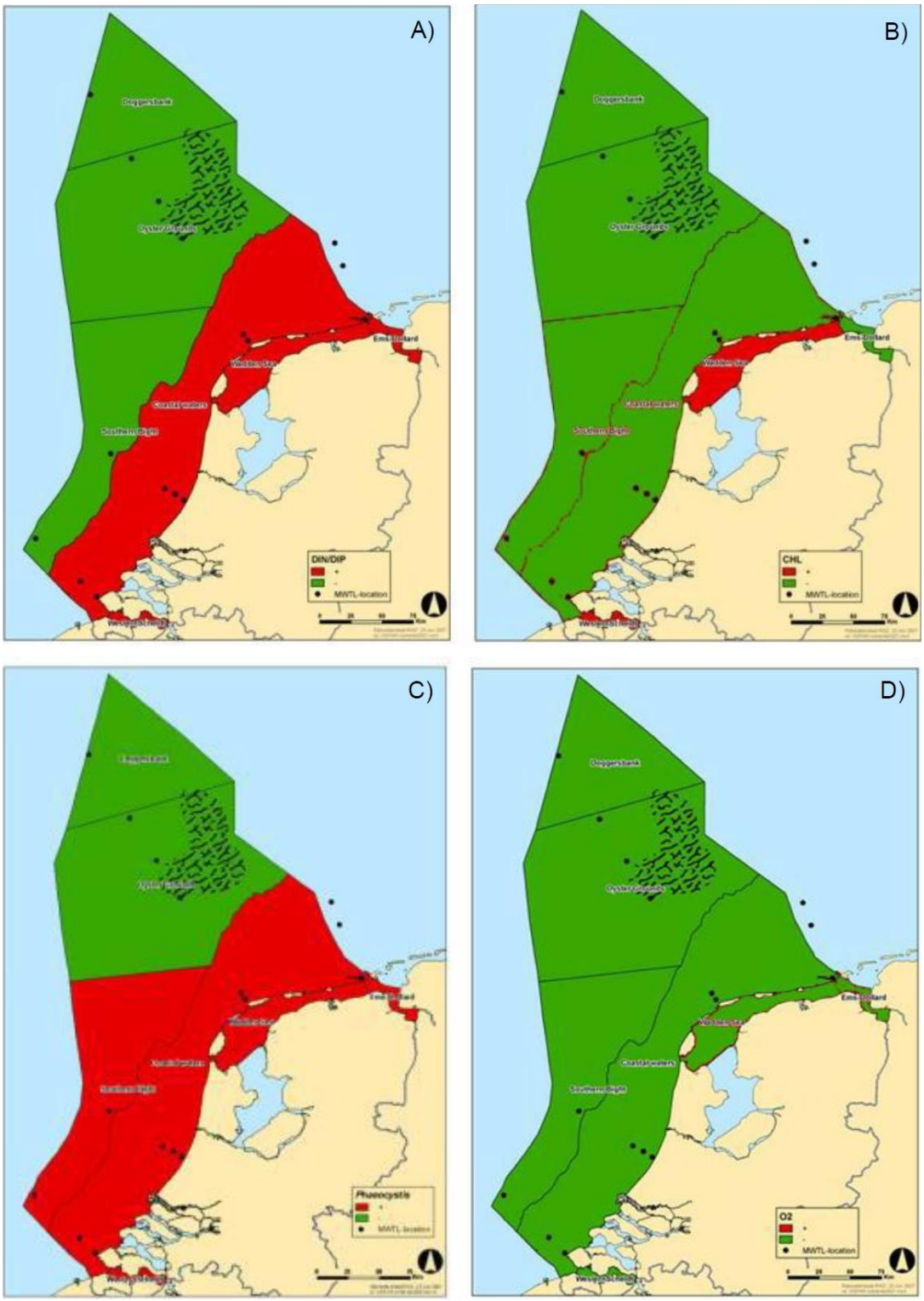

Fig 3.3. Assessment results for 2006-2011 for A) DIN and DIP, B) CHL, C) Phaeocystis and D) oxygen

3.2.4. *Data pre-processing options*

Statistics (either mean, median or 90 percentile) per assessment area over a series of years can be calculated in several ways. Aggregation of observations (either in-situ or from satellites) in space and time can be done step-wise at several spatial and temporal aggregation levels. For aggregation in space there are two aggregation levels:

- Per location (either MWTL or 1 x 1 km grid cell of satellite data)
- Per assessment area.

For aggregation in time there are 4 aggregation levels:

- Individual observation
- Per month
- Per season (either winter or growing season) per year
- Per season per period of several years.

In the most recent OSPAR assessment the following steps have been taken:

- First season means per year have been calculated per assessment area, by averaging over all monitoring locations in that area.
- Next the area mean was calculated over the years of the assessment period.
- The 90-percentile for chlorophyll-a was calculated as twice the growing season mean. In historic MWTL data the 90-percentile was shown to be generally circa two times the season mean for chlorophyll-a (van den Berg, 2004).

In this study we prefer to first aggregate over time per location and next per assessment area because the definition of assessment areas is considered to be revised by OSPAR. Also, the satellite data have a higher spatial resolution, so the effect of this enhanced spatial resolution is a relevant aspect in this pilot assessment study. For comparison we also aggregate the data in the same way as the most recent OSPAR assessment. More specifically we use the following step-wise aggregation in time of the data per location for this study:

- Mean:
  – First monthly average per year (to correct for higher sampling frequency during spring bloom in some years),
  – then growing season mean per year,
  – mean of growing season means of 2006 – 2011.

- Median:
  – median of all chlorophyll observations during the months March through September of 2006 – 2011

- 90-percentile:
  – 90-percentile of all chlorophyll observations during the months March through September of 2006 – 2011

Satellite data are available for the growing seasons of 1998 – 2017 from the quality-controlled merged CHL archive (section 2). We will focus on the period 2006-2011 due to the availability of MERIS data for which we are able to generate the red-NIR based CHL product optimized for turbid eutrophic waters which are found in the coastal area of the Dutch waters.

3.3. Assessment results based on growing season means

3.3.1. Assessment per MWTL location

Table 3.3 shows the mean CHL concentrations for the period 2006-2011 based on both in situ data and the quality-controlled merged CHL data for all MWTL station with the current assessment level at each MWTL station. The satellite CHL products give the same assessment results as in-situ data for all MWTL locations, except for Terschelling 4km where the satellite data observes higher CHL mean values. A color code is appointed to the assessments per stations as an arbitrary indicator based on the ratio between the growing season mean and assessment level. The assessment is considered: 'non-problem' for a ratio smaller than 0.9, 'potential problem' if the ratio is between 0.9 and 1.1 and 'problem' if the ratio is bigger than 1.1.

Table 3.3: Comparison of the CHL growing season means over 2006-2011 from several data sources, with the current assessment level at each MWTL station. A color code is appointed to data source as an arbitrary indicator based on the ratio between the growing season mean and assessment level.

Assessment Area	Station	Assessment level	mean 2006-2011 in situ (µg/l)	mean 2006-2011 EO (µg/l)
Coastal waters	Goeree 2km	7.5 µg/l	10.8	16.54
Coastal waters	Goeree 6km	7.5 µg/l	11.2	12.35
Coastal waters	Noordwijk 10km	7.5 µg/l	6.8	7.55
Coastal waters	Noordwijk 2km	7.5 µg/l	9.9	11.23
Coastal waters	Noordwijk 20km	7.5 µg/l	5.2	5.05
Coastal waters	Rottumerplaat 3km	7.5 µg/l	11.3	8
Coastal waters	Rottumerplaat 50km	7.5 µg/l	2.6	2.29
Coastal waters	Rottumerplaat 70km	7.5 µg/l	1.6	2
Coastal waters	Terschelling 10km	7.5 µg/l	4.1	3.93
Coastal waters	Terschelling 4km	7.5 µg/l	6.1	7.87
Coastal waters	Walcheren 2km	7.5 µg/l	12.4	10.25
Coastal waters	Walcheren 20km	7.5 µg/l	7.3	5.44
Doggerbank	Terschelling 235km	2.25 µg/l	0.9	0.85
Oystergrounds	Terschelling 100km	2.25 µg/l	0.9	0.99
Oystergrounds	Terschelling 135km	2.25 µg/l	0.8	0.83
Oystergrounds	Terschelling 175km	2.25 µg/l	0.6	0.7
Southern Bight	Noordwijk 70 km	2.25 µg/l	2.1	1.97
Southern Bight	Walcheren 70km	2.25 µg/l	2.2	2.5

problem – area — **1.1 < *chl-a assess.***

potential – problem – area — **0.9 < *chl-a assess.* < 1.1**

non – problem – area — ***chl-a assess.* < 0.9**

Figure 3.4 shows the scatterplot of in-situ versus satellite mean CHL concentrations for the period 2006-2011 with the uncertainty estimated with MAD of 0.36µg/l corresponding to an MAPD of 12.68%. The linear regression results in a slope of 1.02 with data close to the 1:1 line ($r^2 = 0.84$).

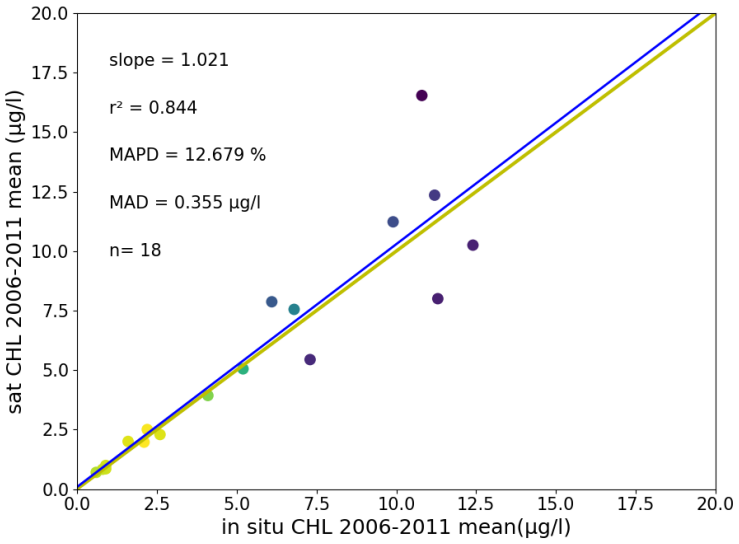

Figure 3.4: Scatterplot of mean CHL concentrations for the period 2006-2011 based on in situ and satellite CHL observations for Dutch waters. The relationship between both data sets are described by the Mean Absolute Difference (MAD), Mean Absolute Percentage Error (MAPD). The determination coefficient (r^2) and the slope characterizes the regression.

3.3.2. Assessment per assessment area

For the assessment per area we aggregated the satellite CHL data in two different ways following the protocol described in section 3.3.1:

- Only consider the satellite CHL observations at the MWTL locations to minimize the differences with the in-situ data
- Consider all satellite CHL observations per assessment area, i.e. all pixels located inside the assessment area

When results are averaged per assessment area only considering the observations at the MWTL locations, the satellite products give similar assessment results as the assessment with in-situ (Table 3.4). When considering all satellite CHL observations at full resolution (Table 3.5), the estimated area CHL mean is for most areas reasonably close to the mean based on MWTL locations only. This agreement can be explained by the fact that the areas are relatively homogeneous with respect to water quality indicators. Only in the assessment area "Coastal waters" the estimated area mean CHL concentrations based on MWTL locations only (7.1 µg/l) is 70% higher as the mean based on all 1x1 km grid cells within the assessment area (4.16 µg/l). This illustrates the bias introduced by sampling a limited number of locations in an area with strong spatial gradients (Figure 2.12). In such areas the higher spatial and temporal resolution provided by satellite observations can provide a more representative assessment, less affected by random variations caused by undersampling critical periods (e.g. spring algal bloom). This is especially valuable in areas characterized with high variability in space and time such as coastal system.

Table 3.4: *Comparison of the CHL growing season means over 2006-2011 from several data sources, with the current assessment level at each MWTL station. The CHL observations are aggregated by grouping the data for all MWTL stations per assessment area, this for both the in situ and satellite data. A color code is appointed to data source as an arbitrary indicator based on the ratio between the growing season mean and assessment level.*

Assessment Area	Assessment level	mean 2006-2011 in situ (µg/l)	mean 2006-2011 EO (µg/l)
Coastal waters	7.5 µg/l	7.1	7.71
Doggerbank	2.25 µg/l	0.9	0.85
Oystergrounds	2.25 µg/l	0.8	0.84
Southern Bight	2.25 µg/l	2.2	2.24

Table 3.5: *Comparison of the CHL growing season means over 2006-2011 from several data sources, with the current assessment level at each MWTL station. The CHL observations are aggregated by grouping the data for all MWTL stations per assessment area for the in-situ data. All satellite CHL observations per assessment area are considered, i.e. all pixels located inside the assessment area. A color code is appointed to data source as an arbitrary indicator based on the ratio between the growing season mean and assessment level.*

Assessment Area	Assessment level	mean 2006-2011 in situ (µg/l)	mean 2006-2011 EO (µg/l)
Coastal waters	7.5 µg/l	7.1	4.16
Doggerbank	2.25 µg/l	0.9	0.76
Oystergrounds	2.25 µg/l	0.8	1.04
Southern Bight	2.25 µg/l	2.2	2.16

problem – area — **1.1 < *chl-a assess.***

potential – problem – area — **0.9 < *chl-a assess.* < 1.1**

non – problem – area — ***chl-a assess.* < 0.9**

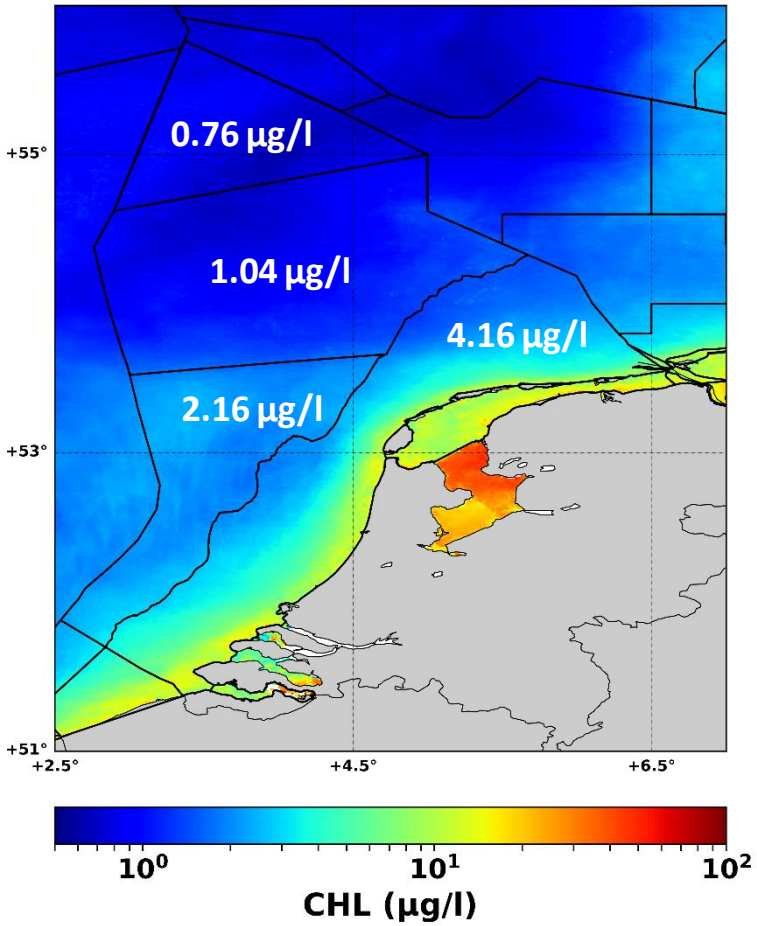

Figure 3.5. Spatial distribution of 6-year growing season mean CHL concentrations in the satellite data. Black lines represent the assessment area boundaries and white numbers in the assessment areas represent the area mean.

3.3.3. Assessment per grid cell of 1x1 km with spatially variable assessment thresholds

Assessment levels in use for eutrophication are presently incoherent between different countries, between MSFD and WFD and between different eutrophication indicators. Results from JMP-EUNOSAT Activity 1 proposed a set of coherent assessment levels for eutrophication in the North Sea based on a step-wise approach. Assessment levels for eutrophication in the North Sea have been defined as a justified area-specific percentage deviation from natural reference conditions not exceeding 50%. Therefore, we first chose a common definition of "natural reference conditions" as the year 1900. The corresponding nutrient loads were calculated with the European catchment model E-HYPE by SMHI. Corresponding nutrient concentrations under natural reference conditions in the North Sea were calculated with the DFLOW-FM model for the North Sea by Deltares. Next, the corresponding CHL concentrations were calculated with two modelling approaches: a statistical GAM model and the deterministic model BLOOM. This approach resulted in spatially variable CHL threshold map as presented in figure 3.6 (right) for the North Sea region with a spatial resolution of 1x1km corresponding to the grid used for the satellite data.

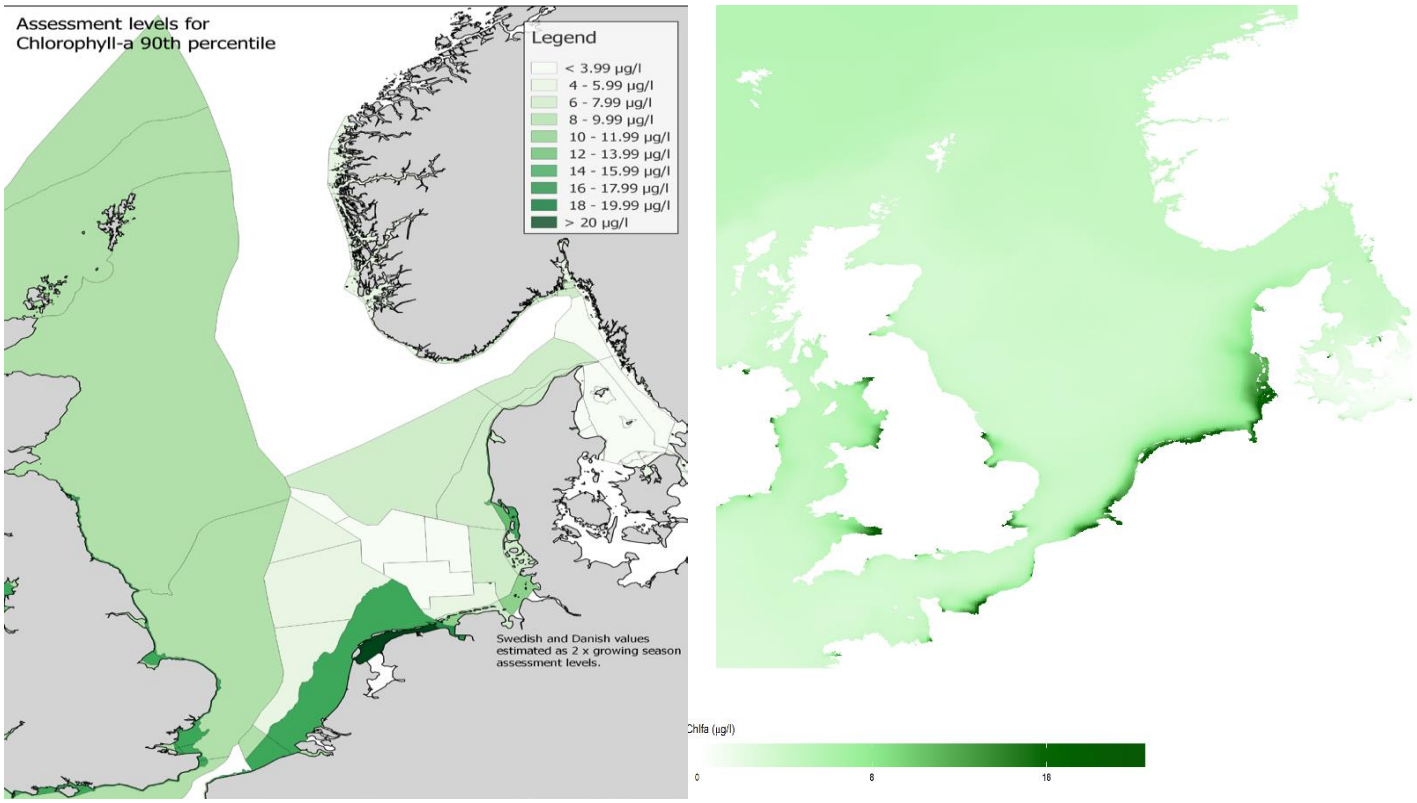

Figure 3.6 (left) Assessment levels for the 90-percentile CHL concentration during the growing season currently used in eutrophication assessment for MSFD showing incoherency between assessment areas. (right) Spatially coherent assessment levels for the mean CHL concentration proposed by Activity 1 with a spatial resolution of 1x1km corresponding to the grid used for the satellite data.

A pixel by pixel eutrophication assessment was performed by directly comparing the satellite data with the assessment thresholds. A color code is appointed to the pixel-wise assessments as an arbitrary indicator based on the ratio between the growing season mean for the period 2006-2011 and assessment level. The assessment is considered: 'non-problem' for a ratio smaller than 0.9, 'potential problem' if the ratio is between 0.9 and 1.1 and 'problem' if the ratio is bigger than 1.1 (Figure 3.7).

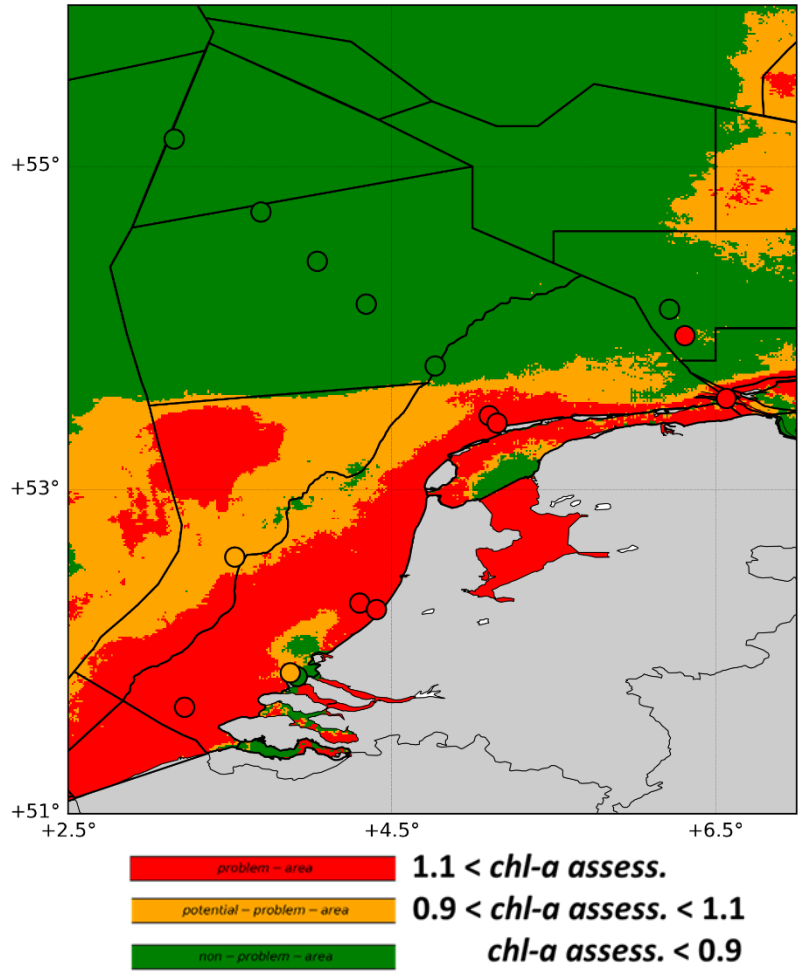

Figure 3.7: Classification map of the mean CHL product (2006-2011) for the Dutch waters with a color code appointed as an arbitrary indicator based on the ratio between the growing season CHL mean and assessment level. Circle markers show the assessment based on in-situ data. The national monitoring zones are overlaid in black

Table 3.6 shows the mean CHL concentrations for the period 2006-2011 based on both in situ data and the quality-controlled merged CHL data for all MWTL station with the new assessment level at each MWTL station as proposed by Activity 1. The satellite CHL products give the same assessment results as in-situ data for all MWTL locations, except for Goeree 2km and Rottumerplaat 50km. Station Goeree 2km shows higher mean CHL concentrations in the satellite data compared to the in-situ data resulting in the different assessment. For station Rottumerplaat 50km the mean CHL concentrations are more comparable between satellite and in-situ data and are both below the assessment level. However, the satellite observations hoover around the threshold value in that pixel.

Table 3.6. Comparison of the CHL growing season means over 2006-2011 from several data sources, with the new assessment levels at each MWTL station. A color code is appointed to data source as an arbitrary indicator based on the ratio between the growing season mean and assessment level.

Assessment Area	Station	Assessment level (µg/l)	mean 2006-2011 in situ (µg/l)	mean 2006-2011 EO (µg/l)
Coastal waters	Goeree 2km	16.52	10.8	16.54
Coastal waters	Goeree 6km	12.38	11.2	12.35
Coastal waters	Noordwijk 10km	5.62	6.8	7.55
Coastal waters	Noordwijk 2km	6.22	9.9	11.23
Coastal waters	Noordwijk 20km	4.40	5.2	5.05
Coastal waters	Rottumerplaat 3km	7.15	11.3	8
Coastal waters	Rottumerplaat 50km	2.71	2.6	2.29
Coastal waters	Rottumerplaat 70km	2.33	1.6	2
Coastal waters	Terschelling 10km	3.86	4.1	3.93
Coastal waters	Terschelling 4km	4.59	6.1	7.87
Coastal waters	Walcheren 2km	4.82	12.4	10.25
Coastal waters	Walcheren 20km	3.62	7.3	5.44
Doggerbank	Terschelling 235km	1.79	0.9	0.85
Oystergrounds	Terschelling 100km	1.84	0.9	0.99
Oystergrounds	Terschelling 135km	1.78	0.8	0.83
Oystergrounds	Terschelling 175km	1.79	0.6	0.7
Southern Bight	Noordwijk 70 km	1.95	2.1	1.97
Southern Bight	Walcheren 70km	1.93	2.2	2.5

Table 3.6 shows the traffic light color system of the OSPAR Common Procedure: problem area (red), non-problem area (green) and potential problem area (amber). Having two (or three) classes is quite limiting in terms of assessing gradual improvement of the GES of an assessment area. With a satellite-based classification CHL product as presented in figure 3.5 it is possible to determine the surface of an assessment zone that is exceeding the assessment threshold, both fixed or variable (Annex I, Figure 3.4). Figure 3.6 (left) shows the evolution in time of the percentage surface of the Dutch assessment areas which falls into the category of 'problem area' (i.e. red zone in Figure 3.5) as an objective indicator of eutrophication based on yearly composites compared to the traditional assessment levels. It shows that when using the standard thresholds, the 'Southern Bight' area has the highest portion of its surface above the assessment level (i.e. 2.25µg/l). It also shows high variability through the years with values ranging from 5.95% (2000) to 84.15% (2013) which is explained by the fact that the observed yearly mean CHL values are very close to the assessment level causing this erratic variation. The 'Coastal waters' area has the second highest percentage surface eutrophied ranging from 1.41% (2000) to 19.60% (2008). It can be considered illogical that the eutrophication problem increases with the distance to the coast between these two areas as the 'Coastal waters' are affected more intensely by riverine input of nutrients. This can be explained by the different in assessment levels between the two areas: 7.5µg/l for the 'Coastal waters' and 2.25µg/l for the 'Southern Bight' where only a limited band of the 'Coastal waters' exceeds this level (Figure 3.3) while the entire surface of the 'Southern Bight' has CHL estimates close to the threshold. This problem can be partially solved by using spatially variable assessment levels (Figure 3.6 right) resulting in a closer match between the areas 'Coastal waters' and 'Southern Bight'. Both areas show similar temporal

eutrophication patterns ranging from 5.76% (2000) to 79.13% (2008) for the 'Coastal waters' and from 19.68% (2000) to 96.10% (2013) for the 'Southern Bight'.

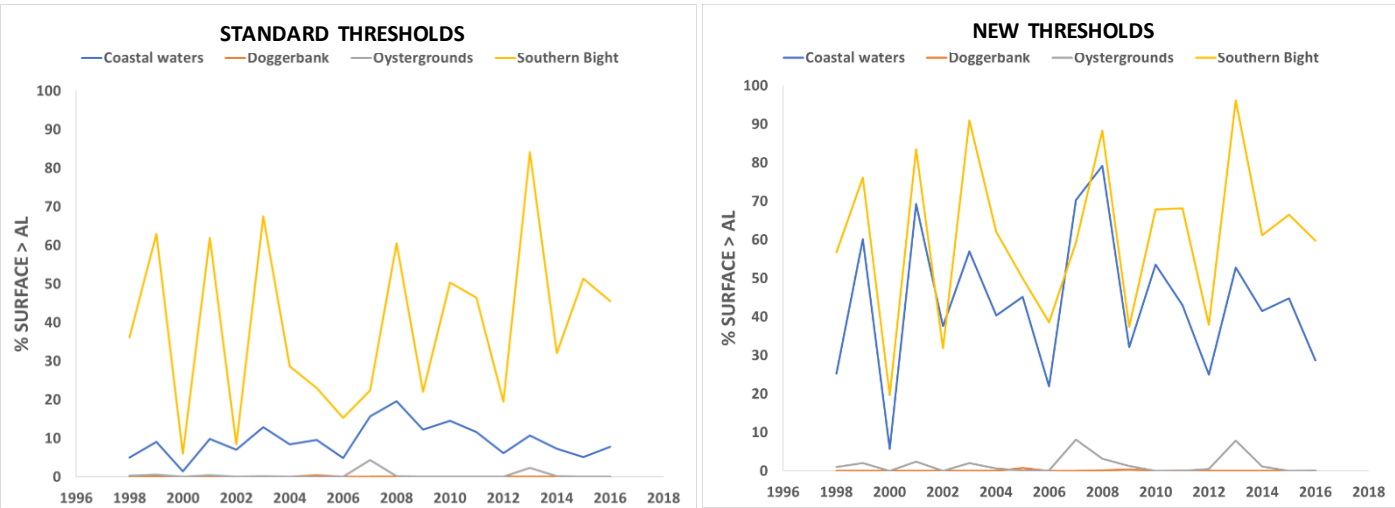

Figure 3.6. The percentage surface of the Dutch assessment areas of which the yearly mean CHL concentrations exceed the traditional (left) or spatially variable (right) assessment levels.

3.3.4. New assessment areas

Next to spatially variable assessments levels, Activity 1 also proposed new assessment areas to replace the current national assessment areas which do not reflect national borders but cross-border areas that are determined by the characteristics of the North Sea ecosystem that are relevant for the assessment of eutrophication. This resulted in assessment areas that share similar environmental conditions within one area which can be distinguished from the conditions in other areas (Annex II). The need for new assessment areas is demonstrated in section 3.3.2 where the Dutch national assessment area 'Coastal waters' shows a strong gradient in CHL concentrations perpendicular to the coast resulting in differences in eutrophication assessments when using in-situ observations compared to satellite observations. Figure 3.7 shows these new assessment areas compared to the national borders.

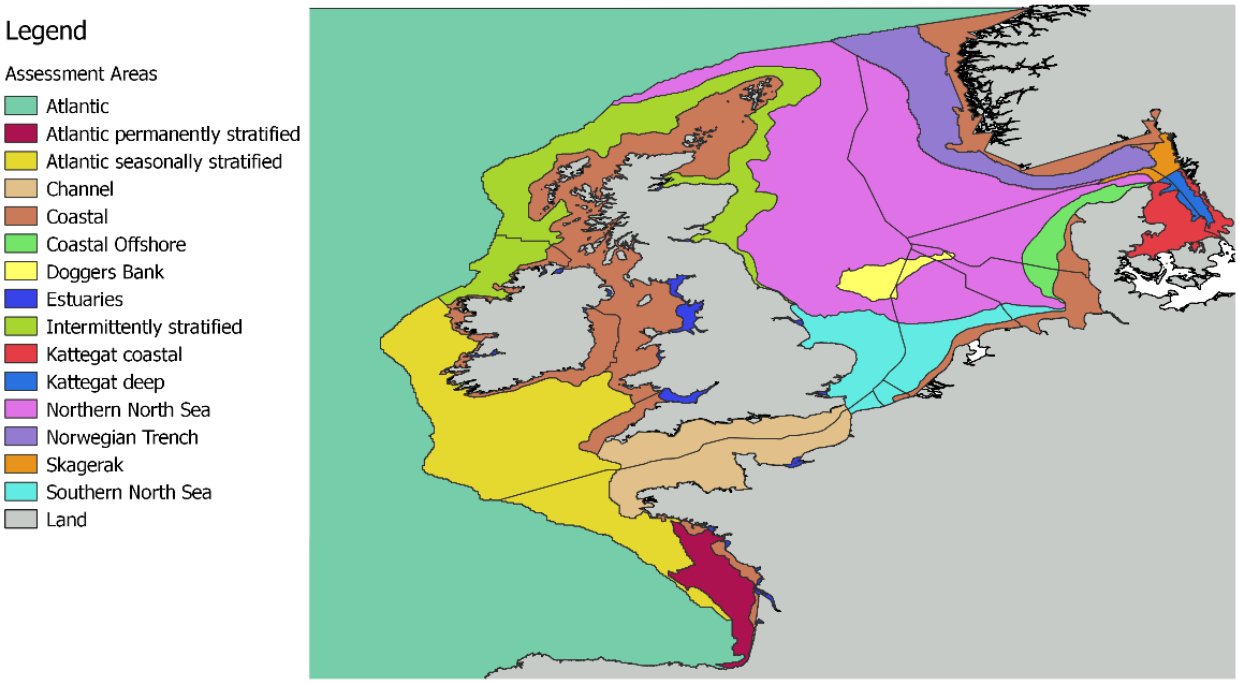

Figure 3.7: Definition of assessment areas based on duration of stratification, mean surface salinity and depth.

Similar to section 3.3.2, we aggregated the satellite CHL data per new assessment area, i.e. all pixels located inside the new assessment areas to obtain a mean CHL concentration for the growing season March-September for the period 2006-2011. Additionally, we calculated the mean assessment level from the spatially variable CHL threshold map enabling a direct assessment by determining the ratio between the mean CHL concentration and mean assessment level per new assessment area. A color code is appointed to the pixel-wise assessments as an arbitrary indicator based on the ratio between the growing season mean for the period 2006-2011 and assessment level. The assessment is considered: 'non-problem' for a ratio smaller than 0.9, 'potential problem' if the ratio is between 0.9 and 1.1 and 'problem' if the ratio is bigger than 1.1. Table 3.7 provides the eutrophication assessment for the period 2006-2011 based on satellite observations, the new spatially variable assessment levels and new assessment areas. The same information is spatially represented in a map product in figure 3.8.

Table 3.7 Comparison of the CHL growing season means over 2006-2011 from satellite observations, with the average assessment levels per new assessment region. A color code is appointed to data source as an arbitrary indicator based on the ratio between the growing season mean and assessment level.

zone	CHL_mean (µg/l)	average threshold (µg/l)
# 1:Atlantic	0.84	2.59
# 2:Atlantic Perm. Strat. (no data)		
# 3:Atlantic Seas. Start.	0.68	1.49
# 4:Atlantic Seas. Start	0.88	1.75
# 5:Channel Fr	1.66	2.05
# 6:Channel UK	1.36	1.78
# 7:Coastal No	1.86	2.23
# 8:Coastal IR	1.66	2.40
# 9:Coastal UK south	1.43	2.11
# 10:Coastal UK North	1.69	2.05
# 11:Coastal BE	9.36	6.40
# 12:Coastal NL	9.66	7.60
# 13:Coastal GE	7.88	8.69
# 14:Coastal DK	6.50	4.71
# 15:Coastal Offshore GE	2.79	2.82
# 16:Coastal Offshore GE	2.66	2.79
# 17:Doggersbank	1.03	1.76
# 18:Doggersbank	0.76	1.82
# 19:Doggersbank	0.76	1.82
# 20:Doggersbank	0.87	1.80
# 21:Estuary Fr	9.39	11.56
# 22:Estuary Gironde (no data)		
# 23:Estuary UK	7.07	5.80
# 24:Interm. Strat. IR	1.00	1.45
# 25:Interm. Strat. UK	1.32	1.95
# 26:Kattegat Coastal	3.60	1.87
# 27:Kattegat Coastal	4.35	1.99
# 28:Kattegat Deep	1.36	2.08
# 29:Kattegat Deep	1.67	2.07
# 30:Central NS (central)	0.84	2.07
# 31:Central NS	0.79	1.82
# 32:Central NS NL	1.04	1.87
# 33:Central NS GE	1.51	2.12
# 34:Central NS	0.93	1.96
# 35:Central NS		
# 36:Central NS	0.92	1.99
# 37:Central NS	0.77	1.82
# 38:Central NS	0.71	1.83
# 39:Norwegian Trench	1.27	2.24
# 40:Skagerrak	0.95	2.17
# 41:Skagerrak	2.12	2.23
# 42:Southern North Sea GE	2.66	3.16
# 43:Southern North Sea FR	4.33	2.36
# 44:Southern North Sea UK	2.76	2.17
# 45:Southern North Sea BE	4.54	3.13
# 46:Southern North Sea NL	2.80	2.54

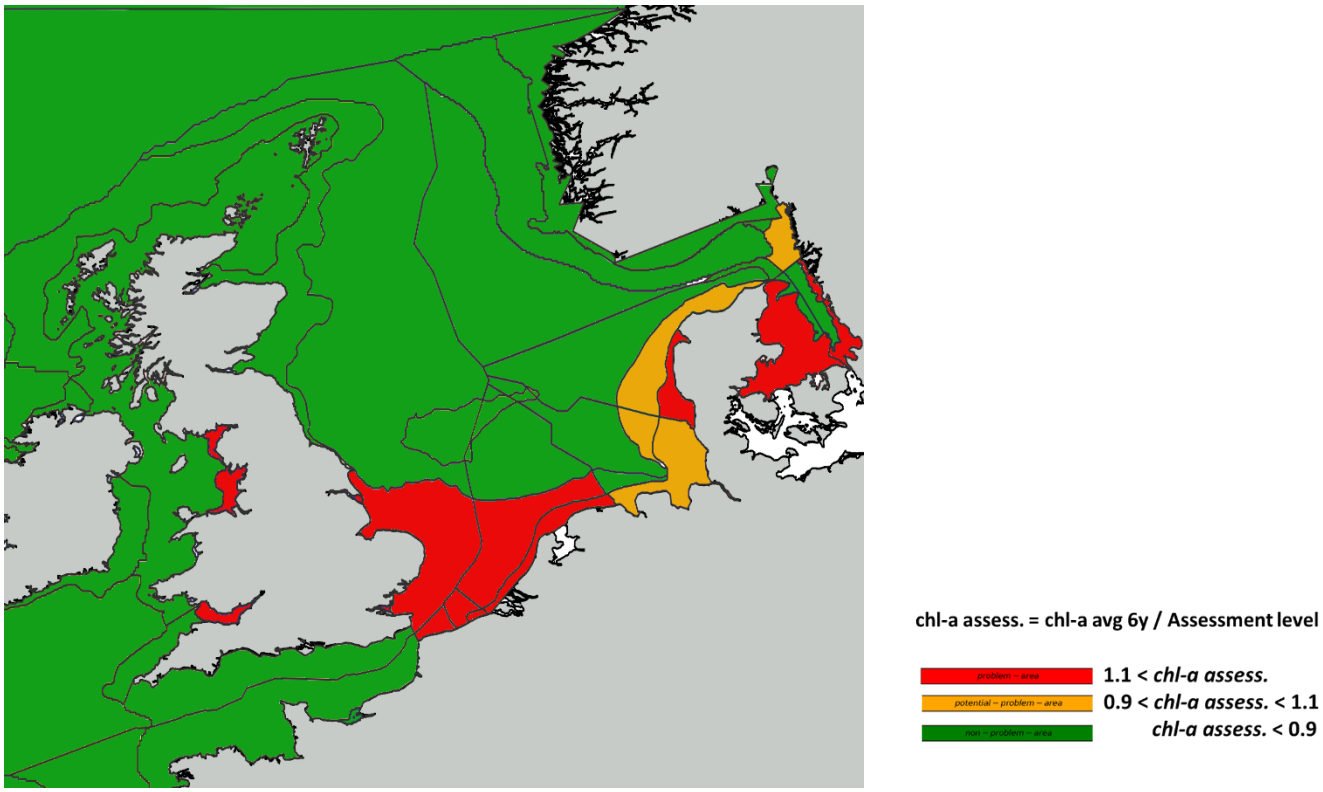

Figure 3.8: Classification map of the mean satellite-based CHL product (2006-2011) for the North Sea region with a color code appointed as an arbitrary indicator based on the ratio between the growing season CHL mean and mean assessment level per new assessment region.

3.4. Conclusions

Including high spatial resolution data into an eutrophication assessment requires different data processing and results may differ from the traditional assessments based on in-situ data. The objective of this Dutch case study was to evaluate how different data sources (in-situ vs satellite data) and data processing methods affect the assessment results.

Assessment using traditional assessment levels with satellite data gave similar results as in-situ data in Dutch waters for assessment at MWTL locations only which is to be expected from the strong correlation between in-situ and satellite 6-year mean CHL concentrations per MWTL station. Still, this approach would completely negate the advantage provide by satellite sensors in terms of spatial resolution. When considering all satellite CHL observations at full resolution, the estimated area CHL mean is for most areas reasonably close to the mean based on MWTL locations only when the areas are relatively homogeneous with respect to water quality indicators. Only in the assessment area "Coastal waters" the estimated area mean CHL concentrations based on MWTL locations only is 70% higher as the mean based on all 1x1 km grid cells within the assessment area. In areas with strong spatial gradients, the assessment results are very sensitive to the area boundaries and the choice of in-situ monitoring locations. The assessment levels for dissolved inorganic nitrogen (DIN) for example are corrected for salinity to take the effect of the cross-shore gradient into account. A similar approach for chlorophyll-a concentrations would make the assessments more robust.
A solution for this problem is the use of spatially variable CHL assessment levels with a spatial resolution of 1x1km corresponding to the grid used for the satellite data. This enables a pixel by pixel eutrophication assessment by directly comparing the satellite data with the assessment levels. In Activity 1 new coherent assessment levels and assessment areas were proposed as used here in the Dutch case study. Spatially variable assessment levels instead of fixed levels result in a more consistent relative exceedance of the assessment levels throughout the assessment area. Consequently, the result is less dependent on the definition of assessment areas. Such spatially varying assessment levels allows for making better use of the full spatial resolution that satellite data can provide. Another possibility is to re-organize the assessment areas into zones that share similar environmental conditions within one area which can be distinguished from the conditions in other areas.

The MSFD system using only two classes (good and bad) is quite limiting in terms of assessing gradual improvement of the status of an assessment area relative to the threshold indicating good environmental status. Using more classes, such as in the WFD, would give more information on changes. Regarding the extent to which good environmental status has been achieved in an assessment area, the satellite-based eutrophication product can easily determine the extent of the area that is not subject to eutrophication, using fixed or variable thresholds, and determine its evolution in time as an objective measure of changes in eutrophication status.

4. Evaluation of suitability of satellite data for coherent CHL assessments in the North Sea

Traditional methods for eutrophication monitoring in coastal waters involve in-situ sampling/measurements of commonly measured parameters such as nutrients concentration, CHL concentration, phytoplankton abundance and composition, transparency and dissolved oxygen concentration. Concerning available methods for in situ measurements, ships provide flexible platforms for eutrophication monitoring, while remote sensing provides opportunities for a synoptic view over regions or sub-regions, but only for CHL concentrations. In the most part of the North Sea, obtaining synoptic observations with in-situ observations is difficult or even impossible, especially in off-shore areas. Remote sensing generally provides data with a higher spatial and temporal resolution compared to in-situ measurements. This makes satellite data useful for large-scale eutrophication assessments and for studies of temporal trends. Such studies enable the mapping of phytoplankton dynamics which differ in terms of algae bloom onsets and peaks between regions and even within the same regional assessment areas. In this section we discuss the factors which determine the quality of the satellite-observations and provide an overview of circumstances where remote sensing observations could be unsuitable for CHL assessments and where in-situ observations are required to obtain relevant information.

One major limiting factor of ocean color remote sensing is cloud cover so high frequency satellite data can be more relied upon in southern Europe than in the north. Additionally, we performed different quality controls and merging techniques to upgrade core ocean color satellite products, as delivered by CMEMS and ODESA, to operational and coherent monitoring products usable for eutrophication assessment in the Greater North Sea giving special attention to optically complex coastal waters (section 2 and 3). Optically complex coastal waters pose many challenges for satellite remote sensing to accurately retrieve biogeochemical parameters such as CHL concentration due to varying concentrations of suspended particulate matter (SPM) and colored dissolved organic matter (CDOM). Still, there were situations (e.g. near-shore coastal waters, CDOM dominated waters) were no suitable CHL product was available which resulted in additional flagged pixels on top of the cloud cover. To identify regions where EO data frequency is low we plotted the number of available satellite observations per growing season (March-September) for the JMP-EUNOSAT region for two years which represent key periods: 2006 as a year with MERIS and MODIS data available and 2015 without with only MODIS data available after the operational failure of MERIS in April 2012 (Figure 4.1). The availability of MERIS data has a significant impact on data availability, especially in turbid coastal waters in non-MERIS periods as the GONS CHL are not available for NASA's sensors due to the missing of the crucial 709nm spectral band.

This can be observed in regions with a critical low number of available EO observations to properly describe the CHL dynamics:

- Estuaries (e.g. Thames estuary, Scheldt Estuary)
- East Anglia Plume
- Wadden Sea
- near-shore coastal zones (e.g. UK, BE, NL, GE, DK)
- Fjords (e.g. Oslo Fjord)

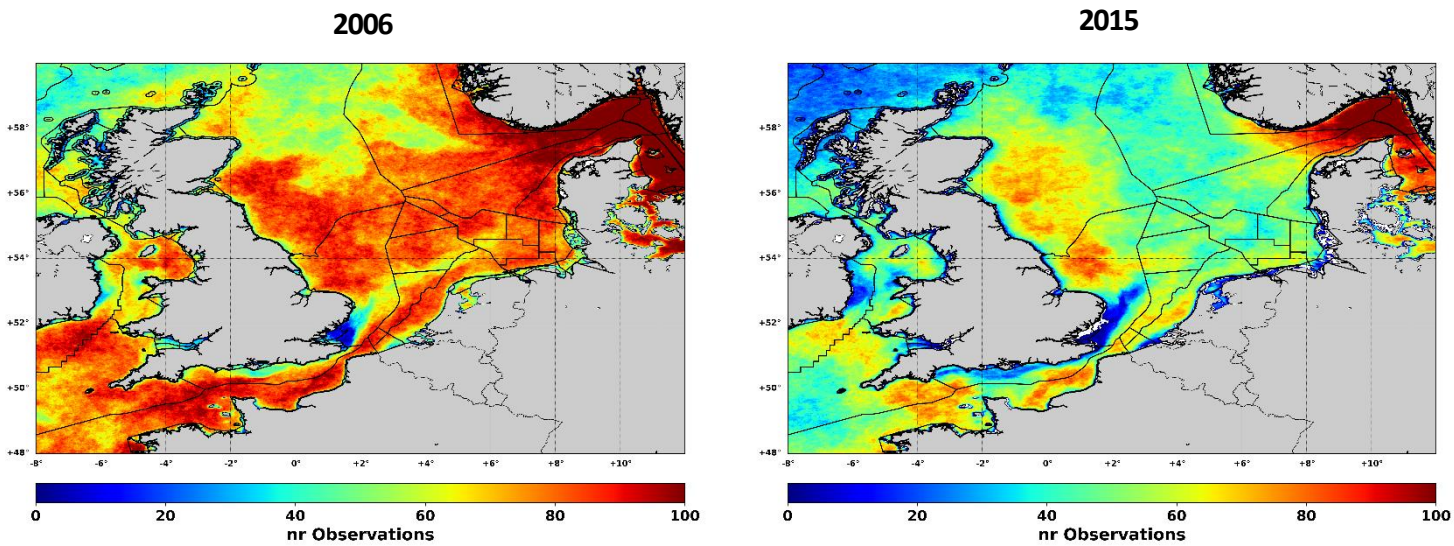

Figure 4.1: Map representing of number of available satellite CHL observations per growing season (March-September) for the years 2006 and 2016. Variability in data availability is caused by cloudiness, quality flagging and sensor malfunction.

Figure 4.2 provides an example of data availability in a near-coast area in turbid Dutch coastal waters near the MWTL Noordwijk stations, located 2km and 10 km from the coast and assessment of the suitability of EO data for eutrophication assessment. For each of these stations we extracted the satellite CHL time series following the protocol described in section 2.5.2 and compared them to in-situ observations collected in the Dutch monitoring programme. The 'Noordwijk 2km' station is located in the near-coast band where we see a significant lower number of available satellite observations, especially in the non-MERIS period. While the quality-controlled EO CHL products provides reliable observations for the period 2003-2011 but no reliable assessment is possible outside of this period due to a critical low number of available EO CHL observations. Future assessments can use the Sentinel-3 data which resembles the MERIS data. For the 'Noordwijk 10km' data is available for the full 1998-2017 period and satellite-based CHL observations can be considered suitable for eutrophication assessment.

Another example of satellite suitability for eutrophication assessment is provided for the Belgian Coastal zone in figure 4.3 showing similar near-coast effects which are strengthened by the presence of the Scheldt estuary and harbor of Zeebrugge (W01 station) resulting in high SPM values ranging from 20 to 75 mg/l (Fettweis et al., 2010). Satellite CHL time series were extracted for the W01 station and compared to in-situ observations collected in the Belgian monitoring programme. We observed a critical lower number of available satellite observations in the non-MERIS period resulting in unreliable EO data for eutrophication assessment.

Still, satellite data are often gappy due to the presence of clouds, lack of satellite coverage and observations rejected by quality control or a coastal mask and there has been work done to fill these gaps using interpolation approaches such as DINEOF. Data Interpolating Empirical Orthogonal Functions (DINEOF) is a self-consistent, parameter-free technique used to reconstruct this missing data based on temporal and spatial information. The suitability of this approach to complete missing data in problematic regions as presented for the Belgian Coastal zone has been investigated. More technical information about the DINEOF approach can be found in Alvera-Azcárate et al. (2005). An example of a reconstructed time series for the Belgian W01 station is demonstrated in figure 4.3. Using this technique, we were able to reconstruct the typical seasonal bloom dynamics as found in Belgian waters which match well with the in-situ observations. As an additional test of the usefulness of the use of DINEOF the daily match up validation using the Dutch in-situ data was redone using the DINEOF interpolated JMP-EUNOSAT CHL archive. Figure 4.4 shows the scatterplots of in-situ observations versus satellite observations, with and without the DINEOF technique applied. Applying the DINEOF technique results in an significant increase of available match ups as expected (216 to 755) without strongly changing the correlation statistics showing the potential of this approach to improve satellite-based observations for regions where satellite data availability is limited.

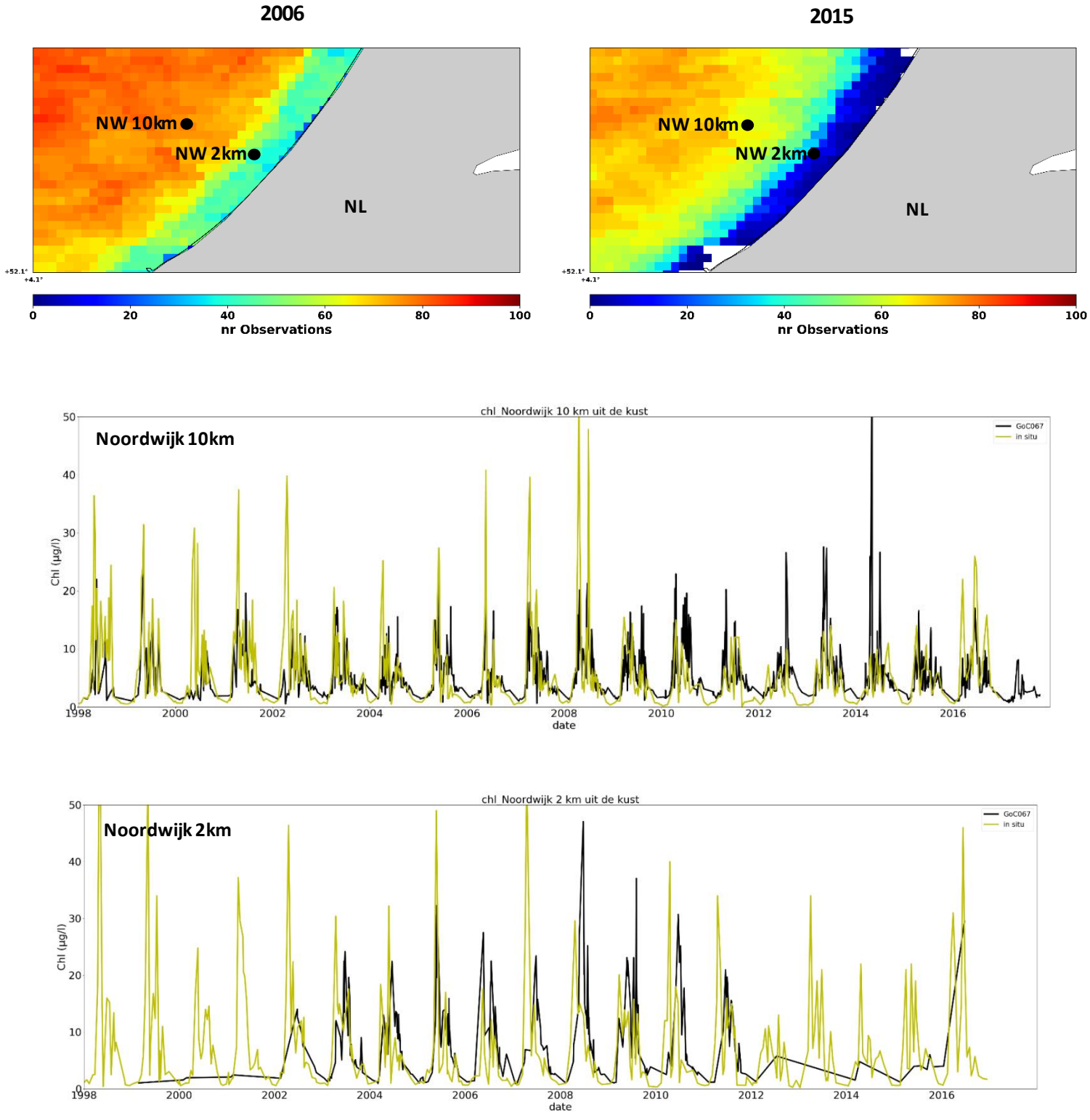

Figure 4.2: Map representing of number of available satellite CHL observations per growing season (March-September) for the years 2006 and 2016 in the Dutch coastal zone near stations Noordwijk 2km (NW 2km) and Noordwijk 10km (NW 10km). For each of these stations CHL time series are presented based on both satellite (black line) and in-situ (yellow line) observations.

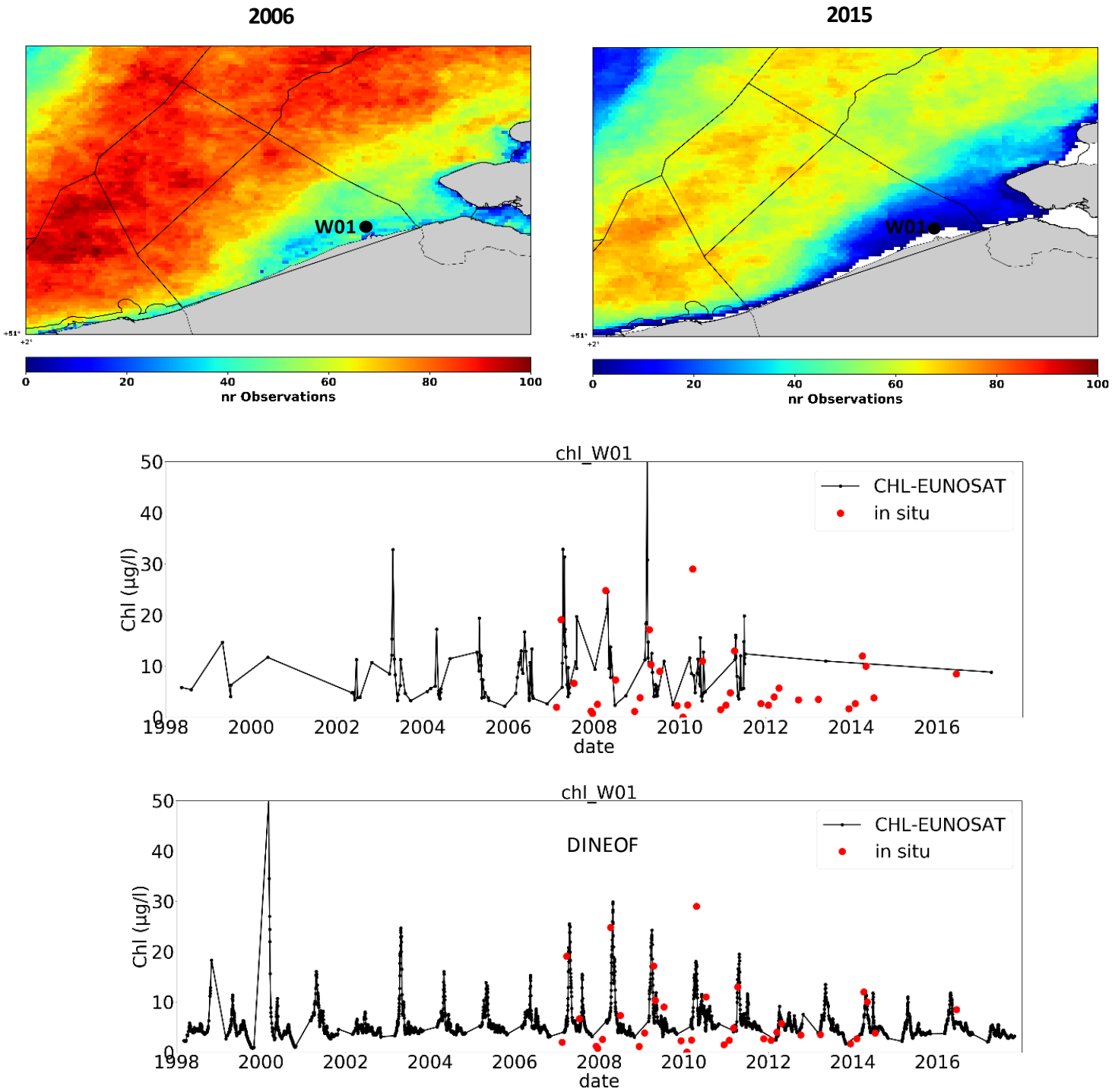

Figure 4.3: (top) Map representing of number of available satellite CHL observations per growing season (March-September) for the years 2006 and 2016 in the Belgian coastal zone. (middle-bottom) Time series of satellite-derived CHL (black line) superimposed on in situ CHL observations (red dots) for station W01 for the period 1998 -2017. The top time series shows the merged JMP-EUNOSAT CHL product with missing observations outside the period 2003-2011 (MERIS period) due to the station's proximity to the coast. The bottom time series shows the reconstruction using DINEOF.

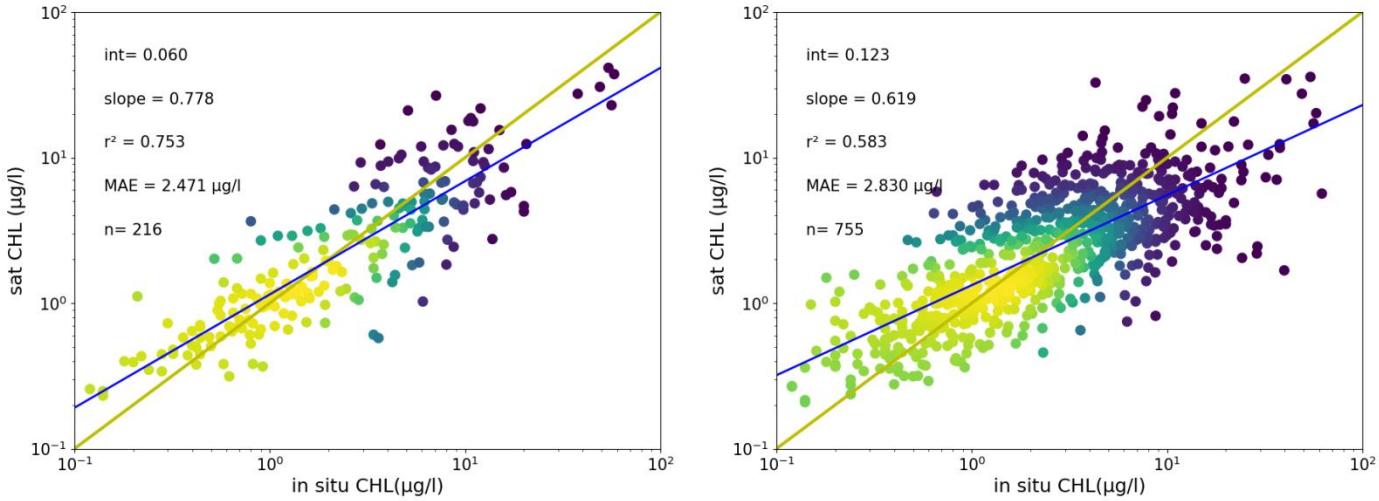

Figure 4.4. Scatterplots of in situ and satellite CHL observations for the Netherlands using the JMP-EUNOSAT CHL archive, without (left) and with DINEOF interpolation (right). The relationship between both data sets are described by the Mean Absolute Difference (MAD), Mean Absolute Percentage Error (MAPD). The determination coefficient (r^2) and the slope characterizes the regression.

Generally, it can be stated that more quality-controlled satellite data is available in the period 2003 to 2011, also in near-coast zones. Sentinel-3/OLCI has a similar spectral bandset as MERIS which is useful to provide more reliable results in turbid coastal waters. Additionally, the full resolution data (300m spatial resolution), compared to the 1km resolution of the products used here, will provide more robust CHL estimates close to the coast and in estuaries. Sentinel-3A was launched early 2016 so we expect to have more quality controlled CHL products available for these problematic regions from 2016 forward. Next to the traditional ocean color sensors, sensors like Sentinel-2/MSI which are originally designed for land observation can also be used to monitor near-coast marine regions providing satellite observation with a spatial resolution of up to 10m (Ruddick et al., 2016).

In summary we can conclude that satellite data are suitable:

- In optically simple waters (case 1 waters)
- In optically complex waters (case 2 waters) after applying the quality control as described in section 2.4.
- in offshore areas where taking in situ measurements is costly
- in areas where no in situ data is available
- for comparisons of the eutrophication status over large subregions
- in addition to in situ measurements.

In situ measurements are more suitable:

- in (sub)regions with an increasing eutrophication problem, and high quality data is required
- in near-shore coastal areas where satellite data availability is insufficient
- in optically complex coastal waters where no optical CHL algorithm can provide accurate CHL estimates (e.g. CDOM rich waters)
- in subregions where for other reasons accurate and reliable data are needed (e.g. river estuaries)

Remote sensing observations can be considered as alternatives or in addition to in situ measurements, depending on the requirements with respect to data. Still, in situ measurements will always remain necessary to validate and calibrate EO-based CHL products.

4.1. Evaluation of suitability of CHL time series for eutrophication assessment

The eutrophication status is not established based on singular CHL observations but is based on a statistical representation (mean or P90) of 6-year CHL time series which can be calculated both using the in-situ data and satellite data. Except for the problem areas described above, satellite observations provide a better temporal and spatial coverage compared to in-situ monitoring and thus are potentially better suited to provide multi-temporal statistical estimates. However, the irregular availability of satellite chlorophyll-a observations both in space and time due to cloudiness, quality flagging, sensor malfunction, etc. has to be considered as it impacts the product accuracy. This impact is two-fold and dependent on (1) the availability of observations during the actual phytoplankton bloom and (2) a proportional distribution of observations in the bloom and non-bloom period. Figure 2.44 illustrates this by showing how a different timing of 50 samples on the same CHL time series can result in significantly different CHL-P90 estimates. From this example it is obvious that sufficient sampling of the bloom period is crucial for generating an accurate CHL-P90 product but can still lead to errors in case of under- or oversampling compared to the non-bloom period.

This effect of irregular sampling on the accuracy of a 90-percentile product (CHL-P90) was studied in detail in simulations by Van der Zande et al. (2011). In this study an ecosystem model was used to generate realistic time series of chlorophyll-a concentrations with high temporal resolution in the most important Belgian monitoring stations. These time series were sub-sampled using the actual observation density of the MERIS satellite in Belgian waters. Results show that a mean relative error of 25.4% on CHL-P90 estimate can be expected due to the effects of irregular sampling. The results of this study were used to improve the CHL-P90 algorithms by adding a weighing procedure taking into account irregular sampling issues to reduce these errors to 9.9%.

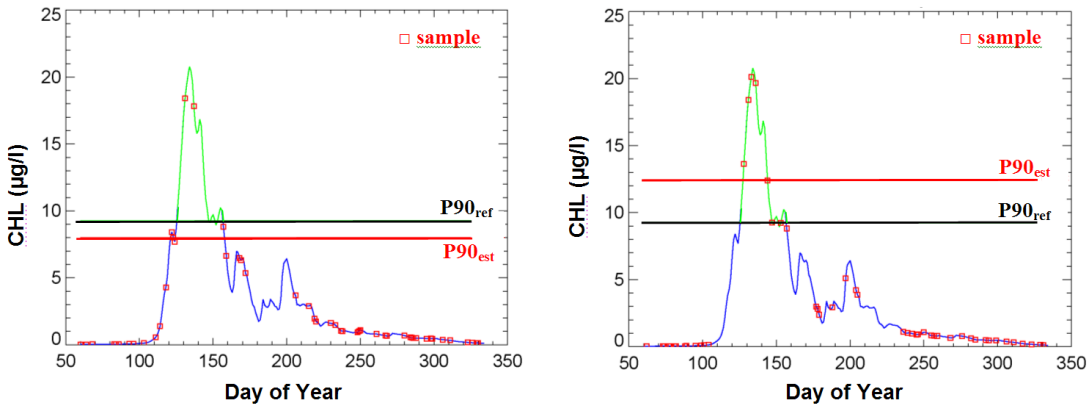

Fig 4.5. Illustration of the impact of two different timings of 50 samples on the same CHL time series on CHL-P90 estimates. Blue/green line: time series of CHL computed by ecosystem model for the year 2006 for a single Belgian monitoring station (51,27°N-2,91°W) with the phytoplankton bloom marked in green. $P90_{ref}$ (black line) and $P90_{est}$ (red line) are the percentile 90 computed respectively from the daily data and from a subsample of 50 data

When using CHL time series, both from in-situ or satellite observation, product quality is essential. While most studies only consider the accuracy of individual satellite CHL measurements, additional errors generated in multitemporal products should not be neglected. This sensitivity study allowed more insight into the impact of sampling irregularities on the final product which should be considered carefully as significant errors were found. The proposed approach provides a tool to consider sampling issues resolving a significant part of this problem without the need for additional data. This theoretical study can be transformed into an operational approach by replacing the ecosystem model by long term satellite climatologies to provide a pixel-based CHL time series. These reference time series can be resampled according to actual in-situ and satellite sampling frequencies providing an evaluation of the quality of the time series. The combination multi-temporal CHL estimates (mean, P90) and an error estimate using this approach can be considered as a more complete product needed by policy makers for WFD and MSFD reporting requirements.

Additionally, these accuracy assessments of both in-situ and satellite CHL time series can be used to objectively determine an optimal way to merge the two data sets together for eutrophication assessment as done in the HELCOM approach (i.e. HEAT tool). In this approach the multi-temporal estimates (in-situ and satellite) are merged together by taking a weighted mean where the weights are chosen arbitrarily or based on expert knowledge. These weights could be determined more objectively based on the accuracy of each of the CHL time series, i.e. more weight given to in-situ observations when accuracy of in situ CHL time series is higher than satellite CHL time series and vice versa.

5. Conclusions and recommendations

For efficient monitoring of eutrophication, it is advised to combine all available monitoring platforms, i.e. dedicated monitoring surveys taking water samples, Ferryboxes mounted on 'ships of opportunity' and satellite observations. In this way, the strengths and weaknesses of one platform can be compensated by another in terms of spatial and temporal resolution, sampling depth, ability to measure different variables, analytical precision and costs. The use of satellite data has been identified as a promising scientific development by JRC in their "In-Depth Assessment of the EU Member States' Submissions for the Marine Strategy Framework Directive under articles 8, 9 and 10" as the use of remote sensing techniques can complement the scarcity of field measurements which has increased during the last decade. Budgets available for marine monitoring are decreasing in many European countries and they struggle to obtain sufficient data for a reliable GES assessment. Efficient use of monitoring resources is therefore needed more than ever. Satellite data of chlorophyll combine cheaper data collection with a much improved geographical and temporal coverage. To enable such a combined use of different data sources, there is a need for a scientifically sound procedure to feed data collected with different methods into one common indicator for the assessment (e.g. CHL) describing both the state and the development of the pelagic environment.

The use of satellite data for assessments requires an open eye for current methods, including baselines and thresholds, and flexibility to achieve better coherence. Satellite data from ocean color sensors (i.e. SeaWiFS, MODIS, MERIS, VIIRS, Sentinel-3) can provide spatially coherent data on CHL concentrations using a variety of CHL retrieval algorithms (e.g. blue/green-ratio algorithms, red-NIR algorithms or Neural Networks). However, because of the optical complexity of coastal waters, retrieving accurate CHL estimates is challenging. The CHL algorithms are often regional or only apply to a certain water type (e.g. clear waters, turbid waters, CDOM rich waters) making it difficult to apply them to a region such as the North Sea as water properties vary between and within regions so that only one algorithm is generally not adapted to the whole study area. To fill this gap, we presented a methodology to determine the reflectance conditions for which these algorithms can deliver an accurate CHL estimate in complex optical conditions as found in coastal waters. Results show that by applying the quality control per algorithm, performances of the selected algorithms are improved and almost reach the standards expected in open ocean for direct match ups (i.e. 30% error). Next, the best combination of quality controlled CHL algorithms is determined to produce a quality controlled multi-algorithm satellite CHL product based on best suited algorithm/water type combination. Data distribution centers such as CMEMS and ODESA online played a key role in this endeavor as they provide analysis-ready validated ocean color products as input for the JMP-EUNOSAT processing chain.

The suitability of the blended CHL product for eutrophication assessment was evaluated by a comparison analysis with in situ datasets for all assessment areas in the greater North Sea provided by the consortium members. Ocean colour algorithms are generally calibrated using HPLC in situ measurements. In this study, in-situ CHL estimates obtained through different techniques were used, i.e. HPLC, spectrophotometry, fluorimetry. As expected there was a better agreement for the HPLC measurements, but it was important for the consortium partners who are using spectrophotometry or fluorimetry methods to have an objective

assessment of how the satellite products compare to their in-situ data sets and how it could impact their eutrophication assessments. A daily match up analysis with the complete in-situ observations resulted in a median error of 45.26%. Eutrophication assessments for the MSFD are performed on multi-temporal composites of these daily CHL products, i.e. mean or P90 over a growing season. A validation of the yearly mean and P90 CHL products yielded a median error of 35.19% and 39.05% respectively showing a good general agreement between in-situ and satellite observations. However, stronger differences between in-situ and satellite products were observed in cases of: 1) complex optical water type (e.g. CDOM dominated waters), 2) use of spectrophotometry or fluorimetry as in-situ analysis technique, 3) proximity of the monitoring station to the coast (e.g. < 1 to 2 km) and 4) the unavailability of the 709nm spectral band (non-MERIS or Sentinel-3 periods) crucial for the GONS and NN CHL products which are optimized for highly turbid and eutrophied coastal areas.

Considering the spatial and temporal availability of the quality-controlled multi-algorithm CHL product we can conclude that remote sensing provides opportunities for a synoptic overview of the CHL concentrations of most part of the North Sea. Gathering similar synoptic observations with in-situ observations is difficult or even impossible, especially in off-shore areas. This makes satellite data useful for large-scale eutrophication assessments and for studies of temporal trends (e.g Annex III). Such studies enable the mapping of phytoplankton dynamics which differ in terms of algae bloom onsets and peaks between regions and even within the same regional assessment areas. However, there are circumstances where remote sensing observations are unsuitable for CHL assessments and where in-situ observations are required to obtain relevant information. There is a significant advantage with the availability of the MERIS sensor (2003-2011) in terms of providing specialized products for optically complex waters. Outside of the MERIS period we observed critically low valid CHL observations in estuaries, the East Anglia Plume, the Wadden Sea, near-shore coastal zones (e.g. UK, BE, NL, GE, DK) and fjords.

With the Copernicus program guaranteeing a reliable source of data to at least the year 2036, special efforts were made to ensure future integration of Sentinel-3/OLCI data into the processing chain. Sentinel-3/OLCI has a similar spectral bandset as MERIS enabling more reliable products for optically complex waters. The full resolution data (300m spatial resolution) will provide more robust CHL estimates close to the coast. Additionally, in the last years considerable progress has been made in the development of water quality products for high resolution sensors such as Sentinel-2/MSI which was designed for terrestrial monitoring (Vanhellemont et al., 2016). This resulted in a portfolio of water quality products which dramatically improves information content of nearshore waters, e.g. 10m instead of 300m resolution providing information within the first nautical mile of coast relevant for WFD monitoring.

To take the next step towards integration of satellite observations into eutrophication assessments for the North Sea, we investigated: 1) different approaches of aggregating the satellite CHL products, 2) use of different assessment levels and 3) use of new assessment areas. In a case study focussing on the Dutch part of the North Sea we tested the impact of the different approaches on eutrophication assessment in order to improve/fine-tune all components before actual implementation. When considering all satellite CHL observations at full resolution, the estimated area CHL mean is for most areas reasonably close to the mean based on in-situ data only when the areas are relatively homogeneous with respect to water quality indicators. However, in areas with strong spatial gradients, the assessment results are very sensitive to the

area boundaries and the choice of in-situ monitoring locations. A solution was proposed by spatially variable CHL assessment levels with a spatial resolution of 1x1km corresponding to the grid used for the satellite data. This enables a pixel by pixel eutrophication assessment by directly comparing the satellite data with the assessment levels resulting in a more consistent relative exceedance of the assessment levels throughout the assessment area. Consequently, the result is less dependent on the definition of assessment areas. Such spatially varying assessment levels allows for making better use of the full spatial resolution that satellite data can provide. Another possibility is to re-organize the assessment areas into zones that share similar environmental conditions (Final report Activity 1 section 9) which is presented in a case study (section 3).

During the study it was also found that the MSFD system using only two classes (good and bad) is quite limiting in terms of assessing gradual improvement of the status of an assessment area relative to the threshold indicating good environmental status. Using more classes, such as in the WFD, would give more information on changes. Regarding the extent to which good environmental status has been achieved in an assessment area, the satellite-based eutrophication product can easily determine the extent of the area that is not subject to eutrophication, using fixed or variable thresholds, and determine its evolution in time as an objective measure of changes in eutrophication status.

We emphasize that the assessment results presented in this report are not proposed as 'the new OSPAR assessment for 2022' but function as a guideline on how to optimally integrate remote sensing data sources into future eutrophication assessments.

References

Alvera-Azcárate, A., Barth, A., Rixen, M., & Beckers, J. M. (2005). Reconstruction of incomplete oceanographic data sets using empirical orthogonal functions: application to the Adriatic Sea surface temperature. *Ocean Modelling*, *9*(4), 325-346.

Bailey, S. W., & Werdell, P. J. (2006). A multi-sensor approach for the on-orbit validation of ocean color satellite data products. *Remote Sensing of Environment*, *102*(1-2), 12-23.

Baretta-Bekker, J. G., Baretta, J. W., Latuhihin, M. J., Desmit, X., & Prins, T. C. (2009). Description of the long-term (1991–2005) temporal and spatial distribution of phytoplankton carbon biomass in the Dutch North Sea. *Journal of Sea Research*, *61*(1-2), 50-59.

Baretta-Bekker, H., Bot, P., Prins, T., & Zevenboom, W. (2008). Report on the second application of the OSPAR Comprehensive Procedure to the Dutch marine waters. *Rijkswaterstaat, The Hague*.

Cloern, J. E., & Jassby, A. D. (2010). Patterns and scales of phytoplankton variability in estuarine–coastal ecosystems. *Estuaries and coasts*, *33*(2), 230-241.

Dall'Olmo, G., & Gitelson, A. A. (2005). Effect of bio-optical parameter variability on the remote estimation of chlorophyll-a concentration in turbid productive waters: experimental results. *Applied optics*, *44*(3), 412-422.

Desmit, X., Ruddick, K., & Lacroix, G. (2015). Salinity predicts the distribution of chlorophyll a spring peak in the southern North Sea continental waters. *Journal of sea research*, *103*, 59-74.

Doerffer, R., & Schiller, H. (2007). The MERIS Case 2 water algorithm. *International Journal of Remote Sensing*, *28*(3-4), 517-535.

European Commission. 2014. The European Commission's assessment and guidance (COM/2014/097_final). Luxembourg: Office for Official Publications of the European Communities.

Fettweis, M., Francken, F., Van den Eynde, D., Verwaest, T., Janssens, J., & Van Lancker, V. (2010). Storm influence on SPM concentrations in a coastal turbidity maximum area with high anthropogenic impact (southern North Sea). *Continental Shelf Research*, *30*(13), 1417-1427.

Gitelson, A. A., Schalles, J. F., & Hladik, C. M. (2007). Remote chlorophyll-a retrieval in turbid, productive estuaries: Chesapeake Bay case study. *Remote Sensing of Environment*, *109*(4), 464-472.

Gohin, F., & Stanev, E. (2011). Annual cycles of chlorophyll-a, non-algal suspended particulate matter, and turbidity observed from space and in-situ in coastal waters. *Ocean Science*, *7*(5).

Gohin, F., Druon, J. N., & Lampert, L. (2002). A five channel chlorophyll concentration algorithm applied to SeaWiFS data processed by SeaDAS in coastal waters. *International journal of remote sensing*, *23*(8), 1639-1661.

Gohin, F., Saulquin, B., Oger-Jeanneret, H., Lozac'h, L., Lampert, L., Lefebvre, A., Riou, P. & Bruchon, F. (2008). Towards a better assessment of the ecological status of coastal waters using satellite-derived chlorophyll-a concentrations. *Remote Sensing of Environment*, *112*(8), 3329-3340.

Gons, H. J. (1999). Optical teledetection of chlorophyll a in turbid inland waters. *Environmental Science & Technology*, *33*(7), 1127-1132.

Gons, H. J., Auer, M. T., & Effler, S. W. (2008). MERIS satellite chlorophyll mapping of oligotrophic and eutrophic waters in the Laurentian Great Lakes. *Remote Sensing of Environment*, *112*(11), 4098-4106.

Gons, H. J., Rijkeboer, M., & Ruddick, K. G. (2002). A chlorophyll-retrieval algorithm for satellite imagery (Medium Resolution Imaging Spectrometer) of inland and coastal waters. *Journal of Plankton Research*, *24*(9), 947-951.

Gordon, H. R., Clark, D. K., Brown, J. W., Brown, O. B., Evans, R. H., & Broenkow, W. W. (1983). Phytoplankton pigment concentrations in the Middle Atlantic Bight: comparison of ship determinations and CZCS estimates. *Applied optics*, *22*(1), 20-36.

Hu, C., Lee, Z., & Franz, B. (2012). Chlorophyll aalgorithms for oligotrophic oceans: A novel approach based on three-band reflectance difference. *Journal of Geophysical Research: Oceans*, *117*(C1).

Jickells, T. D. (1998). Nutrient biogeochemistry of the coastal zone. *Science*, *281*(5374), 217-222.

Joint, I., Wollast, R., Chou, L., Batten, S., Elskens, M., Edwards, E., Hirst, A., Burkill, P., Groom, S., Gibb, S., Miller, A., Hydes, D., Dehairs, F., Antia, A., Barlow, R., Rees, A., Pomroy, A., Brockmann, U., Cummings, D., Lampitt, R., Loijens, M., Mantoura, F., Miller, P., Raabe, T., Alvarez-Salgado, X., Stelfox, C., Woolfenden, J. (2001). Pelagic production at the Celtic Sea shelf break. *Deep Sea Res. Part II Top. Stud. Oceanogr*. 48, 3049–3081.

Le, C., Li, Y., Zha, Y., Sun, D., Huang, C., & Lu, H. (2009). A four-band semi-analytical model for estimating chlorophyll a in highly turbid lakes: The case of Taihu Lake, China. *Remote Sensing of Environment*, *113*(6), 1175-1182.

Lee, Z. (2006). Reports of the international ocean-colour coordinating group. *IOCCG*, Dartmouth, Canada, 5, 122.

Longhurst, A. R. (2010). *Ecological geography of the sea*. Elsevier.

Matsushita, B., Yang, W., Yu, G., Oyama, Y., Yoshimura, K., & Fukushima, T. (2015). A hybrid algorithm for estimating the chlorophyll-a concentration across different trophic states in Asian inland waters. *ISPRS journal of photogrammetry and remote sensing*, *102*, 28-37.

Mélin, Frédéric, and Gert Sclep. "Band shifting for ocean color multi-spectral reflectance data." *Optics Express* 23.3 (2015): 2262-2279.

Morel, A., Claustre, H., Antoine, D., & Gentili, B. (2007). Natural variability of bio-optical properties in Case 1 waters: attenuation and reflectance within the visible and near-UV spectral domains, as observed in South Pacific and Mediterranean waters. *Biogeosciences*, *4*(5), 913-925.

Morel, A.; Antoine, D. Pigment Index Retrieval in Case 1 Waters. Algorithm Technical Baseline Document 2.9. European Space Agency 2011.

Moses, W. J., Gitelson, A. A., Berdnikov, S., & Povazhnyy, V. (2009). Estimation of chlorophyll-a concentration in case II waters using MODIS and MERIS data—successes and challenges. *Environmental Research Letters*, *4*(4), 045005.

Nechad, B., Ruddick, K. G., Schroeder, T., Oubelkheir, K., Blondeau-Patissier, D., Cherukuru, R. C. N., ... & Maritorena, S. (2015). CoastColour Round Robin datasets: a database to evaluate the performance of algorithms for the retrieval of water quality parameters in coastal waters. *Earth system science data*, *7*, 319-348.

Nieke, J., Borde, F., Mavrocordatos, C., Berruti, B., Delclaud, Y., Riti, J. B., & Garnier, T. (2012, November). The Ocean and Land Colour Imager (OLCI) for the Sentinel 3 GMES Mission: status and first test results. In *Earth Observing Missions and Sensors: Development, Implementation, and Characterization II* (Vol. 8528, p. 85280C). International Society for Optics and Photonics.

Odermatt, D., Gitelson, A., Brando, V. E., & Schaepman, M. (2012). Review of constituent retrieval in optically deep and complex waters from satellite imagery. *Remote sensing of environment*, *118*, 116-126.

Oliver, M. J., & Irwin, A. J. (2008). Objective global ocean biogeographic provinces. *Geophysical Research Letters*, *35*(15).

O'Reilly, J. E., Maritorena, S., Mitchell, B. G., Siegel, D. A., Carder, K. L., Garver, S. A., ... & McClain, C. (1998). Ocean color chlorophyll algorithms for SeaWiFS. *Journal of Geophysical Research: Oceans*, *103*(C11), 24937-24953.

OSPAR. 2017. THIRD OSPAR INTEGRATED REPORT ON THE EUTROPHICATION STATUS OF THE OSPAR MARITIME AREA ISBN: 978-1-911458-34-0.

Park, Y. J., Ruddick, K., & Lacroix, G. (2010). Detection of algal blooms in European waters based on satellite chlorophyll data from MERIS and MODIS. *International Journal of Remote Sensing*, *31*(24), 6567-6583.

Patt, F. S., Barnes, R. A., Eplee Jr, R. E., Franz, B. A., Robinson, W. D., Feldman, G. C., Bailey, S.W., Gales, J., Werdell, P.J., Wang, M. & Frouin, R. (2003). Algorithm updates for the fourth SeaWiFS data reprocessing. *NASA Tech. Memo*, *206892*, 22-74.

Pitarch, J., Volpe, G., Colella, S., Krasemann, H., & Santoleri, R. (2016). Remote sensing of chlorophyll in the Baltic Sea at basin scale from 1997 to 2012 using merged multi-sensor data. *Ocean Science*, *12*(2), 379-389.

Rast, M., Bezy, J. L., & Bruzzi, S. (1999). The ESA Medium Resolution Imaging Spectrometer MERIS a review of the instrument and its mission. *International Journal of Remote Sensing*, *20*(9), 1681-1702.

Ruddick, K. G., Gons, H. J., Rijkeboer, M., & Tilstone, G. (2001). Optical remote sensing of chlorophyll a in case 2 waters by use of an adaptive two-band algorithm with optimal error properties. *Applied optics*, *40*(21), 3575-3585.

Ruddick, K., Lacroix, G., Lancelot, C., Nechad, B., Park, Y., Peters, S., & Van Mol, B. (2008). Optical remote sensing of the North Sea. In *Remote Sensing of the European Seas* (pp. 79-90). Springer, Dordrecht.

Ruddick, K., Lacroix, G., Park, Y., Rousseau, V., De Cauwer, V., Debruyn, W., & Sterckx, S. (2003). Overview of Ocean Colour: theoretical background, sensors and applicability for the de-tection and monitoring of harmful algae blooms (capabilities and limitations).

Ruddick, K., Vanhellemont, Q., Dogliotti, A., Nechad, B., Pringle, N., & Van der Zande, D. (2016). New opportunities and challenges for high resolution remote sensing of water colour. *Proceedings of the Ocean Optics XXIII, Victoria, BC, Canada*, 23-28.

Sathyendranath, S. (2000). Reports of the International Ocean-Colour Coordinating Group. *IOCCG, Dartmouth, Canada*, *3*, 140.

Schroeder, T., Schaale, M., & Fischer, J. (2007). Retrieval of atmospheric and oceanic properties from MERIS measurements: a new Case-2 water processor for BEAM. *International Journal of Remote Sensing*, *28*(24), 5627-5632.

Smith, M. E., Lain, L. R., & Bernard, S. (2018). An optimized Chlorophyll a switching algorithm for MERIS and OLCI in phytoplankton-dominated waters. *Remote sensing of environment*, *215*, 217-227.

Steinmetz, F., Deschamps, P. Y., & Ramon, D. (2011). Atmospheric correction in presence of sun glint: application to MERIS. *Optics express*, *19*(10), 9783-9800.

Tilstone, G., Mallor-Hoya, S., Gohin, F., Couto, A. B., Sá, C., Goela, P., Cristina, S., Airs, R., Icely, J., Zühlke, M. & Groom, S. (2017). Which ocean colour algorithm for MERIS in North West European waters? *Remote sensing of environment*, *189*, 132-151.

Van der Zande D., Lacroix G., Desmit X. & Ruddick K. (2011). Impact of irregular sampling by MERIS on eutrophication monitoring products for WFD and MSFD applications *in: Proceedings of the Sixth International Conference on EuroGOOS, 4-6 October 2011, Sopot, Poland*, Vol. - pp. 356–365. Dahlin, H., Flemming, N. C., Petersson, S. E

Vanhellemont, Q. (2012, October). Invalidation of the MEGS 8.0 chlorophyll product in turbid waters. In *3rd MERIS/(A) ATSR and OCLI-SLSTR (SENTINEL-3) Preparatory Workshop, 15-19 October*.

van Leeuwen, S., Tett, P., Mills, D., & van der Molen, J. (2015). Stratified and nonstratified areas in the North Sea: Long-term variability and biological and policy implications. *Journal of Geophysical Research: Oceans*, *120*(7), 4670-4686.

Zibordi, G., Mélin, F., Berthon, J. F., Holben, B., Slutsker, I., Giles, D., D'Alimonte, D., Vandemark, D., Feng, H., Schuster, G. & Fabbri, B. E. (2009). AERONET-OC: a network for the validation of ocean color primary products. *Journal of Atmospheric and Oceanic Technology*, *26*(8), 1634-1651.

Annex I - Technical annex from Belgian MSFD D5 assessment for 2018: CHL by optical remote sensing

Annex I.1. In situ Chl and satellite Chl

In the Belgian Continental Shelf (BCS), the bloom of chlorophyll *a* concentration (Chl) shows high values in the coastal area with a decreasing gradient towards the offshore. The highest values are seen every year during the spring bloom of Chl (usually April), when the colonial haptophyte *P.globosa* accumulates biomass after the early-spring diatom bloom. The 90th percentile of Chl (i.e. the Chl P90) estimated during the growing season (Mar-Oct) is the indicator that measures the size of the Chl spring bloom, and hence the undesirable effect of eutrophication. However, it can only be calculated when a significant amount of data is available (likely once per month).

In the last three decades, however, the in-situ sampling of Chl by the Belgian national monitoring program has decreased from 4-7 samplings per growing season in the 1990's (Ruddick et al. 2008) to 1-3 samplings on average in the 2000-2010's at 10 sites distributed in the BCS. Though in situ data acquisition is still considered the most reliable monitoring tool for pigments, the statistical outputs drawn from such a limited amount of data is dubious and leaves no place for the analysis. This is especially the case in a very dynamic system like the Belgian coastal zone where Chl exhibits very strong variability on both the spatial and the temporal scales (Desmit et al. 2015a).

There is a growing tendency to use optical remote sensing as a supporting tool to achieve the monitoring requirements because of severe resource constraints of available ship time and manpower. Satellite data enables the calculation of Chl P90 pixel-by-pixel, resulting in a map product which is expected to provide more accurate Chl P90 estimates due to an increased temporal and spatial resolution compared to the in situ data (Van der Zande et al. 2011).

Annex I.2. Validation of satellite Chl

Chlorophyll *a* concentration was generated from daily data from ocean colour sensors (i.e. SeaWiFS, MODIS, MERIS, VIIRS) for the years 1998-2017. The algorithms used to derive data from the satellite sensors correspond to the best available algorithms given the optical characteristics of the considered water (i.e. turbid and clear waters) We started from a collection of well-validated operational satellite-based chlorophyll products for the Greater North Sea: 1) CMEMS nr. 67 product where Chl is estimated from the OC5ci algorithm, a combination of OCI (Hu, Lee & Franz, 2012) and OC5 (Gohin, F., et al., 2008.), developed at PML and 2) red-NIR ratio algorithm developed by Gons et al. (2002, 2005) for eutrophic and turbid waters applied to remote sensing reflectance obtained by Envisat-MERIS (MEGS 8.1 processing). For each of these products it was determined for which water types, described in terms remote sensing reflectance (Rrs) spectra, they provided the most accurate chlorophyll estimations (i.e. relative error < 50%) based on a variety of reference datasets from the CCRR project[1] (Nechad et al., 2015). These

[1] Coast Colour Round Robin (CCRR) data set published by Nechad et al. (2015). The CCRR project (http://www.coastcolour.org) funded by the European Space Agency (ESA) was designed to bring together a variety of reference datasets and to use these to test algorithms and assess their accuracy for retrieving water quality parameters. This information was developed to help end-users of remote sensing products to select the most accurate algorithms for their coastal region.

reference data sets were specifically designed to test algorithms and assess their accuracy for retrieving water quality parameters such as Chl concentration. In the next phase of the Chl product generation, a blending process is applied to join chlorophyll-a datasets based on best suited algorithm/water type combination.

Quality control has been applied according to the standard satellite product confidence flags for the MEGS8.1 processor, and a specialized flagging approach designed for the OC5ci and Gons algorithms. Data is supplied at approximately 1 km resolution on a geographical grid with equal spacing in longitude and latitude covering the described region. The daily satellite Chl products are validated by match-up analysis between satellite and available in-situ (seaborne) chlorophyll *a* observations for the entire BCS (Figure A1.1, bottom) following the approach of Bailey and Werdell (2006). This analysis shows a strong correlation between satellite-observed and in situ chlorophyll *a* observations. Outliers in this match up analysis were identified as measurements points at the outer boundary of an algal bloom with a very strong spatial gradient in Chl concentrations. The allowed time difference between in situ and satellite observations was set to two hours which could lead to significant differences in this specific case due to tidal currents.

A time series was produced for the validation period (2007-2016) for the coastal monitoring station W01: the satellite-derived chlorophyll *a* concentrations were superimposed on in situ chlorophyll *a* concentrations (Figure A1.1, top). This allows a qualitative assessment of the ability of the MERIS satellite data to capture the Chl dynamics in the Belgian waters. The use of satellite-observed chlorophyll *a* with a high temporal frequency allows deriving a more accurate Chl P90 since timing and frequency of in situ measurements do not ensure that samples are taken during the peak of the bloom.

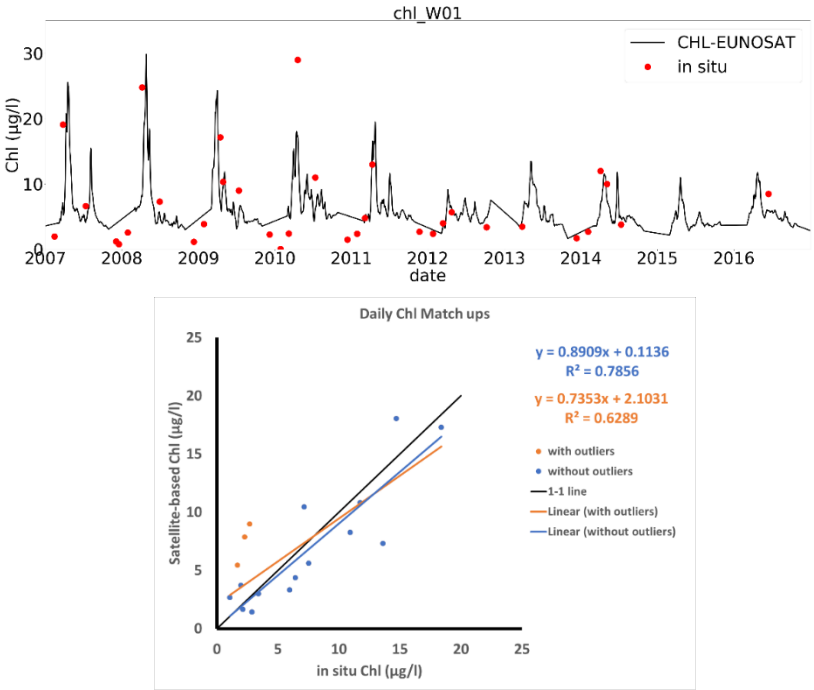

Figure A1.1:. (Top) Time series of satellite-derived CHL (black line) superimposed on in situ CHL observations for station W01 for the period 2007-2016. (Bottom) Regression-plot for CHL match-ups between JMP-EUNOSAT CHL products and in-situ

datasets for the entire Belgian Coastal Zone. Outliers in this match up analysis (orange points) were identified as measurements points at the outer boundary of an algal bloom with a very strong spatial gradient in Chl concentrations

Annex I.2. Analysis of satellite Chl

In order to show a longer-term picture of the Chl P90 in the Belgian waters, the satellite-based Chl P90 product for the period 2011-2016 is presented in Figure A1.2. It shows the highly productive coastal areas and the coastal-offshore gradient in Chl P90.

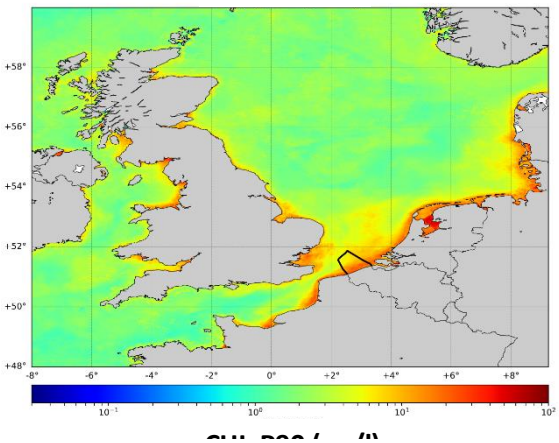

Figure A1.2: The multi-temporal Chl P90 product (March-October, 6-year period) based on satellite observations (JMP-EUNOSAT) in the North Sea used as eutrophication indicator.

The area of the Belgian coastal zone which shows concentrations higher than 15 µg L^{-1} is shown in red on Figure A1.3(a). The surface proportion of the Belgian waters where Chl P90 remains above 15 µg L^{-1} during the period 2011-2016 is 29% Figure A1.3(b). This area is located in the coastal zone and the territorial waters and is subjected to nutrient enrichment.

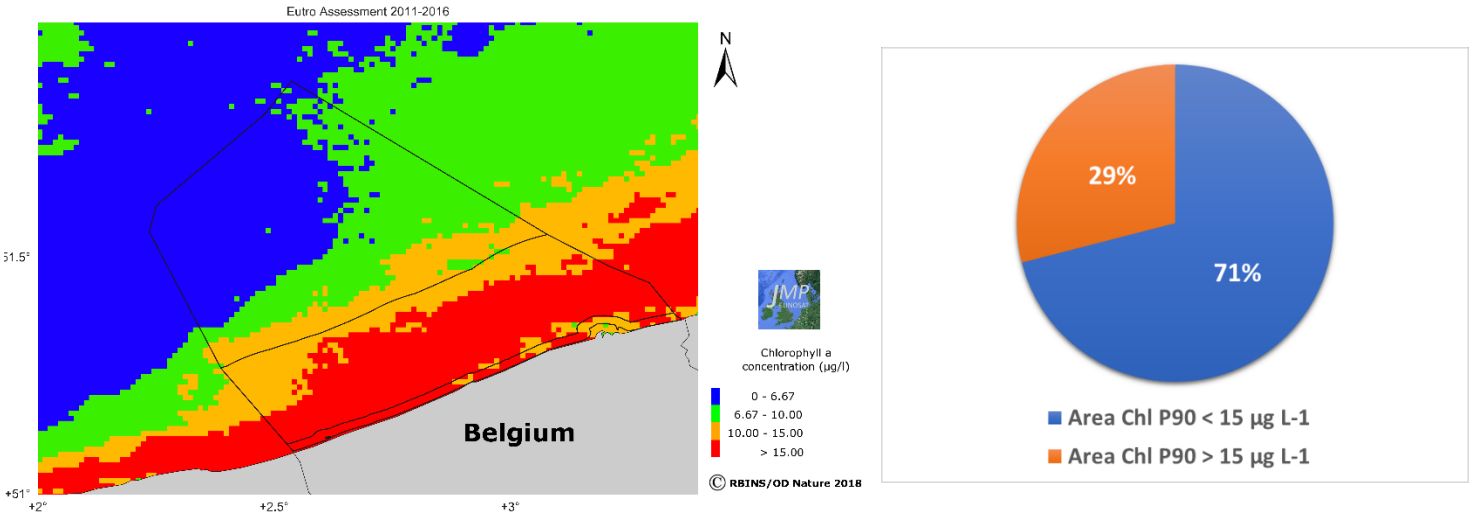

Figure A1.3: (a) Classification of the Chl P90 product (2011-2016) for the BCS with the red class Chl P90 > 15µg L^{-1}. (b) Proportion of pixels where Chl P90 is above 15 µg L^{-1} in the Belgian waters for the period 2011-2016.

Figure A1.4 shows the evolution in time of the percentage surface of the Belgian Coastal Zone which falls into the category of 'Chl P90 > 15µg L^{-1}' (i.e. red zone in Figure A1.3(a)) as an objective indicator of eutrophication based on 6-yearly composites. The surface of the 'Chl P90 > 15µg L^{-1}' class increases strongly (28.74%) between composites 2001-2006 and 2007-2012 but decreases (6.45%) between composites 2007-2012 and 2012-2017.

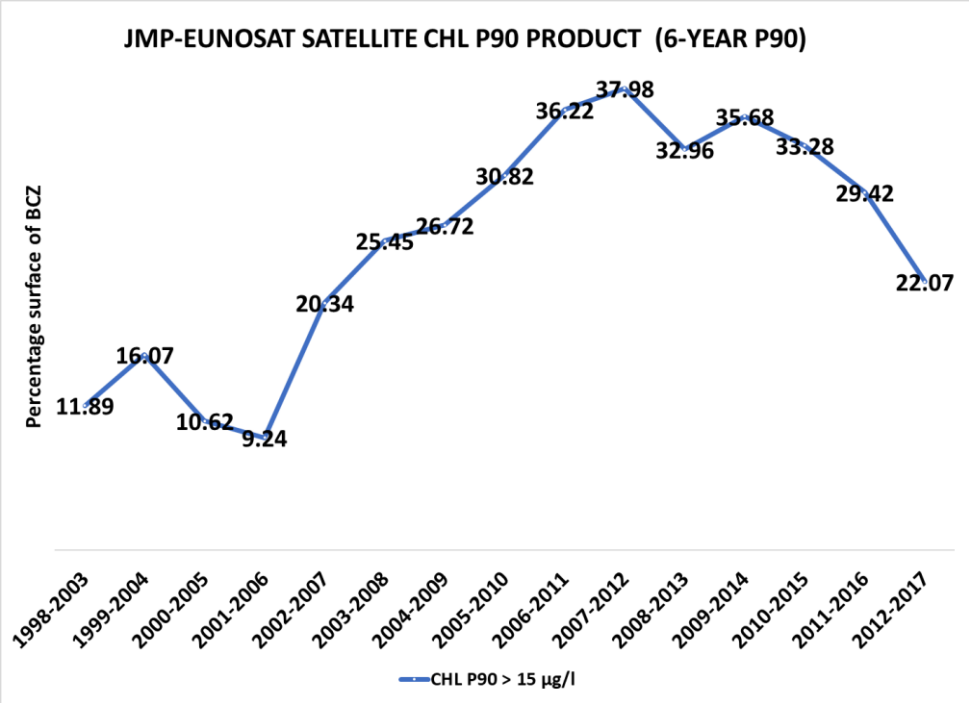

Figure A1.4: The percentage surface of the Belgian part of the North Sea of which the 6-yearly Chl P90 > 15µg L^{-1} as an objective indicator of eutrophication.

This graph shows a strong variation in the Chl dynamics and that a longer time series is needed to determine if this variation is part of a natural cycle. This is made possible with the Copernicus program the European Commission and European Space Agency guarantee ocean colour satellite data up to 2036 with the launch of the Sentinel-3 satellites.

Annex II- Signature patterns of chlorophyll a variability in the Greater North Sea

This section is in preparation for submission to a scientific Journal:

Desmit, X. and Van der Zande. Signature patterns of chlorophyll a variability in the Greater North Sea. In prep.

Along the coastal zone of the Greater North Sea (GNS, [48°N-60°N 10°E-10°W]), high blooms of chlorophyll *a* (CHL) occur between March and October and typically show a steep coastal-offshore decreasing gradient (Baretta-Bekker et al., 2009; Desmit et al., 2015; Jickells, 1998). Due to geomorphological features, the GNS comprises a wide diversity of marine systems within a relatively small geographical area: shallow coastal areas (5-20 m, e.g. in Belgium and The Netherlands) versus deeper waters (~300 m, in the Norwegian Trench), areas subject to freshwater inputs versus areas solely under oceanic influence, permanently mixed versus stratified systems (see van Leeuwen et al., 2015), turbid versus clear waters, and the productive shelf-ocean margin offshore Brittany and Ireland where fluxes of nutrient and organic matter occur between the shelf and the ocean, with deep water ascent bringing nutrients to the euphotic zone (Joint et al., 2001). These geomorphological features influence phytoplankton production and biomass directly or indirectly by controlling the mixed layer depth, the light and nutrient availability and the grazing foodweb. Depending on the local properties of the sea, CHL shows different mean concentrations, and different patterns of temporal variability (annual, seasonal and monthly residual). Cloern and Jassby (2010) have shown how different coastal systems around the world could be distinguished from each other on the basis of their CHL patterns of variability. Therefore, the patterns of CHL variability could theoretically be used to identify sensible biogeographical areas, i.e. to design "the areas within which characteristic ecosystems may be expected to occur", as proposed by Longhurst (2007) at the scale of the global ocean. He used ocean colour data coupled with physical properties of the sea to partition the ocean into biogeographical provinces. Oliver and Irwin (2008) have also partitioned the global ocean by using identical data. They proposed a more objective, statistical technique to aggregate pixels showing similar properties. In this study, we use the annual, seasonal and monthly residual components of CHL variability (derived from satellite ocean colour) to identify biogeographical areas in the GNS, excluding the use of data describing the physical properties of the sea.

Satellite observations of CHL (ENVISAT-MERIS) offer a synoptic picture of the monthly surface Chl over almost a decade (2003-2011). The multiplicative method of Chl signal decomposition (Cloern and Jassby, 2010) was applied to each pixel (see Fig. A2.1) separating the CHL time series into four components: 1) the grand mean, 2) the interannual, 3) the seasonal and 4) the residual components. The grand mean of CHL and the standard deviations of the other components constitute a pool of four numbers characteristic of the time series of CHL in each pixel. The pixel-wise components of Chl variability may be represented in individual maps (annual, seasonal, residual) to depict the spatial patterns of CHL variability (not shown). Subsequently, these numbers may be processed with a K-means cluster analysis to aggregate pixels into different clusters, corresponding to areas of the GNS (Fig. A2.2).

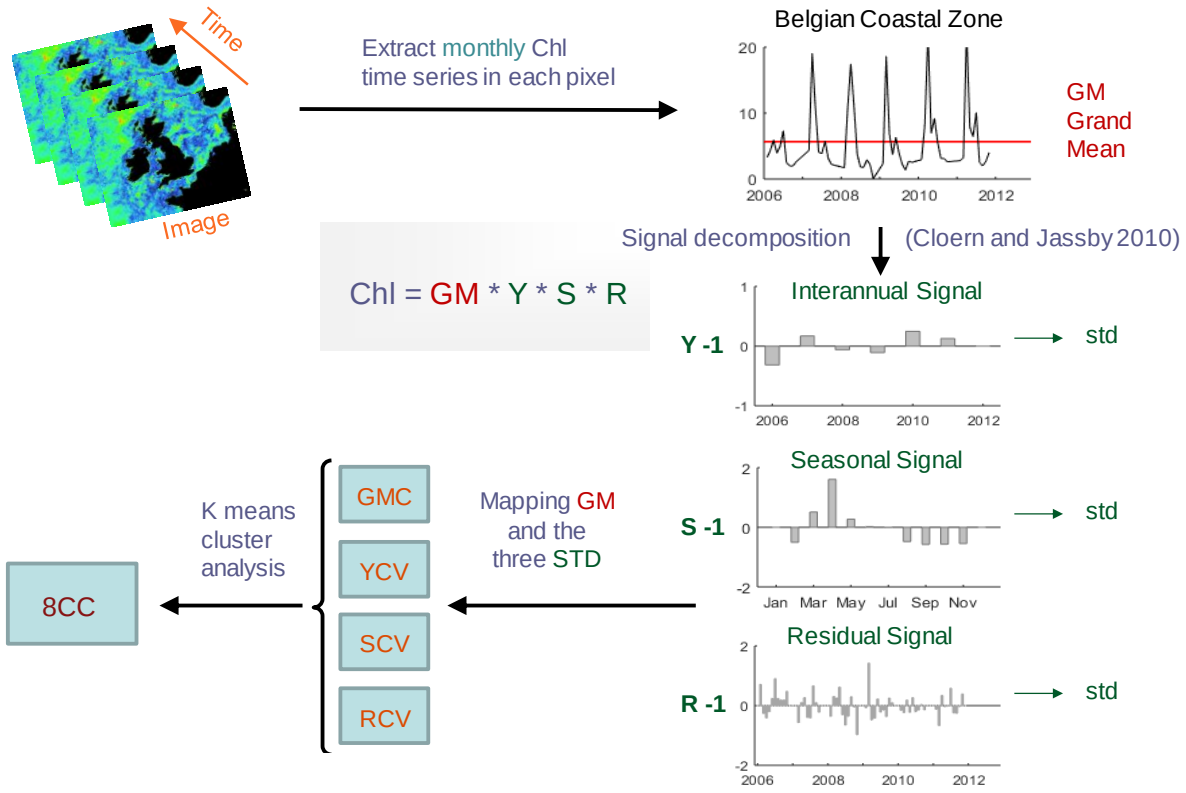

Figure A2.1 Schematic representation of the method used to produce the Figure A2.2. Monthly satellite images of CHL are processed to obtain a map showing eight distinct areas of CHL (see text).

The K-means cluster analysis led to the differentiation of eight distinct clusters of pixels, which define specific areas in the North Sea (Fig. A2.2). These areas correspond to different signature patterns of CHL dynamics for the considered period 2003-2011. There is a clear difference between the continental shelf and the open ocean. The image suggests that bathymetry and distance from the coast are important explanatory factors for the different spatial patterns of Chl. However, bathymetry does not explain all the differences. For instance, the shallower area of Doggerbank in the Central North Sea has approximately the same bathymetry as the southern NS but remains in a different cluster. The stratification regimes in the GNS (permanent, seasonal, intermittent; van Leeuwen et al., 2015) also play a role in defining CHL patterns of variability, as suggested by the boundary between CHL classes in the tidally-mixed Southern North Sea and the stratified Central North Sea. The cluster analysis allowed identifying a specific area along the shelf break, where deep-water nutrients are brought to the euphotic zone enhancing phytoplankton production (Joint et al., 2001). Finally, there is also an area specific to the front where Arctic, Atlantic and continental waters meet, corresponding to the southern part of the Atlantic Subarctic Province (SARC) of Longhurst (2007).

Time series in a few areas indicate the high diversity of CHL patterns that can be observed in the Greater North Sea. In the North Atlantic front, blooms occur in June with relatively high values and some interannual irregularity. Along the margin, west from Brittain, blooms are comparable but occur in April and show irregularity in the monthly residuals. In the North Sea, in an area with intermittent stratification, Chl will show very low regularity in the interannual, seasonal or monthly residual signals. There, the Chl bloom structure seems much less predictable due to the high variability of CHL at all time scales,

suggesting an effect of the intermittent stratification. At the front between the Southern North Sea and the Central North Sea, spring blooms are relatively more intense. They occur in April and there is strong variability in interannual and monthly residual signals. This may be due to the seasonal displacement of the front coupled with intermittent stratification and irregular nutrient enrichment from the continental rivers. The Norwegian Trench shows a systematic main bloom in February because of the permanent saline stratification there allowing CHL accumulation early in the year. Besides, there are additional small CHL blooms occurring with a interannual and monthly variability. The Belgian Coastal Zone shows very regular and predictable blooms, occurring in April with a relatively high intensity most years.

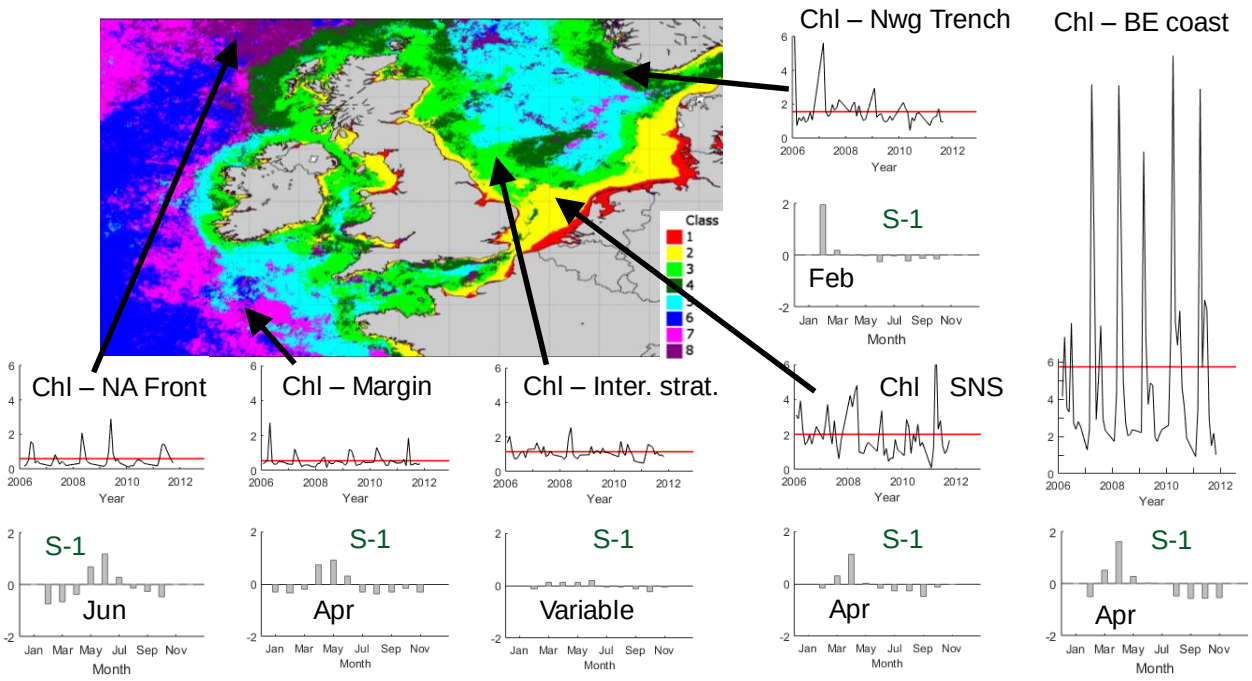

Figure A2.2 Eight clusters of CHL in the Greater North Sea (colours indicate the different clusters). Time series of CHL (µg L^{-1}) are shown with their grand mean (red line) and their seasonal signal (S-1, see Fig. A2.1) for several pixels in typical areas (from left to right: the North Atlantic front, the margin between the ocean and the shelf, an area of intermittent stratification, an area in the Southern North Sea, the Nowegian Trench, and the Belgian Coastal Zone).

Spatial aggregates of CHL can be identified as areas in the North Sea on the basis of patterns of CHL variability. These areas are consistent with the known physical properties of the sea. An additional analysis of CHL dynamics in each area (not shown) allows distinguishing better the different areas that were previously selected by the K means analysis on the basis of standard deviations. The identified areas reflect average CHL spatial patterns in the GNS in a structural way.

Annex III - 20 years of satellite observation of the phytoplankton biomass from the northern Bay of Biscay to the eastern English Channel. Is the water quality improving?

This section is a shortened version of an article submitted to Remote Sensing of Environment.

Francis Gohin, Dimitry Van der Zande, Gavin Tilstone, Marieke A. Eleveld, Alain Lefebvre, Françoise Andrieux-Loyer, Anouk N. Blauw, Philippe Bryère, David Devreker, Philippe Garnesson, Tania Hernández Fariñas, Luis Lampert, Héloïse Lavigne, Florence Menet-Nedelec, Silvia Pardo, Bertrand Saulquin (2019). 20 years of satellite observation of the phytoplankton biomass from the northern Bay of Biscay to the eastern English Channel. Is the water quality improving? Submitted to Remote Sensing of Environment.

Abstract: The variability of the phytoplankton biomass derived from daily chlorophyll-*a* (Chl-*a*) satellite images was investigated over the period 1998-2017 in the surface waters of the English Channel and the northern Bay of Biscay. Merged satellite (SeaWiFS-MODISAqua-MERIS-VIIRS) Chl-*a* was calculated using the OC5 algorithm which is optimized for moderately_turbid waters. The seasonal cycle in satellite-derived Chl-*a* was compared with *in situ* measurements made at seven coastal stations located in the southern side of the English Channel and in the northern Bay of Biscay. The results firstly showed that the OC5 Chl-*a* product applied to a suite of space-borne marine reflectance data, is in agreement with the coastal observations. For compliance with the directives of the European Union on water quality, time-series of 6-year moving average of Chl-*a* were assessed over the region. A clear decline was observed in the mean and 90th percentile of Chl-*a* at stations located in the mixed waters of the English Channel. The time-series at the stations located in the Bay of Biscay showed yearly fluctuations which correlated with river discharge, but no overall Chl-*a* trend was observed. In the English Channel, the shape of the seasonal cycle in Chl-*a* changed over time. Narrower peaks, characteristic of less eutrophic waters, were observed in spring at the end of the studied period. Monthly averages of satellite Chl-*a*, over the periods 1998-2003 and 2012-2017, exhibited spatial and temporal patterns in the evolution of the phytoplankton biomass similar to these observed at the seven coastal stations. Both the *in situ* and satellite Chl-*a* times-series showed a drop in Chl-*a* in the English Channel in May, June and July. This trend in phytoplankton biomass is correlated with lower river discharges at the end of the period and a constant reduction in the riverine input of phosphorus through improvements in the water quality of river catchments in the region. Despite a similar evolution in the riverine nutrient fluxes, the phytoplankton biomass and the risk of eutrophication in summer stay at high level in the Bay of Biscay over the studied period.

Annex III.1. Introduction

To assess the evolution of phytoplankton biomass over a twenty-year period (1998-2017) using both *in situ* and satellite data, the compatibility of the satellite-derived products with the conventional *in situ* retrievals has to be assessed. However, the performance assessment of ocean color satellite data is a difficult task in absolute, particularly for the Chl-a non-gaussian distribution with outliers. It generally relies on mean squared errors, such as the coefficient of determination (r^2), root mean square error, and regression slopes. Seegers et al. (2018) discuss the limitations of these conventional methods and consider that end-user/application criteria should be determinant in the choice of the assessment metrics. The performance assessment of our satellite dataset will be therefore carried out on the 90th percentile during the productive period (from the beginning of March to the end of October). This quantity is the key parameter of the Chl-a distribution involved in the monitoring procedures of the water quality already mentioned.

Another particularity of the quantitative investigations in the field of water quality is also to favour the use of the natural scale and not the logarithm transformation of Chl-*a* (Campbell et al., 1995) as priority is to provide from space accurate estimates of the elevated Chl-*a* concentrations encountered in case of eutrophication. The OC5 algorithm applied to marine reflectance in turbid waters (Gohin et al., 2002) is expected to perform well on a multi-sensor time series. OC5 is robust and provides relatively good retrievals of Chl-*a* compared to other algorithms, not just in north-west European coastal waters (Tilstone et al., 2017) but also in the western Mediterranean Sea (Lapucci et al., 2012; Gomez-Jakobsen et al., 2016), the coastal Vietnamese waters (Loisel et al., 2017), and at global scale (Saulquin et al., 2018). The OC5 Chl-a products that we propose to evaluate and use in this study are interpolated multi-sensor images obtained following the procedure proposed in Saulquin et al. (2011).. These interpolated daily products can be recommended for operational monitoring of Chl-*a* and for providing monthly or yearly bulletins of anomalies based on well-balanced datasets in term of spatial and temporal coverage. A specific attention will be brought to the representativity of the annual cycle of the satellite-derived Chl-*a* compared to those observed *in situ*. A possible improvement in term of eutrophication should be seen not only in the 90th percentile but also in the reduction of the growing period before limitation by nutrients. The annual cycles and the 90th percentile, assessed over years, are therefore the two properties of the Chl-a distribution recommanded for assessing the performance of the satellite method in view of reporting on the assessment of the eutrophication status. Seven stations characteristic of the coastal waters from the northern Bay of Biscay to the eastern English Channel have been selected for this assessment. Figure A3.1 shows the location of the stations superimposed on the mean concentration of non-algal Suspended Particulate Matter (SPM) at the end of winter. All these stations are in nutrient-rich and turbid waters, except the Men er Roue station in the Bay of Biscay.

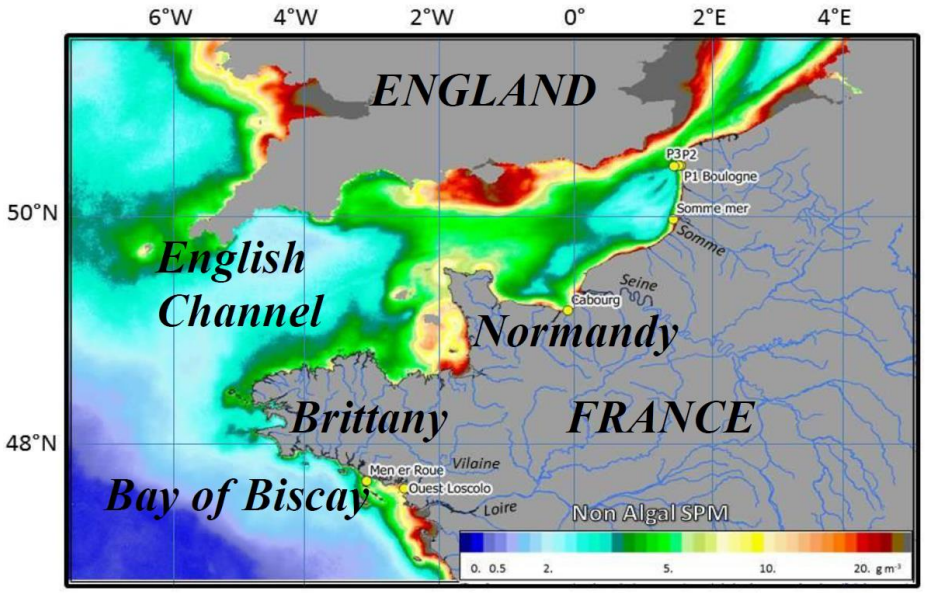

Fig. A3.1. Study area showing in situ station locations superimposed on averaged non-algal Suspended Particulate Matter at the end of winter (March) during the period 1998-2017. **SPM is derived from satellite reflectance using the algorithm described in Gohin et al (2005) and Jafar-Siddik et al., (2017).**

As the directives recommend a period of six years for the reporting of the monitoring programme, the average and the 90th percentile of Chl-*a* retrieved from space or observed *in situ* will be calculated also over this period. The rationale for this assessment period is multiple. It gives time to assess the effect of measures or actions taken in order to achieve or maintain good environmental status while being affordable in practice from *in situ* monitoring.

Annex III.2. Data and methods

The satellite dataset

The images used in this study are interpolated OC5 Chl-*a,* therefore a Level 4 product, following the nomenclature defined by NASA. The interpolation is performed using kriging techniques, which e nable the creation of a daily multi-sensor dataset of complete images over the period 1998-2017 (ftp://ftp.ifremer.fr/ifremer/sextant-data/SATCOAST/atlantic/CHL, Ifremer, 2017). The spatial resolution of the interpolated images is 0.01° in latitude and 0.015° in longitude (about 1.2*1.2 km^2). In practice, the interpolation is carried out on Chl-a anomalies calculated by difference to a 1998-2008 average (SeaWiFS and MODIS/AQUA). Satellite data observed within 5 days before and 5 days after the day of interest and up to 160 km from the pixel location were used to build the data sets used for the interpolation.

The in-situ datasets

The *in situ* data of Chl-*a* (Fig. A3.1) were obtained from the SRN (Suivi Régional des Nutriments), the RHLN (Réseau Hydrologique du Littoral Normandy, SRN 2017), and the Ifremer REPHY phytoplankton network (REPHY, 2017). Three stations (Boulogne 1, 2, 3) are located along a transect off the harbour of Bo ulogne. Somme_Mer-2 is located in front of the mouth of the river Somme (mean annual discharge 35 m^{3}s^{-1}). The Boulogne and Somme_Mer stations belong to the SRN network with a monthly sampling frequency. The Cabourg station, belonging to the RHLN, is located in the vicinity of the Seine plume (mean annual discharge 510 m^{3}s^{-1}). The RHLN and REPHY networks have a 2-weekly sampling frequency. Two stations have been selected in the northern Bay of Biscay, Men er Roué in relatively clear waters and Ouest-Loscolo in the plume of the river Vilaine (mean annual discharge 70 m^{3}s^{-1}) in southern Brittany. The region under the influence of the Vilaine and the Loire rivers is subject to recurrent anoxia events in summer, favoured by high production and stratification (Chapelle et al., 1994). Areas characterised by a strong stratification of the water column have been shown to be sensitive to hypoxia (Conley, 2002).

Annex III.3. Results

The annual cycles at the stations

Figure A3.2 shows the annual cycles of satellite and *in situ* Chl-*a* at the seven sampling stations as well as the mean and the 90th percentile over the productive period. Despite the fact that the satellite data are interpolated, the level and shape of the curves are very similar to those obtained from mono-sensor (non-interpolated) data (Gohin, 2011). Such a result was expected, since the kriging method used for the interpolation is unbiased. The major discrepancy between the satellite and *in situ* data sets is observed in winter along the cross-shore transect off Boulogne. High Chl-*a* concentrations are observed *in situ* very early in the year, even in January. Nevertheless, both SRN and satellite data sets illustrate that the phytoplankton development starts early in the Northern English Channel (as in the North-Sea), though the satellite Chl-*a* is lower. The stations in the river plumes, Somme_Mer, Cabourg and Ouest-Loscolo, exhibit

bell curves typical of eutrophic waters enriched by a constant flux of riverine nutrients. Despite some differences between the datasets, the means and 90th percentileof Chl-*a* are very similar. The correspondence is high between the satellite-derived and *in situ* gradients along the Boulogne transect; with mean levels over the productive period of about 6, 5 and 3 µg m^{-3} from coastal (Point 1) to deeper waters (Point 2 and 3).

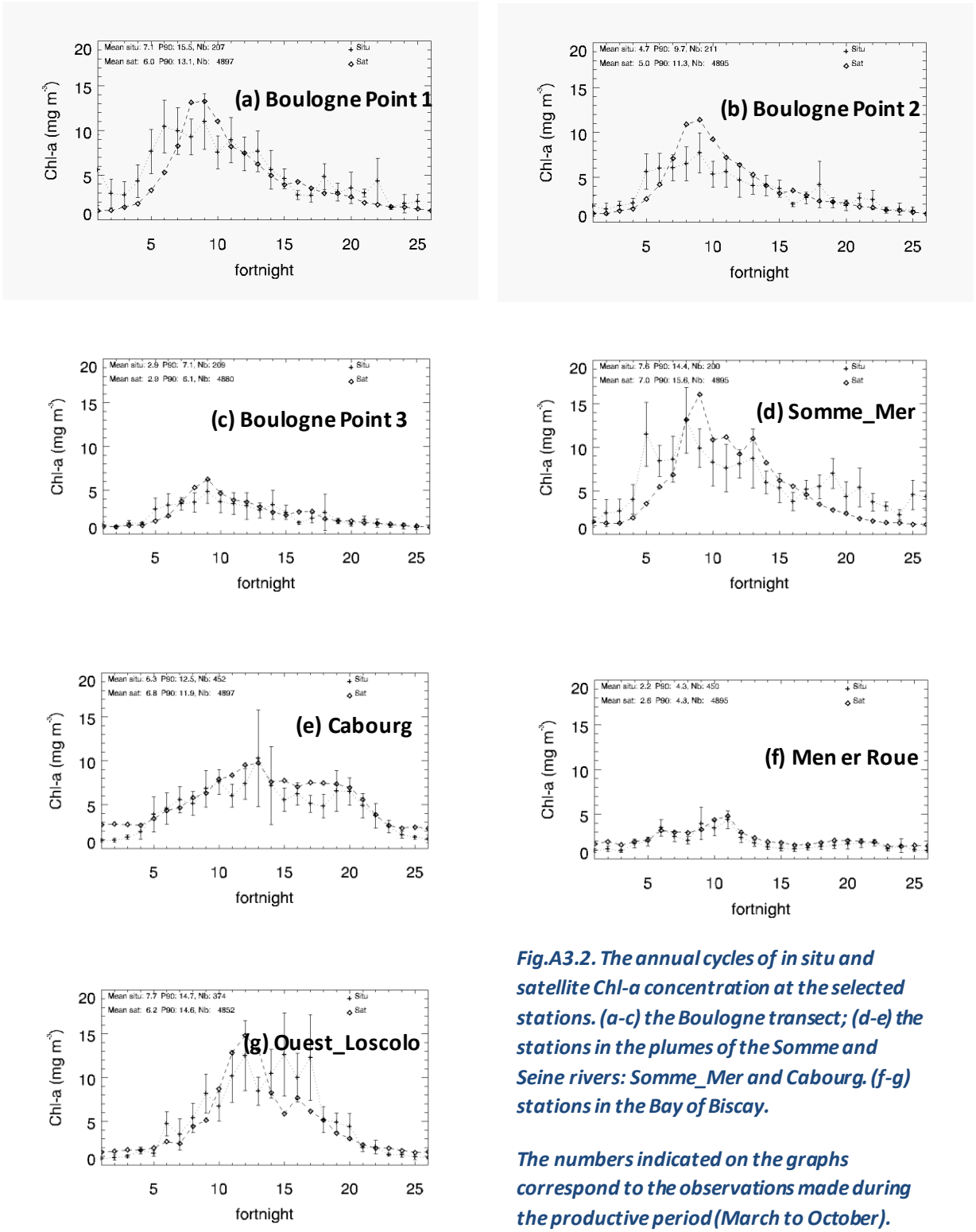

Fig.A3.2. The annual cycles of in situ and satellite Chl-a concentration at the selected stations. (a-c) the Boulogne transect; (d-e) the stations in the plumes of the Somme and Seine rivers: Somme_Mer and Cabourg. (f-g) stations in the Bay of Biscay.

The numbers indicated on the graphs correspond to the observations made during the productive period (March to October). The mean and 90th percentile indicated are also calculated over the productive period. Bars around the in situ averages correspond to 1.65* the standard error

The temporal evolution in Chl-a at the stations

Evolution of the yearly means with time

Figure A3.3 gives the yearly means for the productive season (March-October) at the selected stations. The vertical bars around the *in situ* averages correspond to a approximate confidence interval on the mean at 95% ($\pm 1.65\sqrt{s^2/n}$) where s^2 is the standard deviation and n the number of data) for a Gaussian distribution, indicative of the variability in the *in situ* data. Such a representation is not applicable to the satellite data as these are so numerous (204 retrievals each year within the productive period) that their average is a very accurate estimation of their statistical mean. Thus, the weakness of the satellite averages could concern more the bias that they can show with the *in situ* reference than their variance. That is why it has been so important to roughly assess this bias locally and seasonally by comparing the mean annual curves of satellite and *in situ* Chl-*a* and their major statistics (Figure A3.2). Despite a high variability of the *in situ* measurements, as at the Ouest_Loscolo station in 2007 with two outliers observed at 115 and 75 mg m^{-3}, the time-series of the yearly means derived from the satellite or observed at sea show similar evolutions over years.

The time-series of the six-year moving averages (Figure A3.4) and 90th percentiles (Figure A3.5) show a decrease at the stations in the English Channel whereas no significant trend is observed in the Bay of Biscay (stations Men er Roue and Ouest-Loscolo). Figure A3.6 presents the 90th percentiles of Chl-*a* at the beginning (1998-2003) and at the end of the period (2012-2017) over the area. These maps show that the Men er Roue and Ouest-Loscolo stations are very representative of the Bay of Biscay characterised by an absence of long term trend in the percentile 90 of Chl-*a*, which contrasts with the southern coast of the English Channel and the southern bight of the North-Sea.

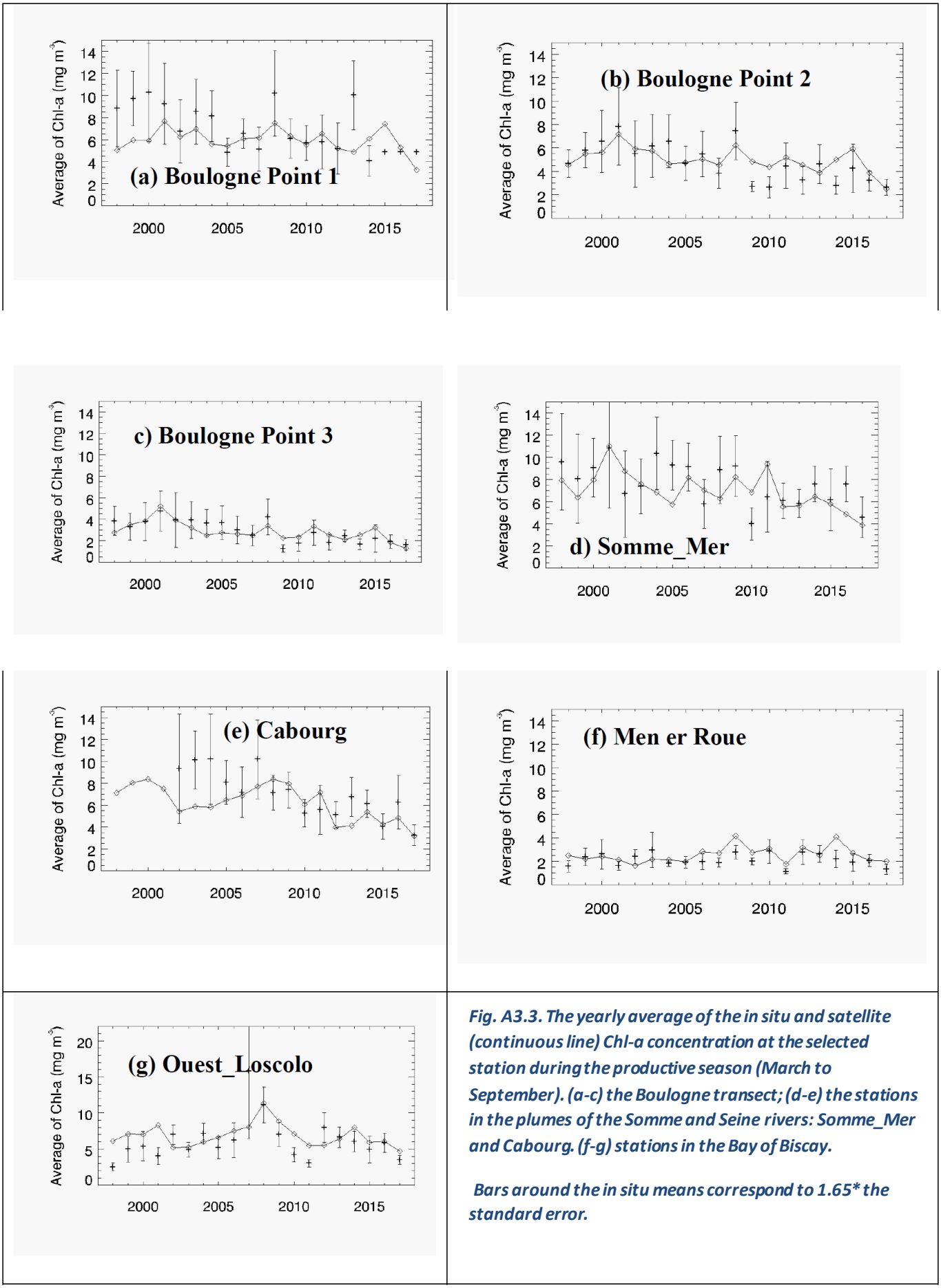

Fig. A3.3. The yearly average of the in situ and satellite (continuous line) Chl-a concentration at the selected station during the productive season (March to September). (a-c) the Boulogne transect; (d-e) the stations in the plumes of the Somme and Seine rivers: Somme_Mer and Cabourg. (f-g) stations in the Bay of Biscay.

Bars around the in situ means correspond to 1.65 the standard error.*

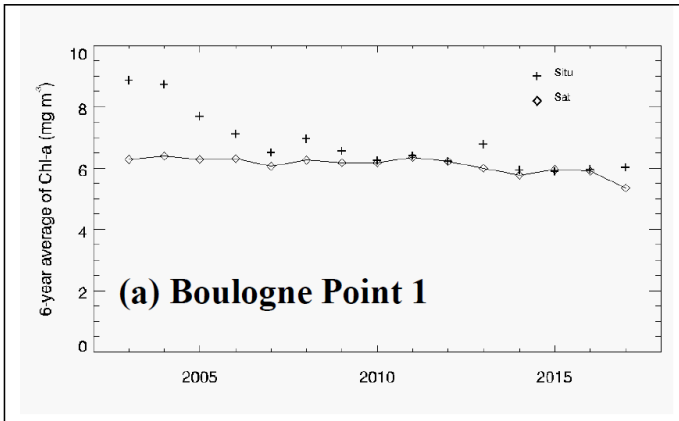

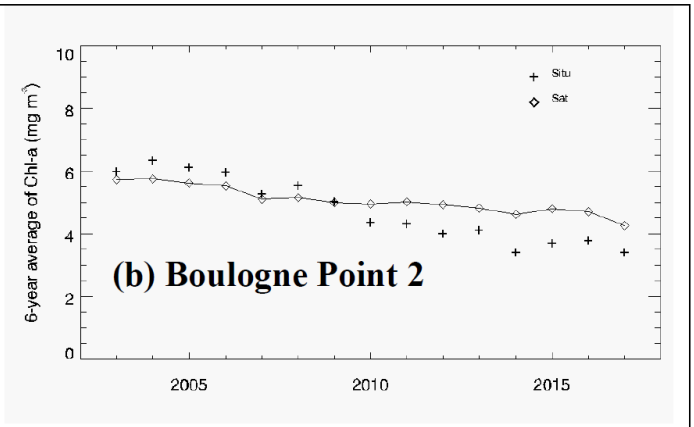

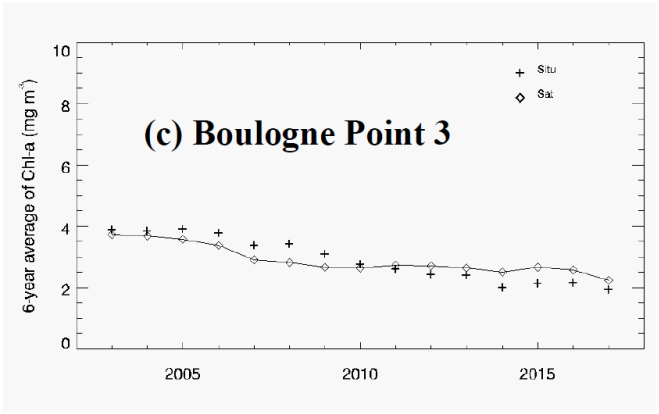

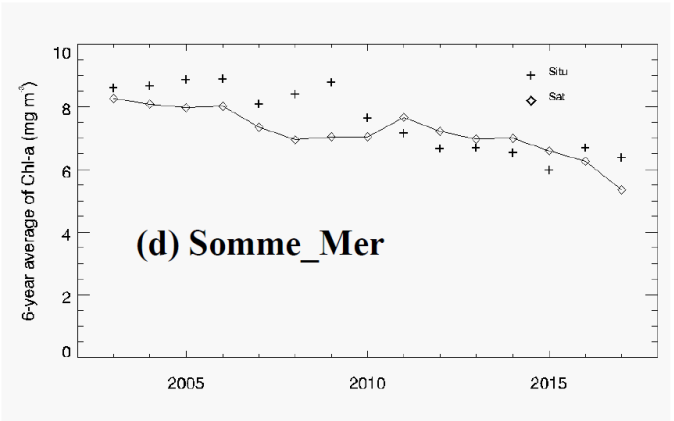

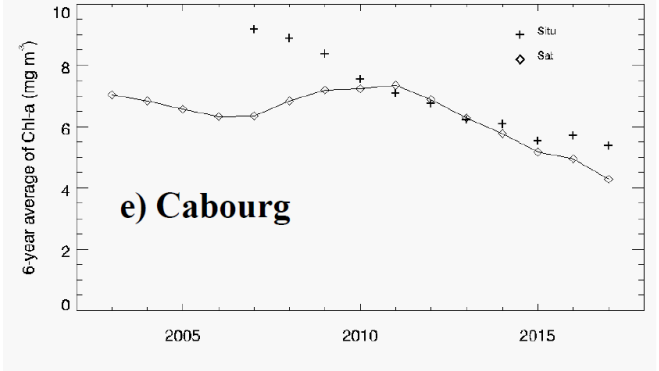

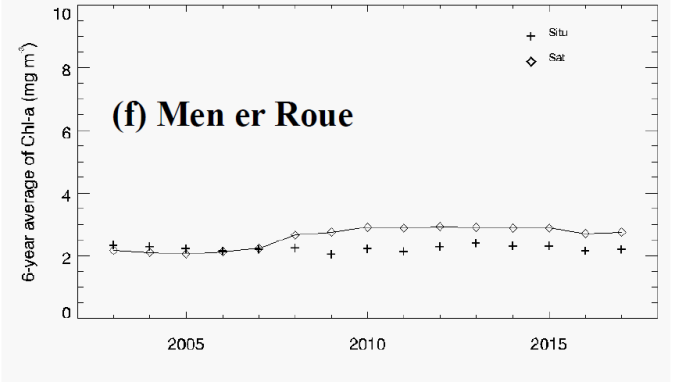

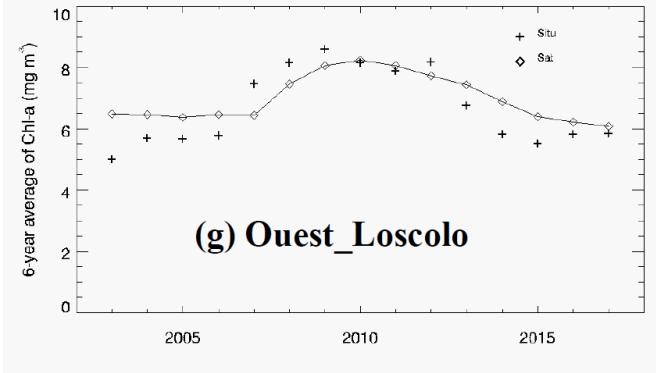

Fig. A3.4. The 6-year moving average of the in situ and satellite (continuous line) Chl-a concentration at the selected stations. (a-c) the Boulogne transect; (d-e) the stations in the plumes of the Somme and Seine rivers: Somme_Mer and Cabourg. (f-g) stations in the Bay of Biscay.

The average is calculated over the productive season (March to October).

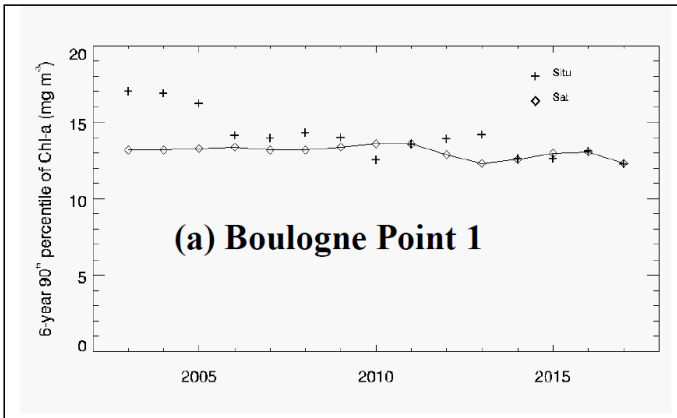

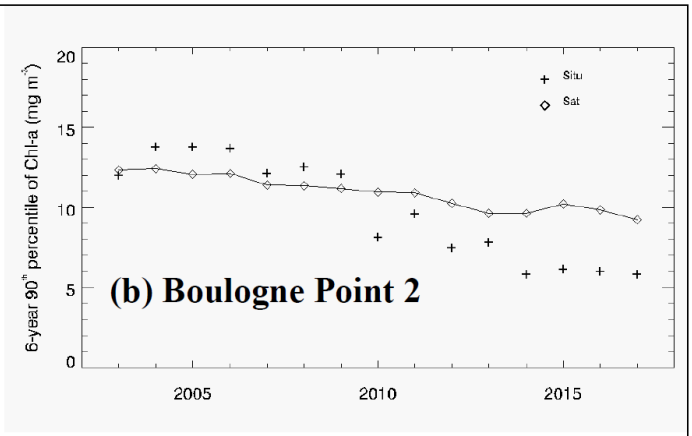

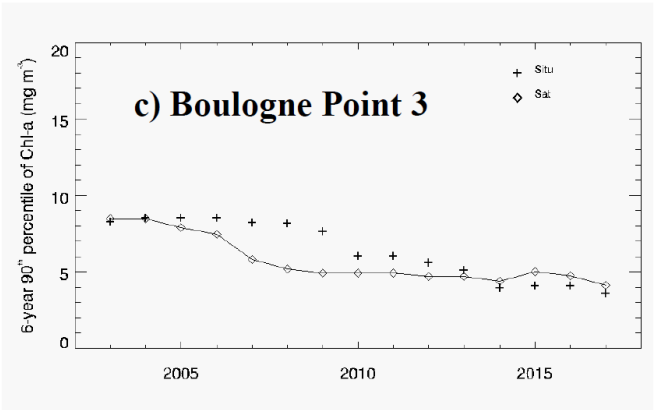

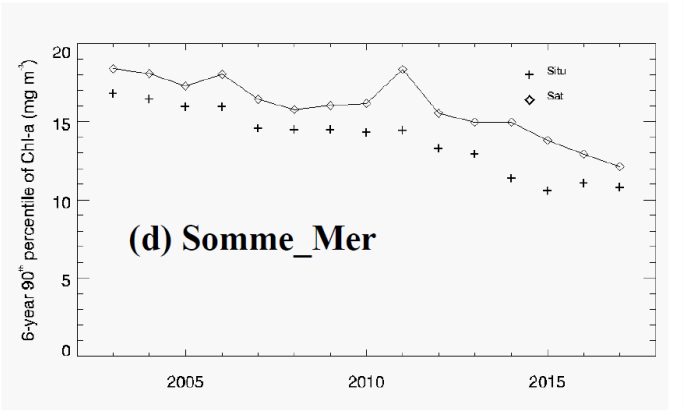

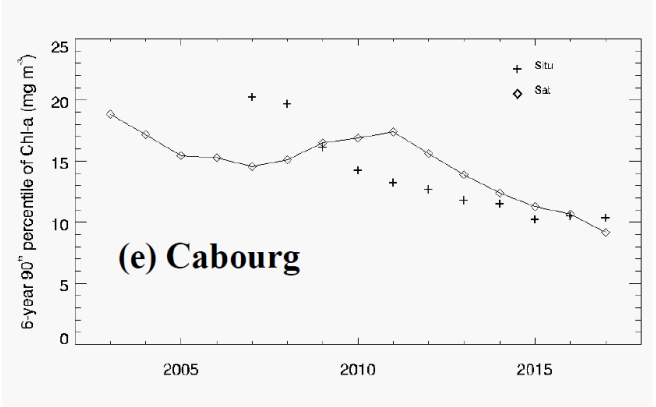

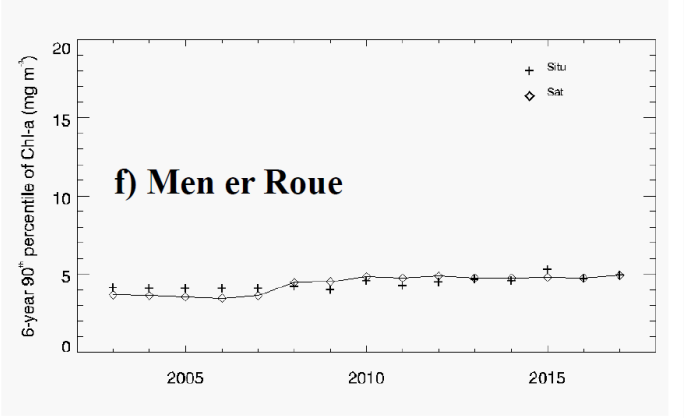

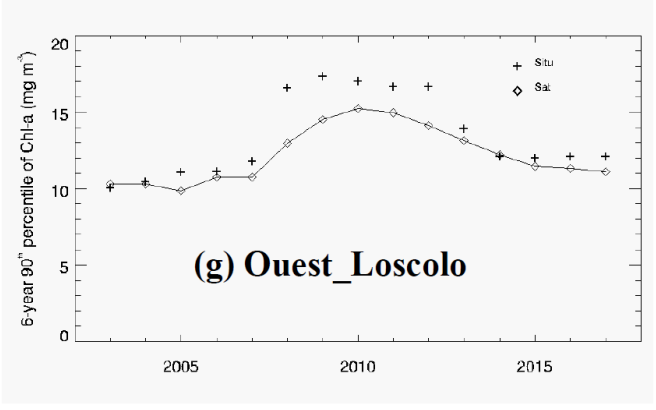

Fig. A3.5.The 6-year moving 90th percentile of the in situ and satellite (continuous line) Chl-a concentration at the selected stations. (a-c) the Boulogne transect; (d-e) the stations in the plumes of the Somme and Seine rivers: Somme_Mer and Cabourg. (f-g) stations in the Bay of Biscay.

The 90th percentile is calculated over the productive season (March to October).

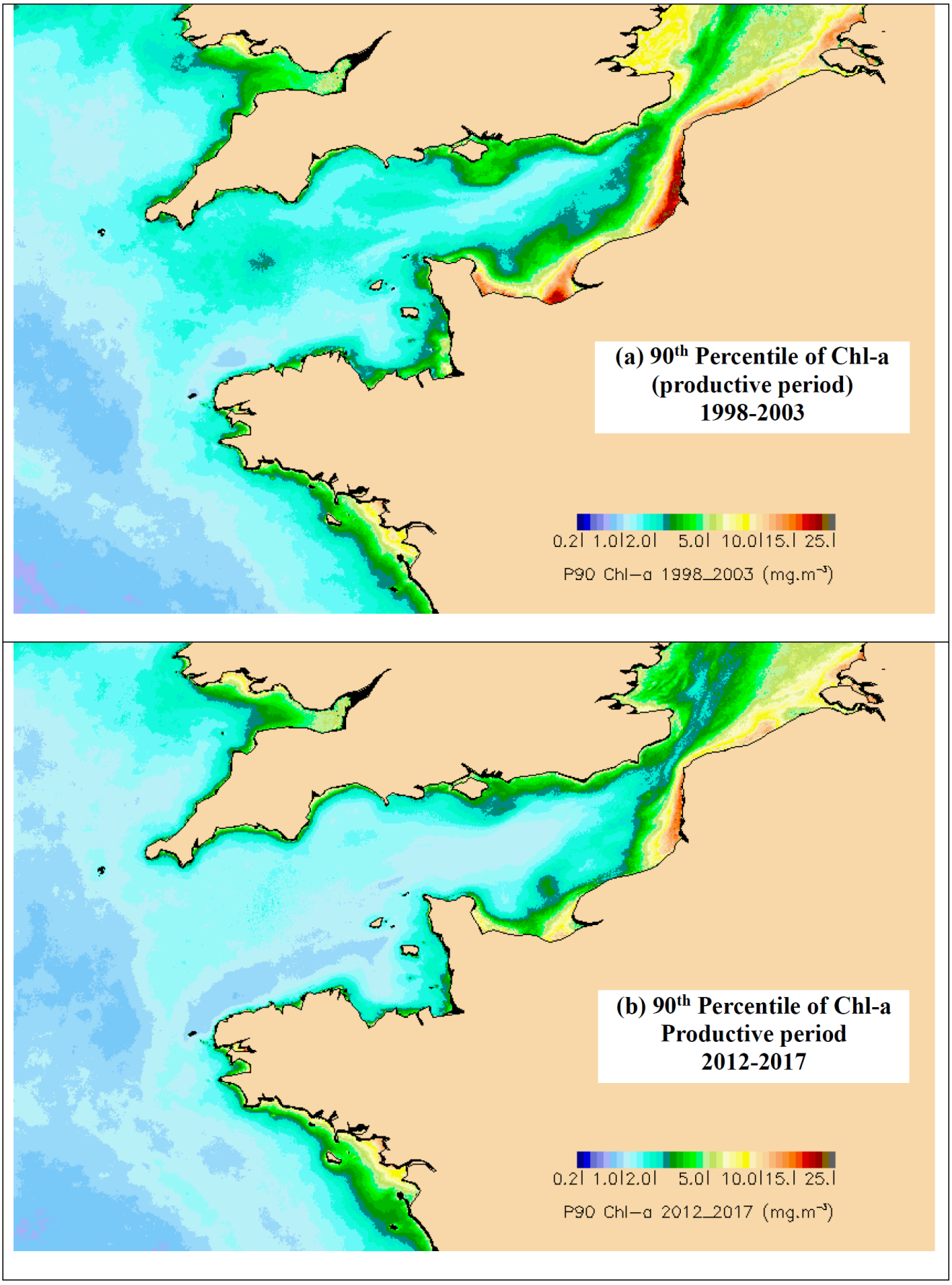

Fig. A3.6. The 90th percentile at the beginning and at the end of the study period. (a) 1998-2003; (b) 2012-2017

Temporal evolution of the annual cycle

If we restrict our samples to periods of 6 years, the lack of *in situ* data makes the representation of the annual cycle from these data less reliable. However, in parallel with lower averages, the shape of the Chl-*a* curve retrieved from satellite and *in situ* data clearly shows an evolution towards those of oceanic regions characterised by a spring peak followed by lower Chl-*a* concentration in nutrient-deprived waters. Figure A3.7 shows the evolution from a "bell shape" to a "peak shape" at the Boulogne Point 2. In 2004-2011 and 2012-2017, the annual cycles of Chl-a show a "peak shape" and are characterised by a decrease of Chl-*a* at fortnightly intervals from 10-15 (May to July), whereas in 1998-2003 Chl-*a* is still high at this period. The decrease in Chl-*a* observed at the last period, 2012-2017, is accentuated in the *in situ* data set by the small number of observations available (73 for the productive period). Figure A3.8 shows typical curves during years of high Chl-*a* (2001 and 2008) compared to years exhibiting lower Chl-*a* (2016 and 2017).
To investigate the phytoplankton dynamics throughout the seasons, the satellite data provide more spatial and temporal coverage as illustrated in Figure A3.9 which shows the monthly means of Chl-*a* at the beginning and the end of the study period. During March and April, Chl-*a* is similar for both periods, while May and June exhibit a clear decline in Chl-*a* in the southern English Channel.

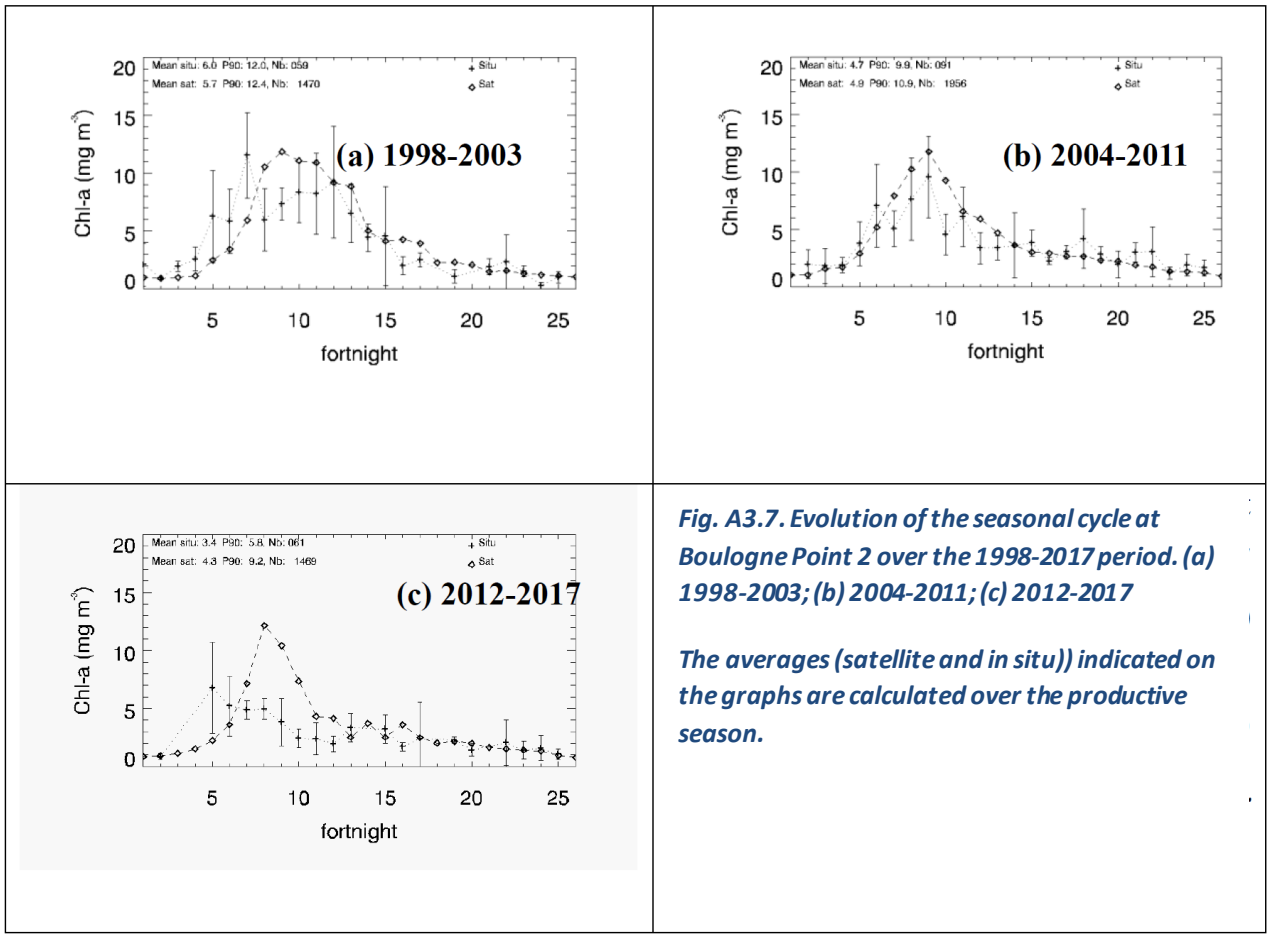

Fig. A3.7. Evolution of the seasonal cycle at Boulogne Point 2 over the 1998-2017 period. (a) 1998-2003; (b) 2004-2011; (c) 2012-2017

The averages (satellite and in situ)) indicated on the graphs are calculated over the productive season.

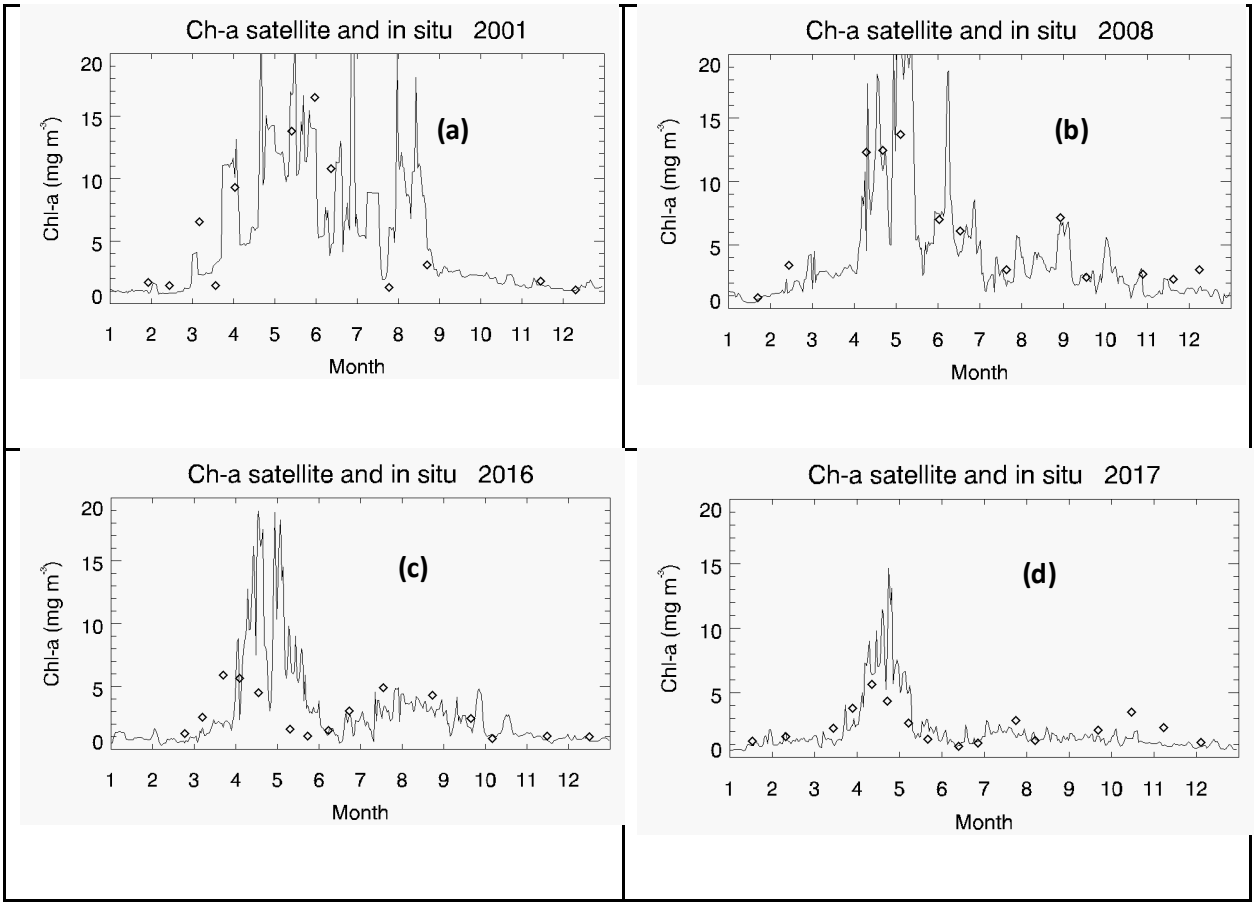

Fig. A3.8. Typical Chl-a cycles at Boulogne Point 2. (a) 2001 and (b) 2008 high Chl-a years; (c) 2016 and (d) 2017 low Chl-a years. diamonds: in situ data; continuous line: satellite data

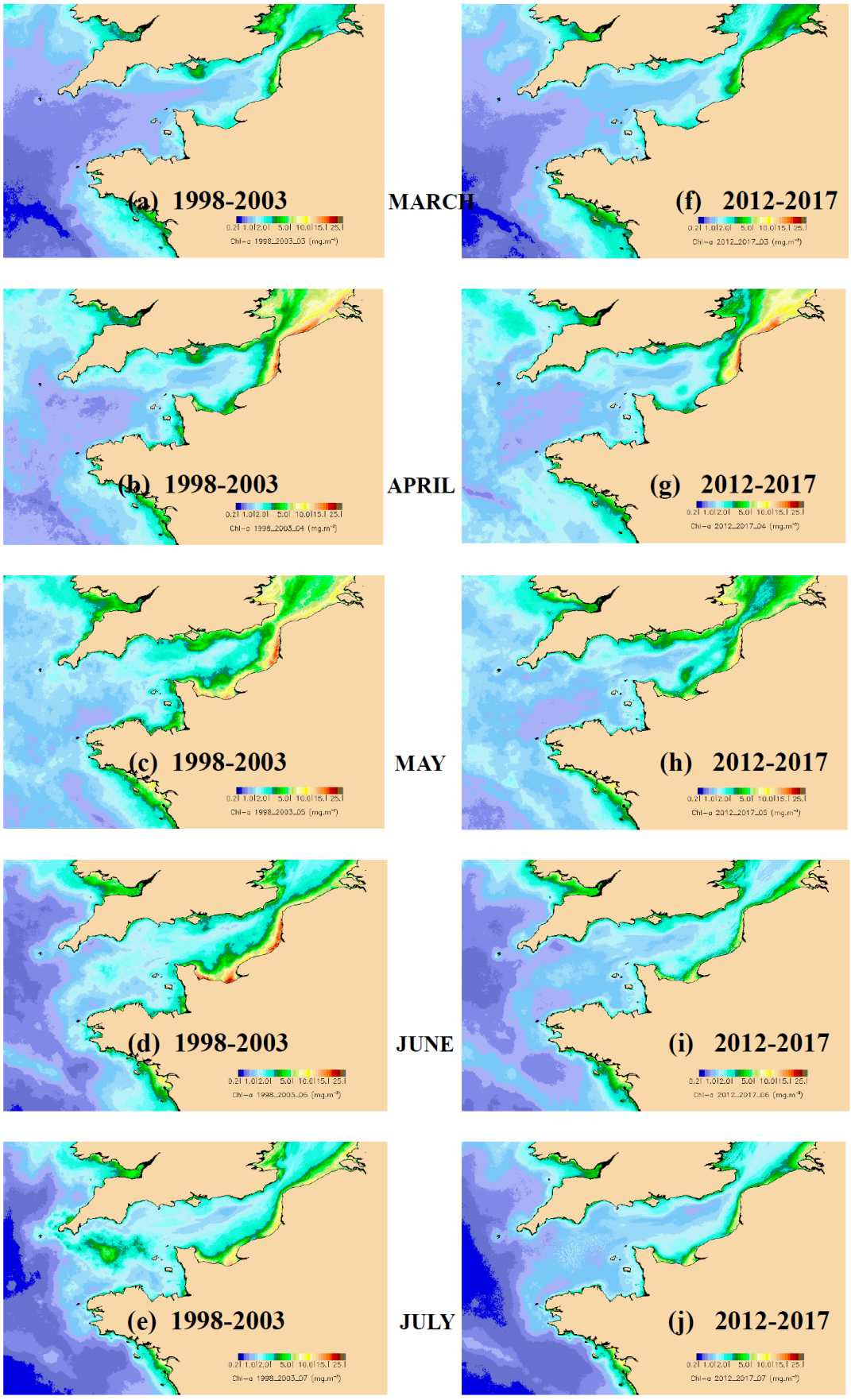

Fig. A3.9. Monthly means of the Chl-a concentration. (a-e) 1998-2003; (f-j) 2012-2017

Annex III.3. Discussion

Regional evolution of the phytoplankton biomass

The evolution of Chl-*a* can be analysed at point scale using *in situ* data or at regional scale using satellite data. The deviation between *in situ* and satellite data shown in Figures A3.4 and A3.5 is enhanced at near-shore coastal stations where patterns of Chl-*a* may exist at a range unreachable at the current 1 km resolution of satellite sensors. The Boulogne Point 1 and Cabourg stations are the most in shore stations and exhibit the highest discrepancy between satellite and *in situ* observations (Fig. A3.4.a and e, Fig. A3.5.a and e). This deviation could come from the remote-sensing technique itself, as particularly complex optical properties, and environment effects, due to the influence of neighbouring land pixels, could affect the quality of the atmospheric correction in waters near the shore. Another plausible explanation is that there has been a substantial improvement in the treatment of the waste waters from neighbouring cities (after application of measures requested by the EU directive on the bathing water quality) since the end of the 1990's, leading to lower nutrient input from sewage effluent into near-shore coastal waters. This may have had strong influence at the Cabourg station which is so close to the coast that, in order to obtain satellite data that are not flagged as land, the location of the pixel was shifted one kilometre northward. There are indeed two scales in the evolution of the nutrient fluxes that affect the coastal waters; one occurs at very short range due to specific improvement locally, for instance in the frame of the bathing water directive, and the second occurs over a larger regional level, which is related to the evolution of the inputs from major rivers, such as the Seine, Loire, Somme and Vilaine rivers which affect the entire area.

At a regional level, there are three main areas that exhibit specific and characteristic evolutions in Chl-*a* from the remote-sensing dataset: the southern Brittany in the Bay of Biscay, the western English Channel, and the so-called "Fleuve côtier", the Region Of Freshwater Influence (ROFI) from the Bay of Seine to the Dover strait in the eastern English Channel (Brylinski et al.; 1990, 1991).
It is in this latter region that the evolution of Chl-*a* is the strongest. Along the southern Brittany coast, there is no significant trend in the pattern and level of Chl-*a* from the beginning to the end of the study period. At the end of the period, the risk of eutrophication remains high in summer when the surface waters stratify and temperature is high.
The western English Channel, particularly the frontal zone between the summer stratified waters of the Atlantic Ocean and the mixed waters of the central English Channel, also has significantly lower levels of phytoplankton biomass at the end of the studied period. This area where high blooms of *Karenia mikimotoi* may occur (Vanhoutte-Brunier et al., 2008) is under the influence of the north-Atlantic hydro-climate and of the inputs in fresh water and nutrients from the rivers flowing into the Bay of Biscay. The evolution of the satellite average of Chl-*a* in July between the periods 1998-2003 and 2012-2017 is also exacerbated by the conjunction of a major heat wave in 2003 that enhanced the thermal gradients and relatively higher fluxes of nutrients from the rivers flowing into the Bay of Biscay.

How do the rivers determine the surface Chl-*a* in the English Channel and the northern Bay of Biscay?

All our stations are in regions of fresh water influence where the physical and chemical environment is partially driven by the river discharges. In consequence, the yearly variability of Chl-*a* is related with the North Atlantic Oscillation, with effects on the river outflows, the inputs in nutrients, the solar irradiance and the sea surface temperature that impact stratification. The decrease in phosphorus is remarkable and it has been identified as a probable cause in the decline of the Chl-a in the Bay of Seine over the period 1990-2010 by Romero et al. (2013). Fig. A3.10, showing the outflows and the averages in nitrate and phosphorus in the Seine and Vilaine rivers, processed over a 6-year basis during the productive season, corroborate the results of Romero et al. (2013). In their case study on the Bay of Seine, they observed that the nitrogen load remained high whilst phosphorus decreased dramatically. Gathering 17 stations from the RHLN Networks in the Bay of Seine over the 2000-2010 period (including the Cabourg station that is particularly well sampled) they also observed a significant decrease in Chl-*a,* a decrease that our study extends to the 2011-2017 period. However, climate is known to contribute significantly to the variability of the coastal environment in western Europe (Goberville et al., 2010). The major effect of the climate on Chl-a at our stations is mostly related with the precipitations and the river discharges. Higher discharges (Fig. A3.10.a) from the Seine river over the period 1998-2003 (particularly winters 2000 and 2001) certainly contribute to accentuate the negative trend in Chl-a that we observed, after Romero et al. (2013), over the period 1998-2017.

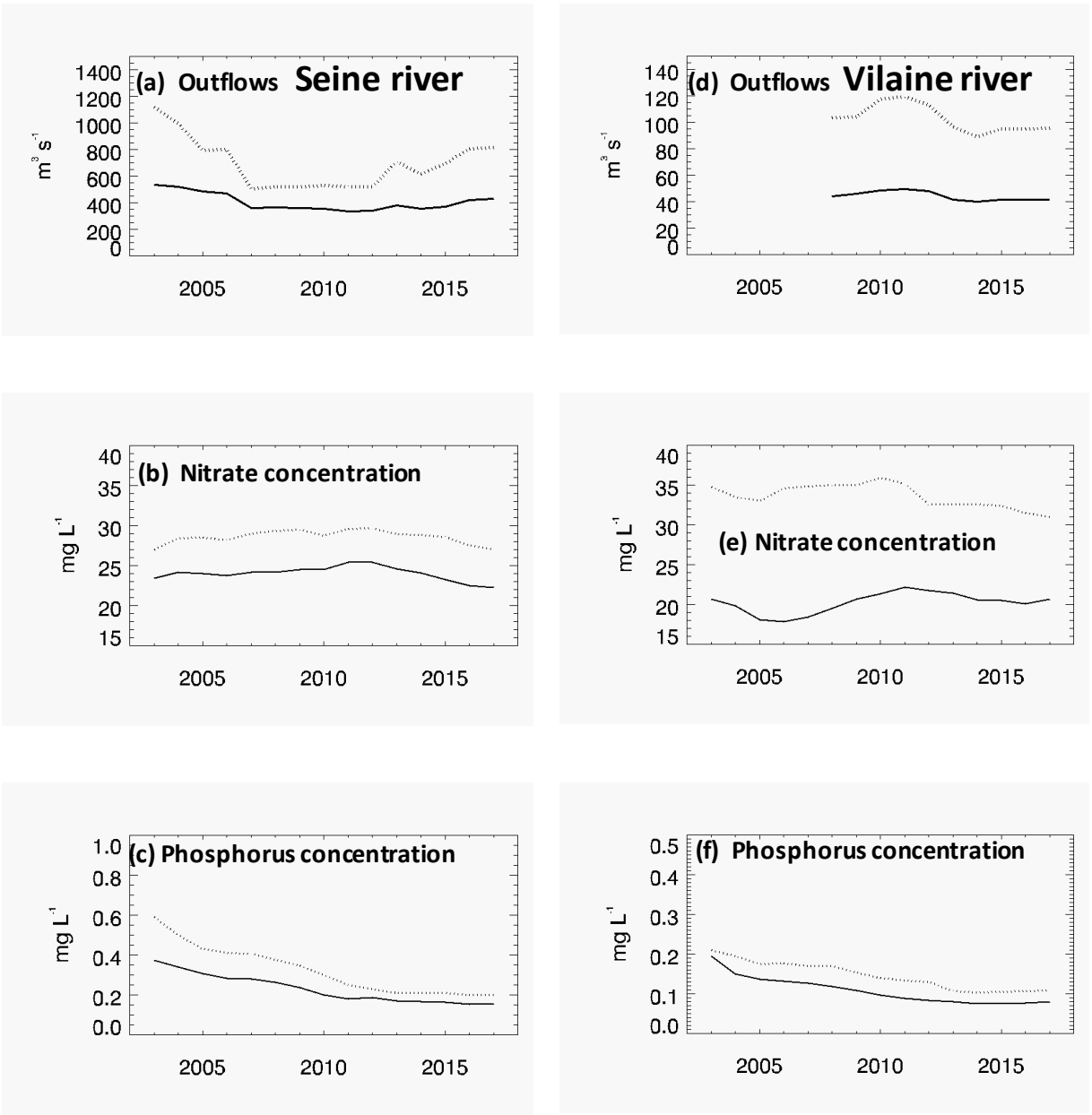

Fig. A3.10. Outflows, nitrate and phosphorus concentration during the productive season for the Seine and Vilaine rivers. (a-c) Seine river; d-f) Vilaine river. The moving average and the percentile 90 are indicated in continuous and dotted line respectively.

By contrast to the English Channel, our Chl-*a* time-series in the northern Bay of Biscay (observed from space and *in situ* at Ouest Loscolo and Men er Roue) do not show any trend over the period despite a decline in phosphorus (Fig. A3.10.f.). Following the patterns of the phytoplankton response to the riverine inputs proposed in Guillaud et al. (2008), the first diatom blooms in the Bay of Biscay appear offshore in late winter, at the edge of the river plume, in relation with haline stratification and anticyclonic "weather windows." In spring, when the central area of the northern shelf is phosphorus-limited, small cells

predominate in the phytoplankton community which competes with bacteria for both mineral and organic phosphorus. In summer, phytoplankton become nitrogen-limited in the river plumes; the central area of the shelf is dominated by small forms of phytoplankton, which are located on the thermocline and use predominantly regenerated nutrients.

References for Annexes

Aminot, A., Kérouel, R., 2004. Hydrologie des écosystèmes marins. Paramètres et analyses. In Ifremer (ed), France.

Andrieux-Loyer, F., Philippon, X., Bally, G., Kérouel, R., Youenou, A., Le Grand, J., 2008. Phosphorus dynamics and bioavailability in sediments of the Penzé estuary (NW France) : in relation to annual P-fluxes and occurrences of *Alexandrium Minutum*. Biogeochemistry, 88, 213-231.

Borja, A, Elliott, M., Carstensen, J., Heiskanen, A.S., van de Bund, W., 2010. Marine management – Towards an integrated implementation of the European Marine Strategy Framework and the Water Framework Directives, Marine Pollution Bulletin, Volume 60, Issue 12, 2175-2186. https://doi.org/10.1016/j.marpolbul.2010.09.026

Bryere, P., Mangin, A., Garnesson P.. Chlorophyll-a evolution during the last 20 years and its relation with mussel growth and optimal repartition for aquaculture and fishery. Ocean State Report 2018, submitted.

Brylinski, J.M., Lagadeuc, Y. 1990. L'interface eaux côtières/eaux du large dans le Pas-de-Calais (côte française) : une zone frontale. C. R. Seances Acad. Sci, 311 (II) : 535–540.

Brylinski, J.M., Lagadeuc, Y., Gentilhomme, V., Dupont, J.P., Lafite, R., Dupeuple, P.A., Huault, M.F., Auger, Y., Puskaric, E., Wartel, M., Cabioch, L., 1991. Le fleuve côtier : un phénomène hydrologique important en Manche Orientale. Exemple du Pas-de-Calais. Oceanol. Acta 11: 197–203.

Capuzzo, E., Lynam CP, Barry J. et al.2018. A decline in primary production in the North Sea over 25 years, associated with reductions in zooplankton abundance and fish stock recruitment. *Glob Change Biol*. 2018;24:e352–e364. https://doi.org/10.1111/gcb.13916

Chapelle, A., Lazure, P., Ménesguen, A. 1994. Modelling eutrophication events in a coastal ecosystem. Sensitivity analysis. Estuar Coast Shelf Sci, 39, 529-548, https://dx.doi.org/10.1016/S0272-7714(06)80008-9

Deborde, J., Anschutz, P., Chaillou, G., Etcheber, H., Commarieu, M.V, Lecroart, P., Abril, G., 2007. The dynamics of phosphorus in turbid estuarines systems : Example of the Gironde estuary (France). Limnology and Oceanography, 52(2), 862-872

Ford, D. A., van der Molen, J., Hyder, K., Bacon, J., Barciela, R., Creach, V. et al., 2017. Observing and modelling phytoplankton community structure in the North Sea. Biogeosciences, 14, 1419–1444. https//doi.org/10.5194/bg-14-1419-2017

Gohin, F., Druon, J. N., Lampert, L., 2002. A five channel chlorophyll concentration algorithm applied to SeaWiFS data processed by Seadas in coastal waters, International Journal of Remote Sensing, 23, 1639-1661 https://doi.org/10.1080/01431160110071879

Gohin, F., Lampert, L., Guillaud, J. F. , Herbland, A., Nezan, E., 2003. Satellite and in situ observations of a late winter phytoplankton bloom, in the northern bay of biscay, Continental Shelf Research, 23, 1117-1141. https://doi.org/10.1016/S0278-4343(03)00088-8

Gohin, F., Saulquin, B., Oger-Jeanneret, H., Lozac'h, L., Lampert, L., Lefebvre, A., Riou, P., Bruchon, F., 2008. Towards a better assessment of the ecological status of coastal waters using satellite-derived chlorophyll-a concentrations, Remote Sensing of Environment, 112, 3329-3340, https://doi.org/10.1016/j.rse.2008.02.014

Gohin, F., 2011. Annual cycles of chlorophyll-a, non-algal suspended particulate matter, and turbidity observed from space and in situ in coastal waters. Ocean Science, 7, 705–732. https://doi.org/10.5194/os-7-705-201

Gómez-Jakobsen, F., Mercado, J.M., Cortés, D., Ramírez, T., Salles, SZ., Yebra, L., 2016. A new regional algorithm for estimating chlorophyll-*a* in the Alboran Sea (Mediterranean Sea) from MODIS-Aqua satellite imagery, International Journal of Remote Sensing, 37:6, 1431-1444, DOI: 10.1080/01431161.2016.1154223

Gons, H. J., Rijkeboer, M. and Ruddick, K.G., 2002. A chlorophyll-retrieval algorithm for satellite imagery (Medium Resolution Imaging Spectrometer) of inland and coastal waters. Journal of Plankton Research, 24(9), 947–951. https://doi.org/10.1093/plankt/24.9.947

Groetsch, P.M.M., Simis, S.G.H., Eleveld, M.A., Peters, S.W.M., 2016. Spring blooms in the Baltic Sea have weakened but lengthened from 2000 to 2014. Biogeosciences 13, 4959-4973. https://doi.org/10.5194/bg-13-4959-2016

Guillaud JF., Aminot A, Delmas D., Gohin F., Lunven M. Labry C., Herbland A., 2008. Seasonal variation of riverine nutrient inputs in the northern Bay of Biscay (France), and patterns of marine phytoplankton response. Journal of Marine Systems. 72: 309-319. https://doi.org/10.1016/j.jmarsys.2007.03.010.

Harvey, E.T., Kratzer, S., Philipson, P., 2015. Satellite-based water quality monitoring for improved spatial and temporal retrieval of chlorophyll-a in coastal waters**.** Remote Sens. Environ., 158, 417-430. https://doi.org/10.1016/j.rse.2014.11.017

Hernández Fariñas T, Soudant D, Barillé L, Belin C, Lefebvre A., Bacher, C., 2014. Temporal changes in the phytoplankton community along the French coast of the eastern English Channel and the southern Bight of the North Sea. ICES Journal of Marine Science 71 (4): 821-833.

Hu, C., Lee, Z., Franz, B., 2012. Chlorophyll a algorithms for oligotrophic oceans: A novel approach based on three-band reflectance difference . Journal of Geophysical Research, 117(C1). https://doi.org/10.1029/2011jc007395

Ifremer : Chlorophylle--a interpolée (données satellite), 2017. http://doi.org/10.12770/9352f74a-7ecb-485e-8ea3-9aa91001b9a1

IOCCG: Remote sensing of ocean colour in coastal and other optically-complex
Waters, 2000. In S. Sathyendranath, & V. Stuart (Eds.), IOCCG report (pp. 1–137). Canada:
Bedford Institute of Oceanography.

Karasiewicz S., Breton E., Lefebvre A., Hernández Fariñas T., Lefebvre, S., 2018. Realized niche analysis of phytoplankton communities involving HAB: Phaeocystis spp. as a case study. Harmful Algae, 72: 1-13. https://doi.org/10.1016/j.hal.2017.12.005

Kratzer, S., Harvey, T., Philipson, P., 2014.The use of ocean colour remote sensing in integrated coastal zone management-A case study from Himmerfjärden, Sweden. Marine Policy 43:29–39. https://doi.org/10.1016/j.marpol.2013.03.023

Lacroix, G., Ruddick, K., Ozer, J., Lancelot, C., 2004. Modelling the impact of the Scheldt and Rhine/Meuse plumes on the salinity distribution in Belgian waters (southern North Sea). Journal of Sea Research, 52 (3), pp. 149-163. doi:10.1016/j.seares.2004.01.003.

Lapucci, C., Rella, M.A., Brandini, C., Ganzin, N., Gozzini, B., Maselli, F., Massi, L., Nuccio, C., Ortolani, A., Trees, C., 2012. Evaluation of empirical and semi-analytical chlorophyll algorithms in the Ligurian and North Tyrrhenian Seas. Journal of Applied Remote Sensing, 6(1). doi:https://doi.org/10.1117/1.JRS.6.063565

Lefebvre A, Guiselin N., Barbet F., Artigas L.F., 2011. Long-term hydrological and phytoplankton monitoring (1992-2007) of three potentially eutrophicated systems in the eastern English Channel and the southern bight of the North Sea. ICES Journal of Marine Science 68(10): 2029–2043. https://doi.org/10.1093/icesjms/fsr149

Le Traon P.Y., Bonekamp, H., Antoine, D., Bentamy, A., Breivik, LA., Chapron, B., Corlett, G., Dibarboure, G., DiGiacomo, P., Donlon, C., Faugère, Y., Gohin, F., Kachi, M., Font, L., Girard-Ardhuin, F., Johannessen, JA., Lambin, J., Lagerloef, G., Larnicol, G., Le Borgne, P., Lindstrom, E., Leuliette, E., Maturi, E., Martin, M., Miller, L., Mingsen, L., Morrow, R., Reul, N., Rio, MH., Roquet, H., Santoleri, R., Wilkin, J., 2015. Use of satellite observations for operational oceanography: recent achievements and future prospects. Journal of Operational Oceanography, 8:sup1, s12-s27, https://ddoi.org/10.1080/1755876X.2015.1022050

L'Helguen, S., Madec, C., Le Corre, P., 1996. Nitrogen uptake in permanently well-mixed temperate coastal waters. Estuarine Coastal Shelf Sci., 42, 803–818.

Loisel., H., Vantrepotte V., Ouillon, S., Ngoc, D. D., Herrmann, M., , Tran, V., Meriaux, X., Dessailly, D., Jamet, C., Duhaut, T., Nguyen, H. H., Nguyen , T. V., 2017. Variability over the Vietnamese coastal waters from the MERIS ocean color sensor (2002-2012). Remote Sensing of Environment, 190, 217-232, doi:10.1016/j.rse.2016.12.016

Lorenzen, C.J., 1967. Determination of Chlorophyll and Pheopigments Spectrophotometric Equations. Limnology and Oceanography, 12, 343-346.

Ménesguen, A., Desmit, X., Dulière, V., Lacroix, G., Thouvenin, B., Thieu, V., Dussauze, M., 2018. How to avoid eutrophication in coastal seas? A new approach to derive river-specific combined nitrate and phosphate maximum concentrations, Science of The Total Environment, 628–629,400-414.
https://doi.org/10.1016/j.scitotenv.2018.02.025

Novoa, S., Chust, G., Sagarminaga, Y., Revilla, M., Borja, A., Franco, J., 2012. Water Quality Assessment Using Satellite-Derived Chlorophyll—A within the European directives, in the southeastern Bay of Biscay. Marine Pollution Bulletin, 65,739-750. https://doi.org/10.1016/j.marpolbul.2012.01.020

O'Reilly, J.E., Maritorena, S.,Mitchell, B. G., Siegel, D. A., Carder, K. L., Garver, S. A., Kahru, M., McClain, C. R., 1998. Ocean color chlorophyll algorithms for SeaWiFS, Journal of Geophysical Research 103, 24937-24953, https://doi.org/10.1029/98JC02160

Ratmaya, W., Soudant, D., Salmon-Monviola, J., Cochennec-Laureau, N., Goubert, E., Andrieux-Loyer, F., Barillé, L., and Souchu, P.: Reduced phosphorus loads from the Loire and Vilaine Rivers were accompanied by increasing eutrophication in Vilaine Bay (South Brittany, France), Biogeosciences Discuss., https://doi.org/10.5194/bg-2018-406, in review.

REPHY – French Observation and Monitoring program for Phytoplankton and Hydrology in coastal waters. REPHY dataset - French Observation and Monitoring program for Phytoplankton and Hydrology in coastal waters. 1987-2016 Metropolitan data, 2017. SEANOE. http://doi.org/10.17882/47248

Romero, E., Garnier, J., Lassaletta, L., Billien, G., Le Gendre, R., Riou, P., 2013. Large-scale patterns of river inputs in southwestern Europe: seasonal and interannual variations and potential eutrophication effects at the coastal zone. Biogeochemistry (2013) 113: 481. **https://doi.org/10.1007/s10533-012-9778-0**

Saulquin, B., Gohin, F., 2010. Mean seasonal cycle and evolution of the sea surface temperature from satellite and in situ data in the English Channel for the period 1986-2006, International Journal of Remote Sensing, 31, 4069-4093. DOI: 10.1080/01431160903199155.

Saulquin, B., Gohin, F., Garrello, R., 2011. Regional objective analysis for merging high-resolution meris, modis/aqua, and seawifs chlorophyll-a data from 1998 to 2008 on the european atlantic shelf, Ieee Transactions on Geoscience and Remote Sensing, 49, 143-154. https://doi.org/10.1109/tgrs.2010.2052813

Saulquin, F., Gohin, F., Fanton d'Andon, O., 2018. Interpolated fields of satellite-derived multi-algorithm chlorophyll-a estimates at global and European scales in the frame of the European Copernicus-Marine Environment Monitoring Service, Journal of Operational Oceanography, https://doi.org/10.1080/1755876X.2018.1552358

Seegers, B. N., Stumpf, R. P., Schaeffer, B. A., Loftin, K. A., Werdell, P. J., 2018. Performance metrics for the assessment of satellite data products: an ocean color case study. *Optics Express*, *26*(6), 7404–7422. https://doi.org/10.1364/OE.26.007404

Smith, M.E., Robertson Lain, L., Bernard, S., 2018. An optimized Chlorophyll *a* switching algorithm for MERIS and OLCI in phytoplankton-dominated waters. Remote Sens. Environ.. 215, 217-227. https://doi.org/10.1016/j.rse.2018.06.002.

SRN - Regional Observation and Monitoring program for Phytoplankton and Hydrology in the eastern English Channel. SRN dataset - Regional Observation and Monitoring Program for Phytoplankton and Hydrology in the eastern English Channel. 1992-2016, 2017. SEANOE. http://doi.org/10.17882/50832

Sundby, B., Gobeil, N., Silverberg, N., Mucci, A., 1992. The phosphorus cycle in coastal marine sediments. Limnology and Oceanography, 37, 1129-1145, https://doi.org/10.4319/lo.1992.37.6.1129

Tilman, D., 1982. Resource competition and community structure, Princeton University Press, New Jersey.

Thomas, Y., Mazurié, J., Alunno-Bruscia, M., Bacher, C., Bouget, JF., Gohin, F., Pouvreau, S., Struski, C., 2011. Modelling spatio-temporal variability of Mytilus edulis (L.) growth by forcing a dynamic energy budget model with satellite-derived environmental data. Journal of Sea Research 66:308-317. https://doi.org/10.1016/j.seares.2011.04.015

Tilstone, G., Mallor-Hoya, S., Gohin, F., Belo Couto, A., Sa, C., Goela, P., Cristina, S., Airs, R., Icely, J., Zühlke, M., Groom, S, 2017. Which Ocean colour algorithm for MERIS in North West European waters? Remote Sens. Environ.. 189, 132-151. https//doi.org/10.1016/j.rse.2016.11.012

Vanhoutte-Brunier, A., Fernand, L., Menesguen, A., Lyons, S., Gohin, F., Cugier, P., 2008. Modelling the karenia mikimotoi bloom that occurred in the western English channel during summer 2003, Ecological Modelling, 210, 351-376. https://doi.org/10.1016/j.ecolmodel.2007.08.025

Vermaat, J.E., McQuatters-Gollop, A., Eleveld, M.A., Gilbert, A., 2008. Past, present and future nutrient loads of the North Sea: causes and consequences. *Est. Coast. Shelf Sci.* *80*(1), 53-59. https://doi.org/doi:10.1016/j.ecss.2008.07.005